UNIVERSITÀ
DEGLI STUDI
DI MILANO

TECHNISCHE
UNIVERSITÄT
DARMSTADT

Bi-national PhD in the area:

Molecular and Cellular Biology

Research field: ion channels biophysics

vom Fachbereich Biologie

der Technischen Universität Darmstadt

and

from Dipartimento di Bioscienze

of Università degli Studi di Milano

Submitted in fulfillment of the requirements

for the degree: PhD

DISSERTATION

by Paolo Zuccolini

Supervisors: Prof. Gerhard Thiel (Darmstadt)

Prof. Anna Moroni (Milano)

Author: Paolo Zuccolini

Title: Application of optogentetic principles for the modulation of the pacemaker current I_f

Thesis work performed at:

- **Università degli Studi di Milano - Dipartimento di Bioscienze, Via Celoria 26 Milano (IT)**
- **Technische Universität Darmstadt, Schnittspahnstraße 3 Darmstadt (DE)**

Uploaded on TUprints in the year: 2019

Date of oral exam: 22/03/2019

1

INDEX

2

ABSTRACTS

2.1 Abstract in English

HCN4 channels control pacemaking of the heart. They are activated by negative voltage and modulated by cAMP. Recently it had been discovered that cyclic di-nucleotides bind to a second site in the channel C-terminus. This counteracts the effect of cAMP on shifting channel activation positive. A bacterial cyclase, which synthesizes c-di-GMP in response to red light, allows engineering of an optogenetic system for remote HCN4 modulation and hence for controlling the heart pace.

Two cyclases were used in this work: one constitutively active (Slr1143) and one red ligh-regulated (BphS). Because the latter has some dark activity, it is co-expressed with a phosphodiesterase (YhjH). Recordings of HCN4 activity in HEK293T cells show that Slr1143 affects the voltage dependence of the channel, shifting the activation curve negative with respect to the control.

Experiments with BphS show no difference in HCN4 activity between light and dark treated cells. The combined BphS-YhjH expression seemed to be unable to increase the c-di-GMP concentration in a light dependent manner. To examine the effect of light on c-di-GMP production we quantified the cyclic di-nucleotide with an established ELISA assays in HEK293T cells and with an immune-fluorescence method. The latter consisted of monitoring expression of interferon-β in BphS-YhjH expressing T cells. Cyclic di-nucleotides can activate the STING pathway, which augments synthesis of interferon-β. Both methods underlined that Slr1143 and BphS-YhjH system increased the level of c-di-GMP in cells. This activity, however, was not light regulated. The immuno-fluorescence data indicate a slightly higher expression of the constitutive compared to the light-regulated cyclase. This may explain why we observed an effect of the former but not of the latter on HCN4 gating. Eliminating YhjH did not affect the level of c-di-GMP, suggesting that the phosphodiesterase is insufficient for eliminating c-di-GMP dark production. The data confirm previous results in that c-di-GMP is able to modulate HCN4 activity. BphS is not yet suitable as an optogenetic tool because of its high dark activity. This problem may be overcome by increasing the expression/activity of the phosphodiesterase in the next iteration of engineering an optogenetic tool.

2.2 Abstract in italiano

I canali HCN4 sono i principali regolatori della frequenza cardiaca. Si aprono in iperpolarizzazione e sono modulati da cAMP. Recentemente si è scoperto che anche i nucleotidi di-ciclici interagiscono con il canale, legandosi in un altro sito localizzato al C-terminale. Ciò contrasta la capacità del cAMP di spostare la voltaggio dipendenza verso potenziali più positivi. Una ciclasi batterica, che sintetizza c-di-GMP in risposta a luce rossa, permette di costruire un sistema per il controllo remoto di HCN4 e dunque del pacemaker.

In questo lavoro sono state utilizzate due ciclasi: una costitutivamente attiva (Slr1143) ed una regolata da luce rossa (BphS). Dato che quest'ultima presenta attività ciclasica anche al buio, va co-espressa con una fosfodiesterasi (YhjH). Registrazioni delle correnti attivate da HCN4 in HEK293T, mostrano che Slr1143 modifica la voltaggio dipendenza del canale spostandone la curva di attivazione rispetto ai controlli.

Gli esperimenti con BphS non mostrano alcuna differenza nell'attività di HCN4 tra buio e luce. L'espressione combinata di BphS e YhjH sembrava non aumentare la concentrazione di c-di-GMP in modo luce-dipendente. Per analizzare l'effetto della luce sulla produzione di c-di-GMP, esso è stato quantificato con un consolidato test ELISA e con immuno-fluorescenza. Quest'ultimo metodo consisteva nel monitorare l'espressione di interferone β in cellule T esprimenti Bphs-YhjH. I nucleotidi di-ciclici attivano infatti il pathway di STING, che aumenta la sintesi dell'interferone. Entrambi i metodi hanno evidenziato che Slr1143 e il sistema BphS-YhjH aumentavano il c-di-GMP nelle cellule. Tuttavia, questa attività non era luce-dipendente. I dati di immuno-fluorescenza indicano un'espressione leggermente maggiore della ciclasi costitutiva rispetto a quella luce-regolata. Ciò può spiegare perché abbiamo osservato un effetto del primo costrutto sul gating di HCN4 ma non del secondo. L'eliminazione della fosfodiesterasi YhjH non aumenta la concentrazione finale di c-di-GMP e ciò indica che essa non è in grado di compensarne la produzione al buio. I dati confermano osservazioni precedenti sulla capacità del c-di-GMP di modulare l'attività di HCN4. Tuttavia BphS non è ancora adatto per essere usato in optogenetica per via della sua attività al buio. Questo problema potrebbe essere risolto aumentando l'espressione e l'attività della fosfodiesterasi nelle successive fasi di sviluppo del sistema.

2.3 Abstract auf Deutsch

HCN4-Kanäle steuern die Frequenz des Herzschlags. Sie werden durch negative Spannung aktiviert und durch cAMP moduliert. Kürzlich wurde entdeckt, dass auch zyklische Dinukleotide an eine zweite Stelle im C-Terminus des Kanals binden können. Dies wirkt dem Effekt von cAMP auf die Aktivierung des Kanals entgegen. Eine bakterielle Cyclase, die c-di-GMP als Reaktion auf Rotlicht synthetisiert, ermöglicht die Entwicklung eines optogenetischen Systems zur ferngesteuerten HCN4-Modulation und damit zur Steuerung des Herzrhythmus.

Zwei Proteine wurden verwendet: eine konstitutiv aktive (Slr1143) und eine rotlichtregulierte (BphS) Cyclase. Da letztere eine gewisse Dunkelaktivität aufweist, wird eine Phosphodiesterase (YhjH) koexprimiert. Aufzeichnungen über die HCN4-Aktivität in HEK293T-Zellen zeigen, dass Slr1143 die Spannungsabhängigkeit von HCN4 beeinflusst; Slr1143 verschiebt die Aktivierungskurve des Kanals relativ zur Kontrolle in Richtung negativer Membranspannungen.

Experimente mit BphS zeigen keinen Unterschied in der HCN4-Aktivität zwischen Zellen, die im Hellen oder Dunklen inkubiert wurden. Die kombinierte BphS-YhjH-Expression schien nicht in der Lage zu sein, die c-di-GMP-Konzentration in einer lichtabhängigen Weise zu erhöhen. Um die Wirkung von Licht auf die c-di-GMP-Produktion zu untersuchen, haben wir die zyklische Dinukleotid-Konzentration mit einem etablierten ELISA-Assay in HEK293T-Zellen und mit einer Immunfluoreszenzmethode quantifiziert. Letztere bestand in der Überwachung der Expression von Interferon-β in BphS-YhjH exprimierenden T-Zellen. Zyklische Dinukleotide können den STING-Pfad aktivieren, der die Synthese von Interferon-β verstärkt. Beide Methoden zeigten, dass sowohl Slr1143 als auch das BphS-YhjH-System zu einer Erhöhung des zellulären c-di-GMP-Spiegels führen. Diese Aktivität war jedoch nicht durch Licht reguliert. Die Eliminierung von YhjH hatte keinen Einfluss auf das c-di-GMP-Level, was darauf hindeutet, dass die Phosphodiesterase nicht in der Lage ist, die Produktion von c-di-GMP im Dunklen zu unterbinden. Die Daten bestätigen die bisherigen Ergebnisse, dass c-di-GMP in der Lage ist, die HCN4-Aktivität zu modulieren. BphS ist aufgrund seiner hohen Dunkelaktivität noch nicht als optogenetisches Werkzeug geeignet. Um dieses Problem auf dem Weg zur Konstruktion eines funktionsfähigen optogenetischen Werkzeugs zu überwinden, muss die Expression/Aktivität der Phosphodiesterase erhöht werden.

3

INTRODUCTION
AND
AIM OF THE THESIS

3.1 Birth and development of a powerful technique

Optogenetics is an innovative and powerful approach that combines methods of genetic and optical techniques to trigger or inhibit well defined events in specific cells of living tissues (Deisseroth, 2015). The principle of optogenetics is to remotely modulate cellular events of interest with light. The effective light stimulations can be applied in a very fast manner and further fine tuned by grading the power and/or the wavelengths of the stimulating light. The final light stimulation can then penetrate, with or without the help of specific light guides, deeply into the tissues. The modulation of cellular processes by light stimulation can be achieved by the expression of specific photo-regulated proteins in the target cells. An activation of these light sensitive proteins then leads, directly or indirectly, to the desired effects (Rost et al., 2017).

The principle of optogenetics was introduced in 2015 by Boyden and colleagues as a tool for selectively controlling the activity of specific types of neurons (Deisseroth, 2011). The neural circuits are highly complex systems in which different types of neurons stimulate or inhibit each other. The great challenge for neurobiologists was to experimentally dissect these complex circuits and investigate the role of each class of neuron in the information processing (Boyden, 2011). Before the introduction of optogenetics important insights into the role of different neurons within a circuit could be provided by direct electrical stimulation of cells in intact brain tissue. The drawback of this method is that neurons belonging to a specific class are often sparsely embedded within the tissue (Fenno et al., 2011). An alternative approach for dissecting complex neuronal circuits was provided by pharmacological methods. This type of manipulation indeed offered a more precise way of targeting a specific cell type of interest with certain expression patterns. The drawback of this approach is that it requires the diffusion of chemical compounds to the site of action, which is in most cases too slow for manipulating the desired activity of neurons (Fenno et al., 2011). Scientists realized since the late seventies that to understand more deeply how the brain works they needed a method by which neurons of just one type could be manipulated, leaving the others unaffected (Crick, 1979). The ideal technique would employ a genetically encoded tool, which is selectively expressed in a defined class on neurons and which is able to affect excitability in response to a diffuse and fast stimulus. The first step in this direction was the intuition that light could be such a stimulus, fulfilling the need for speed, diffusion and simplicity of delivery.

Before optogenetics was introduced, other researchers already had the idea of using light as a remote and non-invasive stimulus to elicit neuronal firing. Zemelman and colleagues conferred photo-sensitivity to hippocampal neurons by co-expressing in these cells the elements of the phototransduction machinery of *Drosophila* (Zemelman et al., 2002). In invertebrates, the stimulation of the photoreceptors activates a pathway that eventually causes cell depolarization *via* opening of cation channels. By expressing the phototransduction elements in hippocampal neurons, they were able to elicit the firing of action potentials in response to light irradiation. The light activated firing was obtained also in neurons treated with

inhibitors of glutamate receptors, proving that the observed action potentials were not provoked by excitatory synaptic inputs. However, the recordings of action potentials in these light-sensitive neurons indicated that there was a delay of 0.5÷34 seconds between the beginning of the irradiation and the appearance of the firing. The technique, although interesting, was not providing the desired temporal precision.

To achieve an activation of neural firing with a higher temporal precision, the pioneers of optogenetics expressed in neurons an ion channel that is directly gated by light. This system does not require any signaling cascade or second messenger between light perception and membrane depolarization. The crucial channel, which provided these features, was channelrhodopsin-2 (ChR2), a light-activated ion channel from *Chlamydomonas reinhardtii*, first characterized by Nagel and colleagues in 2003 (Nagel et al., 2003). Before the publication of this seminal work it was already known that this channel uses retinal as a chromophore to sense light, and that the activity of the channel was involved in the generation of "photocurrents" in the algae when the latter are irradiated with blue light (Sineshchekov et al., 2002). When Nagel and colleagues characterized this protein, they clearly demonstrated that it was both a light sensor and an ion channel. They expressed the protein into *Xenopus laevis* oocytes supplied with all-trans retinal. In these oocytes they were able to measure a blue light-activated inward current that displayed a peak followed by a decay to a steady state level (Fig. 3.1 A). The channel turned out to be permeable for mono and divalent cations, while anions did not contribute in any way to the measured currents. The authors furthermore performed inside-out patch clamp experiments: with this technique it is possible to measure currents flowing through a small piece (patch) of membrane that is isolated from the rest of the membrane and the cytoplasm. In this configuration channel gating cannot depend on potential regulators or signaling cascades from the cytoplasm. Using excised patches the authors confirmed that even after isolating the channel from the cytoplasm it was still able to elicit a light-activated current similar to that observed in whole-cell measurements (Fig. 3.1 B). With this work it was proven that ChR2 is cation channel, which is directly gated by blue light.

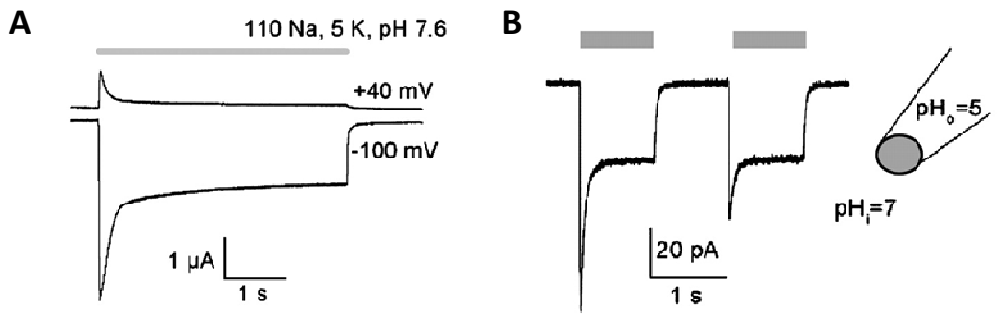

Fig 3.1 Characterization of ChR2. (A) Currents recorded in *Xenopus laevis* oocytes expressing ChR2. When the voltage was clamped at -100 mV, blue light illumination elicited the activation of an inward cation currents. (B) Inside-out patch-clamp recordings of a patch of membrane from an oocyte expressing ChR2. (figures from Nagel et al., 2003).

Boyden and co-workers understood that this peculiar channel from an alga could be used to elicit action potentials in neurons in a light dependent manner (Boyden et al., 2005). The channel opens upon blue light illumination and is selective for cations. Because of the electrochemical gradient across the membrane of neurons, the opening of a cation channels will cause an inward flux of positive ions and hence a depolarization of the membrane potential. This in turn will trigger the generation of action potentials. For a proof of concept, Boyden and coworkers infected cultured rat neurons with lentiviruses containing a Chr2-YFP fusion protein. In these cells they were able to measure blue light activated inward currents similar to those measured by Nagel one year before (Fig 3.2 A and B). Under continuous blue light irradiation they observed an appreciable depolarization of the membrane potentials and the rise of spiking activity. The latter appeared few milliseconds after the light stimulation began but the frequency decreased dramatically during the stimulation (Fig. 3.2 C). Given the rapid activation of Chr2 by light and the consequent depolarizing current, they also succeeded in eliciting single action potentials by short single blue light flashes. They found that a light flash of 15 ms was able to generate a complete action potential and that multiple light pulses separated by dark periods were able to generate high frequency firing in the neurons (Fig. 1.2 D). Thanks to such an incredible temporal precision, they were able not only to elicit neuronal firing but also to regulate the frequency of their spikes by modulating the light pulses frequency. The results of these experiments show that the concentration of retinal in neurons is evidently sufficient for a proper Chr2 function. Collectively this implied that this optogenetic tool is totally genetically encoded and does not require to treat the cells with any exogenous compound. This is an important feature for an optogenetic tool, as its ability to response to light will not depend on the delivery of chemicals to cells. In the same period in which Boyden and colleague developed optogenetics, another research group engineered a light-activated channel called SPARK (Banghart et al., 2004). The shortcoming of this channel is that it needs to be supplied with an exogenous molecule that confers light dependence to the gating. The system developed by Boyden and colleagues is, on the contrary, intrinsically light regulated.

In the past decade the optogenetics methods have been further developed and the technique has been enriched with new tools, some of which are present in nature and belonging to the opsin family (Mei and Zhang, 2012). An example of these proteins is the yellow light regulated chloride pump halorhodopsin from *Natronomonas pharaonis* (NpHR). This is a pump that is able to transport chloride ions across the membrane into the cytoplasm (Bamberg et al., 1993). The transfer of negative charges into an excitable cells should hyperpolarize the membrane potential, preventing the rise of action potentials. This is indeed what happened when NpHR was expressed into neurons: an illumination with yellow light led to a hyperpolarization of the membrane potential and an inhibition of firing (Fig. 1.3, Zhang et al., 2007). Action potentials were in this case induced by injecting positive currents into the cells. The ability of this stimulation to induce firing promptly disappeared when the yellow light was turned on.

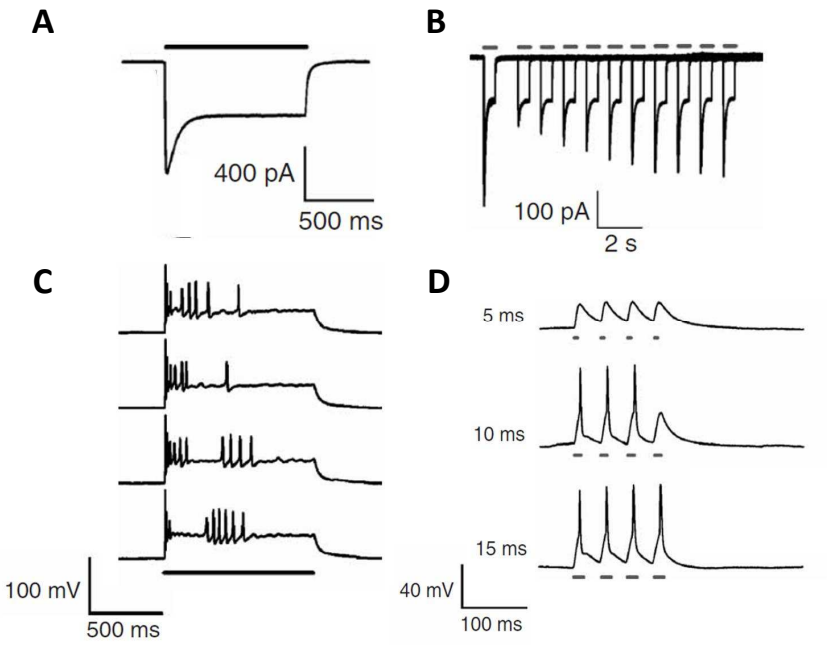

Fig 1.2 Expression of Chr2 in neuronal cells. (A) Currents recorded in cultured rat neurons expressing Chr2 when they were exposed to continuous blue light. (B) Multiple inward currents elicited by irradiating the cells with short light pulses. (C) Membrane potential in Chr2-expressing neurons: upon illumination with continuous light the frequency of the spikes decreases with time. (C) Short light pulses allowed to finely modulate the frequency of the action potentials: 15ms long pulses were the best to generate complete action potentials. In the four figures light pulses are indicated with bars. (Figures from Boyden et al., 2005).

It was interesting to note that NpHR was able to counteract the effect of Chr2 when the two proteins were coexpressed in neurons. In this scenario the pump inhibited the firing caused by Chr2 upon irradiation with blue light. This inhibitory optogenetics tool NpHR was also expressed into moto-neurons of *Caenorhabditis elegans*. In this context the activation of the pump caused a complete inhibition of the animal's swimming activity (Zhang et al., 2007).

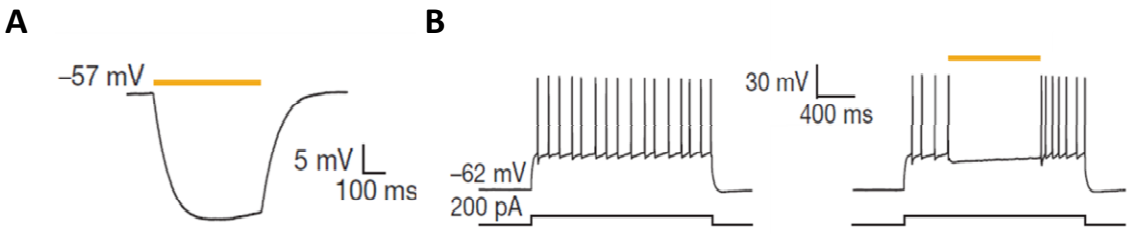

Fig 3.3 NphR is able to silence the neurons. (A) Membrane potential variation recorded in cultured rat neurons expressing NphR when they were exposed to continuous yellow light. (B) Action potential recorded in neurons expressing NphR: the hyperpolarization caused by the yellow light inhibited the neurons electrical activity. (Figures from Zhang et al., 2007).

Some other more recently developed optogenetic tools are proteins that cannot be found in nature; they are the product of protein engineering. These constructs are usually designed to confer light sensitivity to a protein responsible for the effect that one wants to control. For this purpose the photosensitive domain of a light regulated protein is in most of the cases fused with the protein of interest. In the past years, new synthetic proteins for optogenetic applications have been engineered using, as regulatory domain in these chimeras, the LOV2 domain of the plant phototropin 1 (Cosentino et al., 2015; Niopek et al., 2014; Pham et al., 2011; Strickland et al., 2008). This domain, which is part of a blue light sensor in plants, is composed by antiparallel β-strands that form an hydrophobic cavity (cage or core), in which the chromophore flavin mononucleotide is held uncovalently. The C terminus of the cage contains an amphipathic alpha helix called Jα, whose apolar side docks onto the core (Fig 1.4 A, Christie, 2007). Irradiation of the domain induces the formation of a covalent adduct between the C(4a) carbon of the flavin chromophore and a conserved cysteine residue within the LOV2 domain. The conformational rearrangements in the cage, that occur after the formation of the covalent bond, cause the disruption of the interaction between the cage and the Jα, which partially unfolds. This unfolding of the Jα results in an activation of the kinase domain of the phototropin, located at the end of the helix (Fig. 1.4 B, Christie, 2007). The LOV2 domain is therefore able to keep a catalytic domain blocked against its core and to "release" it in response to blue light.

An elegant example for the construction of new optogenetics tools using the LOV2 domain, is the light gated potassium channel BLINK (Cosentino et al., 2015). Potassium channel opening drives the membrane voltage negative and hence terminates in this way action potentials and prevents firing in excitable cells (Hille, 2001). Such a light sensitive K^+ channel could be very useful for optogenetics because opsin-based hyperpolarizing optogenetic tools have some shortcomings. First, these ion pumps are rather inefficient because they move only one ion per photocycle. Notably a channel conducts in contrast up to 10^8 ions per second. Moreover the pumps also create abnormal ion gradients in cell. For these reasons, the optogenetic community had been looking for a more efficient and genuine light-gated channel, which can be used to hyperpolarize cells. In 2015 Cosentino and co-workers constructed a light-gated potassium channel by fusing the LOV2 domain to a viral potassium channel called Kcv (Fig 1.4 C). This is a very small potassium channel composed by only the pore module of a K+ channel lacking any regulatory domain (Plugge et al.,2000). The design of this synthetic channel was inspired by the finding that channel proteins are often modular elements in which the pore, which conducts the ions, is connected with regulatory domains (Arrigoni et al., 2014). Conformational changes of the regulatory domain can be transmitted to the pore unit were they alter the flux of ions. This natural architecture of ion channels can be mimicked in synthetic proteins in which a channel pore unit is coupled in an intelligent manner with a foreign regulatory or sensor unit (Arrigoni et al., 2014, Difrancesco et al., 2015). The native fusion of the a viral potassium channel pore to the LOV2 domain resulted, after some optimization steps, in a potassium channel that could be reversibly gated by blue light (Fig. 1.4 D, Cosentino et al., 2015).

Optogenetic principles can also be used to regulate different types of cellular processes beyond the control of changes in the membrane voltage. An interesting example for such a system that does not involve ion currents, is presented in the work from the Di Ventura's group (Niopek et al., 2014; Niopek et al., 2016; Di Ventura, 2016). They were able to control, precisely and reversibly, nuclear translocation of proteins in human cells. They used the LOV2 domain as photo-switch and added at the C terminus of the Jα a nuclear localization signal (NLS). The latter is concealed from the nuclear import machinery in the dark state but, in the light, the Jα helix unfolds and undocks from the *As*LOV2 core domain, exposing the NLS to the cytoplasm (Fig 1.4 E). In this condition the NLS can be recognized and bound by the endogenous importins. They named this light-inducible nuclear localization signal LINuS. A construct made by Mcherry and LINuS (Fig 1.4 F) was expressed in different cell types. In cells expressing this construct it was possible to see that the mCherry fluorescence signal was present both in the nucleus and the cytoplasm in the dark. To reduce the background nuclear localization of LINus, they added also a nuclear export signal (NES). This new construct was, in the dark, dispersed in the cytoplasm but was not present in the nucleus. Upon illumination, they observed the occurrence of a mCherry signal in the nucleus, which indicated that the protein was being relocated there (Fig 1.4 G). With LINuS as an optogenetic tool they are now able to control cellular events that involve nuclear translocation of a protein or a set of proteins. Examples are mitotic entry or gene expression. In the next step they used the same principles behind LINuS to create a light dependent export signal called LEXY.

With this brief overview, I want to show the principles optogenetics and the importance of this new technology in biological sciences. A number of recent reviews underscore the great impact on this new concept on progress in research in many fields (Rost et al., 2017; Boyle at al., 2018). To complete the picture I also described some examples of synthetic proteins, which were designed to expand the collection of neurophysiology tools or to achieve the modulation of new and different cellular events.

Optogenetics is a dynamic and rapidly evolving field that can be enriched with new light-inducible proteins to control different phenomena. This PhD work was motivated by the idea to further expand the optogenetics toolbox. The particular goal was to create a system which allows a light-regulated gating of the HCN4 channel and, with this, a way to modulate the heart rate in an non invasive manner. The rationale behind this approach will be presented in the next chapter.

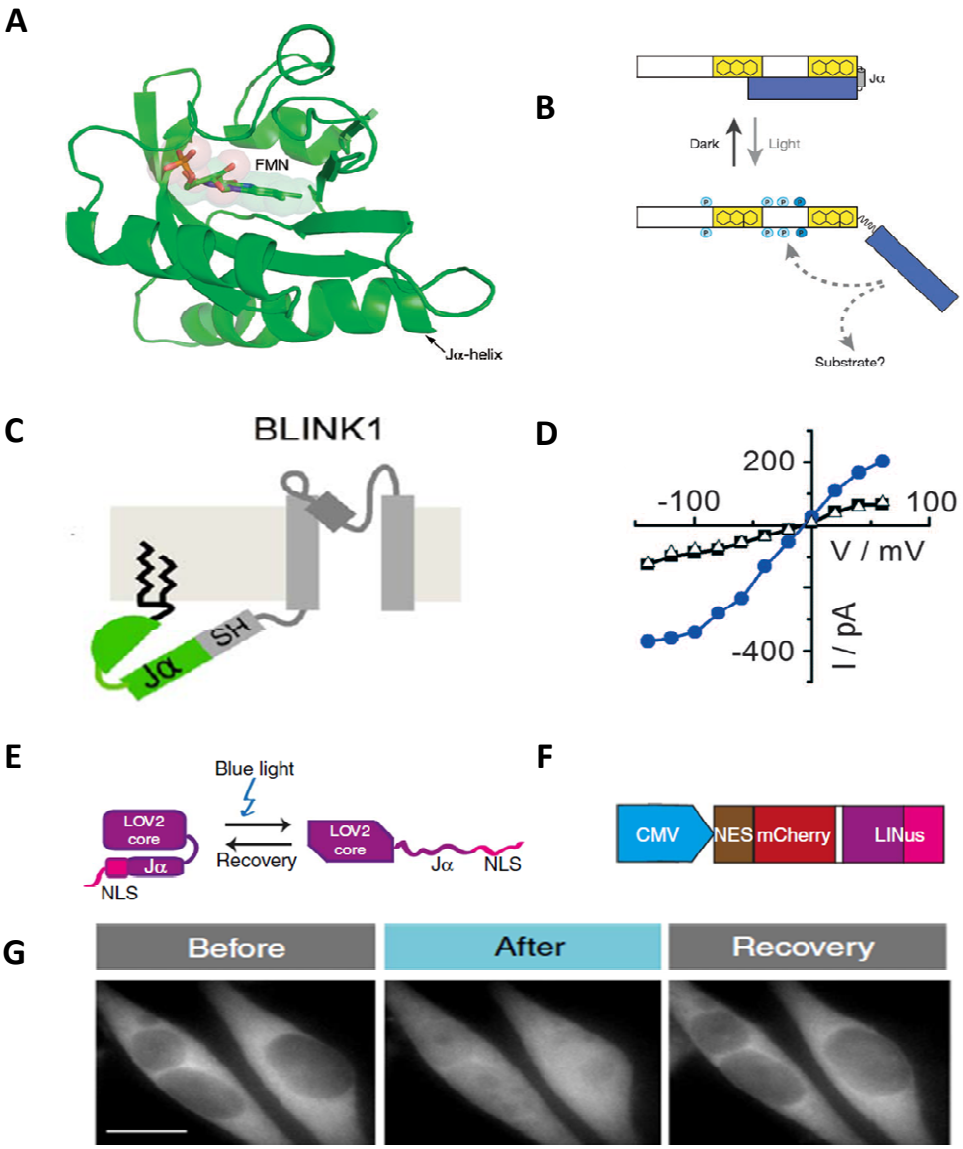

Fig 1.4 New synthetic LOV2-based proteins for optogenetics. (A) Structure of LOV2 domain of phototropin 1 (Christie, 2007). (B) The unfolding of the Jα helix leads to the activation of the effector domain of the phototropin 1 (Christie, 2007). (C) Schematic representation of BLINK1, a synthetic light-gated potassium channel in which the LOV2 domain is fused to the N terminus of the potassium channel Kcv (Cosentino et al., 2015). (D) I/V curves obtained from HEK293T cells expressing BLINK1 in the dark (black squares), after irradiation with blue light (blue dots) and after dark recovery (empty triangles) (Cosentino et al., 2015). (E) Cartoon representing how, upon light irradiation, the NSL is exposed to cytoplasm in LInuS (Niopek et al., 2014). (F) The fusion protein LINuS (Niopek et al., 2014). (G) Reversible nuclear migration of LINuS in response to blue light can be observed by monitoring the mCherry fluorescence (Niopek et al., 2014).

3.2 The HCN channel family and the role of HCN4 in sinoatrial node cells.

Hyperpolarization-activated cyclic nucleotide gated channels (HCN1-4) are a family of ion channels, which are expressed both in the brain and in the heart. They are voltage dependent and open upon hyperpolarization of the plasma membrane; at depolarized voltages they are closed. In addition to a regulation by voltage, the activity of these channels is also modulated by the binding of the second messenger cAMP to a cytosolic binding domain (Biel et al., 2009). With respect to their regulation HCN channels share therefore characteristics with both voltage-gated and ligand-gated channels. A peculiar feature of HCN channels is that they are, different from K^+ channels with the same architecture, not strictly K^+ selective. This means that not only K^+ is permeating the pore, but also Na^+ (Santoro and Tibbs, 1999; Biel et al., 2009). The selectivity ratio is approximately 3:1 meaning that for three K^+ ions one Na^+ is on average transported by these channels.

The currents mediated by HCN channels were first discovered in the heart and immediately attracted the attention of physiologists because of their peculiarities in gating and selectivity. Different from all other channels known at this time, HCN channels were activated by hyperpolarization while all other voltage gated channels were activated by depolarization (Brown et al., 1979). As mentioned before the current carried by these channels was not selective for K^+ alone but a mix of both K^+ and Na^+ (DiFrancesco et al., 1986). For these reasons the current was named “funny” current (I_f) in the first place although now is often called I_h (Barbuti and DiFrancesco, 2008). Later, an hyperpolarization activated current, named I_h, was measured also in neurons (Pape, 1996) and the genes of the HCN isoforms began to be identified at the end of the nineties (Ludwig et al., 1998; Ludwig et al., 1999; Santoro et al., 1997; Santoro et al., 1998; Vaccari et al., 1999).

Recently the structure of HCN1 was solved by high resolution cryoEM. Hence new information and possible explanations for the particular behavior of these channels are now available (Lee and MacKinnon, 2017). From the structural data it becomes evident that HCN channels share some features with voltage gated K^+ channels (Kv). The channel is composed of four subunits and each of them presents three modules: the voltage sensor domain (VSD), the pore module and a cyclic nucleotide–binding domain (CNBD) (Fig. 3.5). The latter is connected to the pore module via the so-called C-linker region, which is protruding into the cytoplasm. The four subunits are organized to form a central pore surrounded by the four VSDs, as in Kv channels (Fig. 3.6; Lee and MacKinnon, 2017).

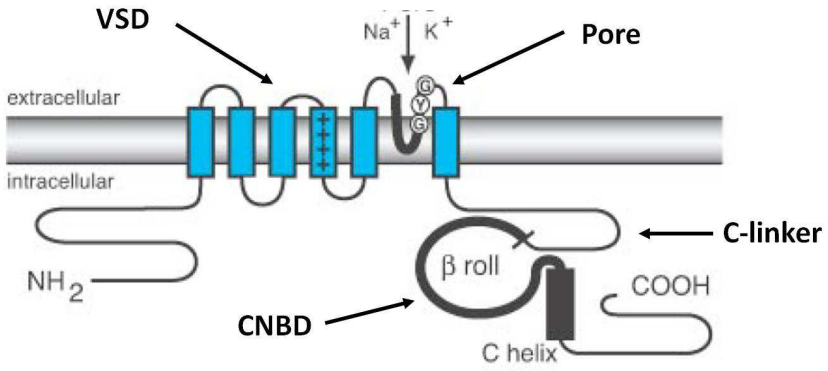

Fig. 3.5 HCN channel subunits. General structure of one HCN subunit (Robinson and Siegelbaum 2003).

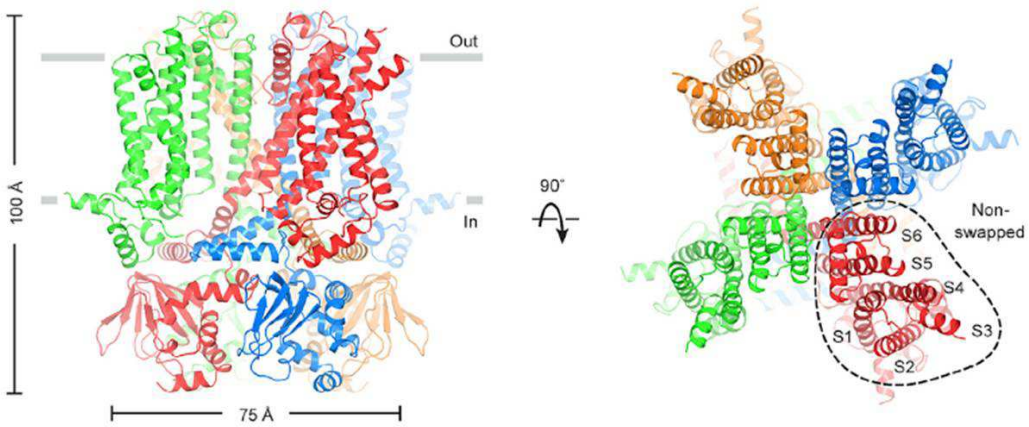

Fig. 3.6. Structure of an HCN channel. Spatial organization of the four subunits to form a functional HCN1 channel. HCN1 present a central pore surrounded by four VSDs. The C-linker and the CNB are in the cytoplasm underneath the pore (Lee and MacKinnon, 2017).

Pore opening in HCN channels is regulated by the four VSDs, each of them composed of four transmembrane helices (S1-S4) as in channels of the Kv family. In the latter channels the S4 segment contains positively charged residues, known as gating charges. Their position in the membrane is strongly affected by the polarity of the transmembrane electric field (Larrson et al., 1996; Börjesson et al., 2008; Bezanilla 2008). During depolarization, the S4 segment undergoes a combined movement of rotation, tilt and vertical translation toward the extracellular side of the membrane: this conformational change in the VSD controls the gating of the pore (Long et al., 2005; Blunk and Batulan, 2012). Interestingly, in HCN channels the voltage sensor has an S4 segment with positive charges as well. Early studies about S4 movement were done using an HCN channel from sea urchin and suggested that the vertical translation of this segment was conserved in HCN channels (Männikko et al., 2002). However, later studies showed that for human HCN channels the mechanism seems to be more complicated (Vemana et al., 2004; Bell et al., 2004; Gross et al., 2018). These studies pointed out that a lateral displacement of S4, rather than a vertical movement, seems to be of central importance in HCN voltage sensing, which may be modulated by a rearrangement of the TMDs surrounding the S4 domain (Bell et al., 2004; Gross et al., 2018) . Moreover,

the S4 segment in HCN channels is longer than that of Kv channels and it extends in the cytoplasm (Fig. 3.7 A; Lee and MacKinnon, 2017). It has been proposed that this extraordinary length of the S4 helix allows an interaction between the C-linker and the so-called S4-S5 linker, which connects the S4 to the S5 helix (Lee and MacKinnon, 2017; Gross et al., 2018). This interaction, when the S4 helix is in the "depolarized position", may stabilize the closed state of the pore and may be involved in cAMP effect on the voltage dependence.

The voltage sensor is directly connected to the pore via the so-called S4-S5 linker, consisting of few amino acids (Lee and MacKinnon, 2017). The pore module is made of two transmembrane helices (S5 and S6) separated by the pore helix and the selectivity filter. It has already been mentioned that HCN channels allow the permeation of both K^+ and Na^+ with a permeability ratio *P*Na:*P*K of about 1:3 (Santoro and Tibbs, 1999). Surprisingly, HCN channels contain the same essential amino acids that are required to form the K^+ selectivity filter in highly selective K^+ channels (Biel et al., 2009). The structure of the HCN1 obtained by Lee and MacKinnon in 2017 is now able to explain the low K+ selectivity of HCN channels. It shows that the first two amino acids of the selectivity filter have a different orientation compared to that of canonical potassium channels (Lee and MacKinnon, 2017). As a consequence, the outer half of the selectivity filter appears to be dilated. In K^+ selective channels this part of the filter contains two of the four binding sites that coordinates the entrance of K+ ions. The presence of four sites in selective K+ channels allows two K^+ ions to bind simultaneously (Zhou et al., 2001). The outer part of the filter in HCN1 in contrast is much wider so that sites 1 and 2 are absent (Fig. 3.7 B). Lee and MacKinnon hypothesized that "a filter in which only a single ion can bind, even if the binding is thermodynamically favorable for K^+ over Na^+, will not exhibit strong kinetic selectivity because an entering Na^+ ion, which will only reside very briefly, will rapidly exit to either side (i.e., it can permeate)" (Lee and MacKinnon, 2017). On the contrary, in K^+ selective channels a multi-K^+-ion occupancy in the filter can augment the probability of Na^+ exiting from the same side that it entered. The latter is favored by a K^+ ion hindering the transition into the other direction. Given the particular nature of this selectivity filter architecture in HCN1, channel opening at the resting membrane potentials of neurons or cardiomyocytes will result in an inward current, which depolarizes the membrane. This depolarization brings the voltage to the threshold for activation of an action potential. The importance of this depolarization is explained in details in the next paragraphs.

As mentioned previously the pore is connected, at its C-terminal end, to the regulatory domain CNBD. This ligand binding domain includes α-helices (A, P, B, C, D and E) and a β-roll between the A and B helices (Zagotta et al., 2004; Lolicato et al., 2011; Saponaro et al., 2014; Lee and MacKinnon 2017). The latter also contains the so-called phosphate binding cassette, which forms the cAMP binding pocket. cAMP binding to this site causes major spatial reorientation of the helical components of the CNBD; in particular, the B and C helices move toward the core of the CNBD (Fig. 3.7 C, Saponaro et al., 2014; Lee and MacKinnon 2017). This

movement is propagated to the C-linker region, which connects the CNBD to the S6 helix of the pore (Gross et al. 2018). The final effect of cAMP binding is an acceleration of the activation kinetics of the channel concomitant with a positive shift of the voltage dependency of activation. As a consequence the channel opens, in the presence of high concentrations of this cyclic nucleotide, at less hyperpolarized voltages (Fig. 3.7 D). Important to note here is that the binding of the cyclic nucleotide to the CNBD is not sufficient for channel opening. The primary stimulus for channel opening is provided by negative membrane voltage. Binding of the ligand to the CNBD is only modulating in an allosteric manner the effect of membrane voltage on the channel. Binding of cAMP to the CNBD is in this scenario effectively lowering the energy barrier for channel activation by negative voltage.

When Lee and MacKinnon presented the structure of HCN1, they pointed out that the N-terminal part of the protein is organized in a 3-α-helical domain (called HCN domain). This domain forms a contact with both, the S4 helix of the same subunits and the CNBD of a neighbor subunit (Lee and MacKinnon, 2017). Since the HCN domain is in contact with both regulatory elements of the channel, e.g. the voltage sensor and the ligand binding domain, it may have a key role in the dual regulation of HNC channel gating.

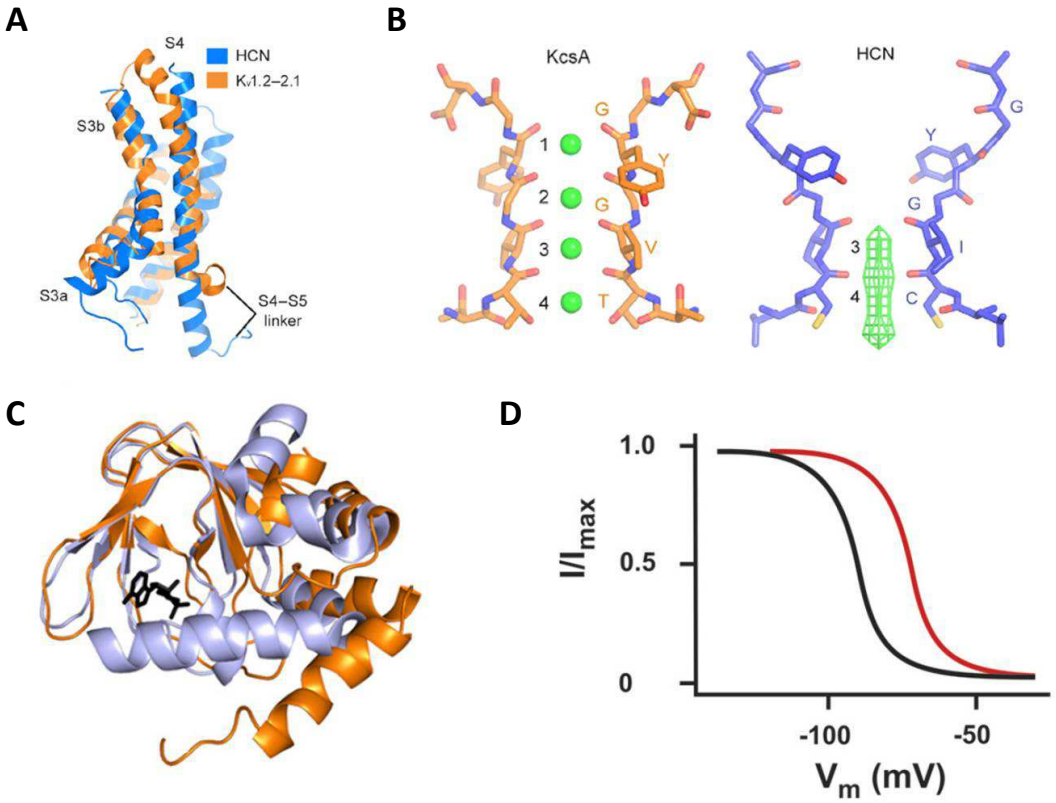

Fig. 3.7 Unique features of HCN channels. (A) HCN channels display a gating behavior opposite of that observed in other voltage dependent K^+ channels. This may be due to the length of the S4 segment: this helix is longer in HCN (blue) compared to that of Kv channels (orange) (Lee and MacKinnon, 2017). (B) Comparison between the structure of the selectivity filter in HCN1 and in KcsA, a well known and characterized potassium channel (Lee and MacKinnon, 2017). (C) The binding of cAMP to the CNB causes the conformational reorientation of the helical parts, that are evident when comparing the structures of the unbound (orange) and bound (violet) state (Saponaro et al., 2014). (D) cAMP effect on the voltage dependency of the channel: the opening is shifted to less negative voltages as shown in this illustration by Biel et al. (2009).

The present work focuses on one member of the HCN family namely the HCN4 isoform. This channel plays a key role in the generation and the regulation of the spontaneous electrical activity of the heart. HCN4 is indeed the HCN isoform, which is most highly expressed in the sinoatrial node (SAN), the natural pacemaker of the heart (Shi et al.,1998; Difrancesco 2010; Baruscotti et al.,2010). Therefore HCN4 provides the main contribution to the I_f current and in this way to the autonomous pace making of the SAN. SAN cells display a spontaneous and rythmic electrical activity, which means that they are able to fire continuously action potentials, without the requirement of any excitatory input from the nerves. The electrical signals generated in the SAN propagate through the whole heart causing the rhythmical contraction of the cardiac muscular tissue and, therefore, the beating of the heart.

The spontaneous firing of the SAN is possible thanks to the peculiar characteristics of the HCN channels, which were described in the previous paragraphs: the opening at hyperpolarized voltages and the ability to conduct both Na^+ and K^+. The mechanism was first proposed in the seventies and eighties of the last century on the basis of several experimental observation (reviewed in DiFrancesco 2010). It was observed that an action potential depolarizes at its peak up to +30 mV before returning back to negative voltages (repolarization) by the opening of K^+ channels. This repolarization phase causes the membrane voltage to hyperpolarize up to -60 mV, a voltage at which the HCN channels start to open. The opening of the HCN channels at negative voltages results, because of the electrochemical gradient existing across the membrane, in the depolarizing current I_f. As a consequence the membrane potential slowly depolarizes, a phenomenon known as slow diastolic depolarization (SDD). The SDD brings the voltage to the threshold for the subsequent action potential (Fig. 3.8). Thanks to the unique biophysical properties of HCN channels, the SAN cells are able to continuously generate firing: the last phase of an action potential triggers the mechanism that leads to the activation of another one.

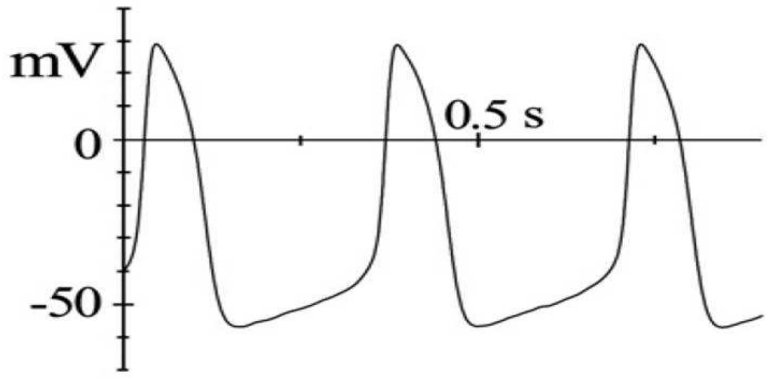

Fig. 3.8 Spontaneous generation of action potential in SAN cells. Membrane voltage recording of a SAN cell. The SDD brings the potential from about -60 mV to the threshold for the activation of a subsequent action potential (Baruscotti et al., 2010).

As previously mentioned, the voltage dependency of the channel is shifted to positive voltages following cAMP binding. The degree of the shift along the voltage axis is in this case a function of the cAMP concentration (DiFrancesco and Tortora, 1991). This mechanism allows a fine tuning of the I_f current by physiological changes in the concentration of this second messenger in the cytoplasm. As a result of this tuning of HCN4 activity in SAN cells, the timing and the duration of the SDD is modulated by the cAMP concentration. The latter, in SAN cells, increases and decreases after beta-adrenergic and cholinergic stimulation, respectively (Sicchitano et al., 2012). The adrenergic and muscarinic receptors are in this scenario the initiators of pathways, which eventually affect the concentration of cAMP and therefore the opening of HCN4 channels (Barbuti and DiFrancesco, 2008). An increase of the intracellular concentration, of cAMP as output of a signal cascade, will in this way augment opening of the channel already at less negative voltages. This in turn affects the activation of theSDD, causing a faster frequency of the firing (Di Francesco, 1993; Biel et al.,2009). Fig. 3.9 illustrates the dependency of heart rate on cAMP concentration. An elevation of cAMP concentration due to the presence of Isoprenaline, causes a decrease in the time interval between two action potentials resulting in an acceleration of the heart beat. The reverse occurs when the cAMP level decreases in response to Acetylcholine stimulation. Thanks to its dual gating regulation by hyperpolarization and ligand binding, the HCN4 channel not only has the ability to elicit spontaneous auto-rhythmic activity, but it is also the final effector of the mechanism that determinates the beating frequency. This is the reason why the I_f current is also often called “pacemaker current”.

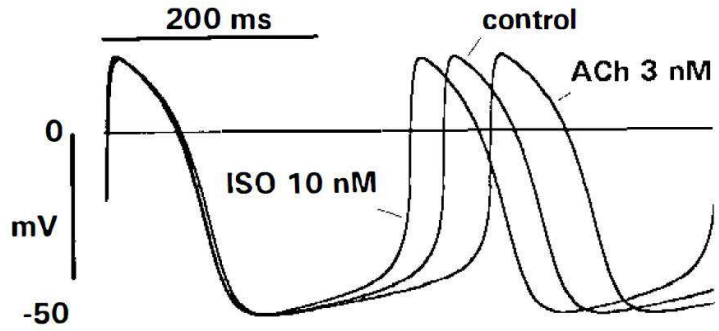

Fig. 3.9 Pacemaking regulation. The slope, and therefore the duration, of the SDD is influenced by opposite types of stimulation: in the present example treatment with 10 nM isoprenaline and 3nM acetylcholine (DiFrancesco, 1993). The steepness of the SDD is a reflection of the modulation on intracellular concentration of cAMP, which can influence the opening of the HCN channels.

In 2014 Lolicato and colleagues discovered a new and unexpected property of the HCN4: the response of the channel to cAMP can be counteracted, in an isoform specific manner, by cyclic di-nucleotides (Lolicato et al., 2014). In the latter study the HCN4 channel was crystalized in complex with cGMP. This cyclic nucleotide is also known to bind like cAMP the CNBD and affect pace making in the heart. Surprisingly, by analyzing the crystal structure, Lolicato and co-workers found a second binding site for cGMP (Lolicato et al.

2014). This binding site in the C-linker was called C-linker poket (CLP). The CLP is located between the second and the third helices of the C-linker, a region important for the propagation of conformational changes between the CNBD and the pore (Fig.3.10 A) (Gross et al. 2018). Further scrutiny of the structural data suggested that the pocket might be wide enough to bind a molecule about twice the size of cGMP. For this reason and supported by docking studies, the authors of this study tested, whether c-di-GMP or other cyclic di-nucleotides could bind the CLP and affect channel opening.

For this purpose, they measured HCN4 activity in patch clamp recordings in HEK293 cells in presence and absence of 100 uM c-di-GMP, c-di-AMP and cGAMP in the recording pipette. The electrophysiological assay revealed that the cyclic di-nucleotides had by itself no effect on the voltage dependency of the HCN4 channel. However when the measurements were repeated in presence of saturating concentration of cAMP (delivered via pipette as well) they found that cyclic di-nucleotides completely reversed the positive shift of the HCN4 activation curve. Only when cAMP was added to the pipette solution alone they observed the expected right shift; a co-presence of cAMP and cyclic di-nucleotides completely suppressed the positive shift of cAMP (Fig. 3.10 B). Control experiments confirmed the view that this effect was due to the specific binding of cyclic di-nucleotides to the newly discovered binding site. Mutations of amino acids, which were presumably involved in the binding of cyclic di-nucleotides to the respective site, eliminated the effect of these molecules. To test whether this antagonistic action of cyclic di-nucleotides on cAMP regulation of the HCN4 channel could affect a key physiological function of the channel such as peacemaking, the authors recorded the membrane potential of SAN cardiomyocites. Consistent with the effect of cyclic di-nucleotides on the HCN4 activation curve, the presence of cyclic di-nucleotides (in this case cGAMP) in the recording pipette caused a decrease in the spontaneous firing rate of SAN cells (Fig. 3.10 C). Binding to CLP seems to prevent β-adrenergic stimulation on the I_f current, mimicking the physiological effect of acetylcholine. Since the newly discovered CLP is located in a region of the channel that connects the CNBD and the pore it was hypothesized that ligand binding to the CLP may hamper the transmission of the conformational change from the CNBD to the pore.

Cyclic di-nucleotides are small molecule commonly used as second messenger in bacteria. The only second messenger present in mammals is the cGAMP, which is synthesized only in cells of the immune system in response to exogenous DNA in the cytoplasm. C-di-GMP is not present at all in mammals and, in particular, in humans. Therefore it is tempting to exploit this system in an orthogonal pathway for regulating HCN4. In this work I tried to establish a system with a light regulated di-guanylate cyclases from bacteria, which might be used as a tool for a remote control of HCN4 channel activity and hence heart rate.

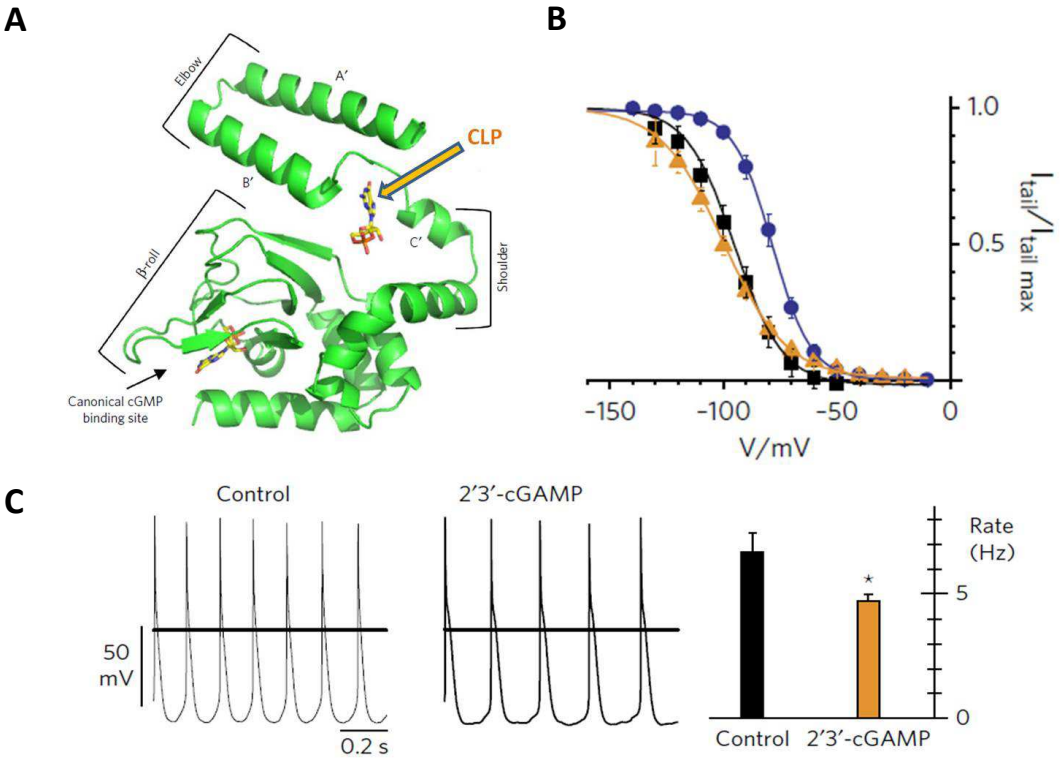

Fig. 3.10 The HCN4 channel is regulated by cyclic di-nucleotides. (A) The CLP found by Lolicato and colleagues is located between the so-called elbow and shoulder of the C-linker domain in HCN4. (B) The graph are reports three activation curves which describe the dependency of the channel open probability and voltage. Activation curves were measured in different conditions: recording pipette filled with standard intracellular solution (black squares); intracellular solution + 15 uM cAMP (Blue circles); intracellular solution + 15 uM cAMP + 100 uM c-di-GMP (orange triangle). (C) Recordings of the membrane potential in SAN cells in absence (left) or presence (right) of 100 uM cGAMP in the recording pipette. The rate observed in each condition is reported in the small graph. Data from Lolicato et al., 2014.

3.3 A photo-regulated diguanylate cyclase.

Cyclic di-nucleotides have emerged as important second messengers in bacteria, where these molecules regulate many important cellular processes in response to diverse extracellular cues (Fig. 3.11 A, Kalia et al., 2013). Among them, c-di-GMP, a universal bacterial second messenger, was first described in 1987 by Ross and colleagues as a cofactor of cellulose synthase (Ross et al., 1987). In the subsequent years it occurred that c-di-GMP is an ubiquitous signaling molecule synthesized from two GTP and is involved in cellular processes such as biofilm formation, motility, virulence, the cell cycle, differentiation (Romling et al., 2013).

The final intracellular concentration of c-di-GMP is determined by the antagonistic action of the diguanylate cyclase (DGC) and phosphodiesterase (PDE) enzymes, which are responsible for the synthesis and the breakdown of this second messenger (Romling and Galperin, 2017). There are two types of enzymatic domains that display DGC or PDE activity, respectively: the GGDEF domain and the EAL domain (Fig. 3.11 B; Jenal et al., 2017; D'Argenio and Miller, 2004). The GGDEF and EAL domains are often found on the same polypeptide chain as parts of multi-domain proteins: about one third of all GGDEF domains and two thirds of all EAL domains are found in the same proteins (as reviewed in Romling et al., 2013). Most of these proteins containing a GGDEF-EAL tandem are not bifunctional and have therefore either DGC or PDE activity. In this type of proteins one of the two domains is not functional and has a different function, like in the CC3396 from *Caulobacter crescentus* (Christen et al., 2005). In this protein the GGDEF domain has no cyclase activity but instead binds GTP and in response activates the EAL domain.

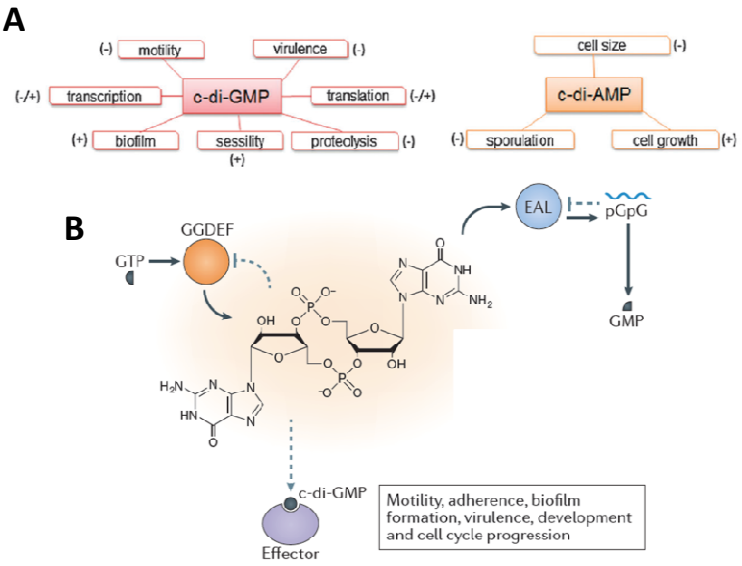

Fig. 3.11 Cyclic di-nucleotides are bacterial second messengers. (A) c-di-GMP and c-di-AMP are involved in many cellular pathways that modulate important cellular events like translation, biofilm formation, growth etc. (Kalia et al., 2013). (B) The cellular concentration of c-di-GMP is regulated by the antagonist action of GGDEF and EAL domains (Jenal et al., 2017).

One GGDEF-EAL domain tandem has been found also in a bacterial phytochrome, where it acts as the effector domain of the light sensitive protein (Tarutina et al., 2006). Bacterial phytochromes are a family of homodimeric photo-receptors that use biliverdin as a chromophore. Each subunit consists of a "photo-switch" module and an output "effector" domain, that is typically a histidine kinase (Rockwell and Lagarias, 2010). The photo-switch module is composed of three conserved domains: the PAS (Per-ARNT-Sim repeats), the GAF (cGMP phosphodiesterase/adenylate cyclase/FhlA transcriptional activator), and the PHY (phytochrome-specific) domains (Aldridge and Forest, 2011). The biliverdin is located in the chromophore-binding pocket of the GAF domain and it forms a thioether bond with a conserved Cys in the neighboring PAS domain (Wagner et al., 2005). A scheme of the domain organization of each monomer is reported in Fig. 3.12 A. The C-terminal helix of the GAS domain is continuous with the first helix of the PHY domain, so a single long helix runs the length of the photosensory core and the PAS, GAF, and PHY domains are arrayed along it (Aldridge and Forest, 2011, Piatkevich et al., 2013, Takala et al., 2014). The PHY domain has a 49 amino acids-long extension, called tongue, that reaches and contacts the cromophore-binding poket in the GAF domain (Takala et al., 2014). In the dark the BV is the cis form, that absorbs light at 670-700 nm; when irradiated with red light in this range of wavelengths, it converts into the trans form (Fig. 3.12 B, Piatkevich et al., 2013).

In 2014 Takala and co-workers solved the structure of a bacterial phytochrome from *Deinococcus radiodurans* in the resting and activated states (Fig. 3.12 C, Takala et al., 2014). They observed that in the dark the monomers are fairly close to each other, while in the activated state the dimer adopts an open Y-like shape of the PHY domains, which move apart by circa 3nm. They also found out that the transition of biliverdin into the trans form has an effect on the folding of the tongue, which changes its secondary structure from a β-sheet to an α-helix. As a result, the tongue is shortened and the distance between the GAF and PHY domain is reduced. As a consequence of this, the dimer opens up between the PHY domains.

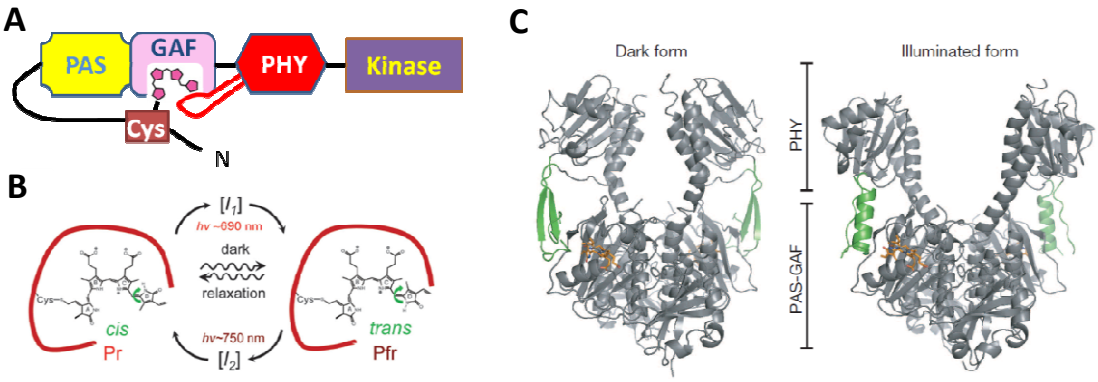

Fig. 3.12 Bacterial phytochrome photosensors. (A) Schematic representation of a bacterial phytochrome monomer with its domains. (B) Photo-cycle of the biliverdin (Piatkevich et al., 2013). The chromophore in the cis form (also called Pr) has the absorption peak at 690 nm, while the trans form (Pfr) absorbs light at 750 nm. Irradiation with red light at 750 nm causes a fast recovery to the cis form. (C) Structure of a phytochrome from *Deinococcus radiodurans*; the tongue is colored in green (Takala et al., 2014).

As mentioned above, in 2006 Tarutina and colleagues discovered that a phytochrome in *Rhodobacter sphaeroides*, named BphG1, has a GGDEF-EAL tandem as output domains (Tarutina et al., 2006). This phytochrome has a canonical PAS-GAF-PHY photo-switch, that is connected to GGDEF and EAL domains (Fig. 3.13 A). To understand the function of this unusual phytochrome, they added a His tag to the C terminus for purification and performed *in vitro* biochemical characterization after over-expressing the protein in *E. coli*. The *E. coli* strain they used for this purification expressed also heme oxigenase and therefore synthesized biliverdin as well. When they purified the protein, they observed a small amount of monomer, a presumed tetramer and other bigger oligomers. They found out that the whole protein BphG1 had the typical photochemical properties of bacterial phytochromes: it was binding biliverdin and displayed absorption-emission peaks of these photoreceptors. This protein exhibited PDE activity but, surprisingly for a phytochrome, this activity was not light regulated (Fig. 3.13 A). They noticed that, together with BphG1, another small protein was co-purified. This small protein turned out to be a dimer of EAL domains, which had PDE activity as well (Fig. 3.13 B). They concluded that BphG could undergo a partial cleavage in *E. coli* and so they decided to characterize the remainder of the protein, i.e the PAS-GAF-PHY-GGDEF. Since the His tag was at the C terminus of the EAL domain, to purify this fragment they added a C-terminal tag to it. When they tested the enzymatic activity of this fragment they discovered that it worked as a light regulated diguanylate cyclase (Fig. 3.13 B). With these experiments Tarutina and colleagues showed that not only kinases but also other functional domains, can serve as output modules for phytochromes and that BphG1 is a bifunctional protein with both c-di-GMP synthesis and hydrolysis function. Moreover, when BphG1 undergoes partial cleavage, the truncated protein (that they began to call BphG) is able to synthesize the cyclic di-nucleotide in a light dependent manner.

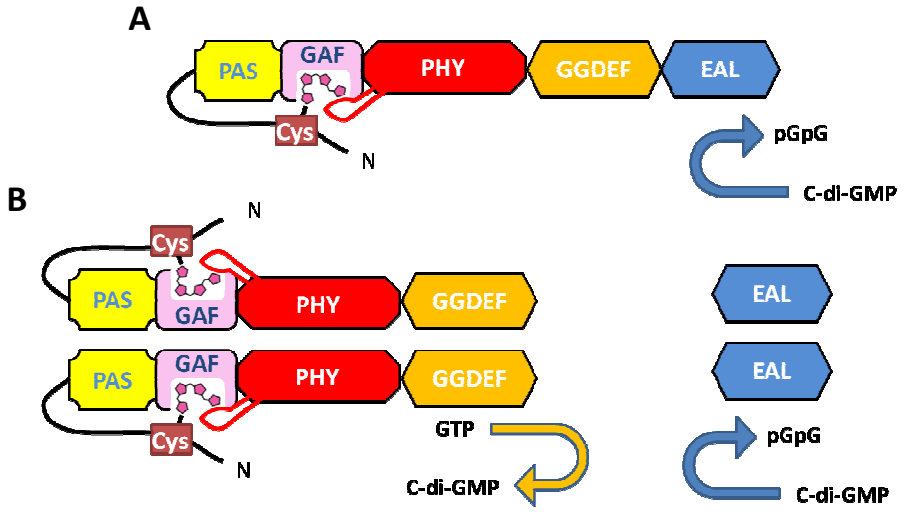

Fig.3.13 The BphG1 phytochrome. (A) The BphG1 protein is a bacterial phytochrome, with the typical photo-switch module, to which are connected a GGDEF domain and an EAL domain. The entire protein showed a light-independent PDE activity. (B) BphG1 undergoes cleavage to obtain two distinct proteins: EAL dimmers with PDE activity and a light-regulated DGC. (modified from Tarutina et al., 2006: colors have been changed to match those used in subsequent publications from the same group).

Some years later, the same group had the idea to use BphG for developing an optogentic tool, which is able to synthesize the second messenger c-di-GMP in a light dependent manner (Ryu et al., 2014). They monitored the production of c-di-GMP in *vivo* in *E. Coli* cells and found that the activity of the protein was very poor. The intracellular concentration of the second messenger was indeed incompatible with the activation of many c-di-GMP dependent processes. To improve the cyclase activity, they substituted the GGDEF domain of BphG with the GGDEF domain of a more active DGC from *Synechocystis sp.* called Slr1143: this Chimeric protein was called BphS1. Upon irradiation with red light, the BphS1 construct showed a circa 2.5-fold higher DGC activity compared to BphG. To further improve the cyclase activity of the chimera, they introduced a mutation in the conserved RXXD sequence motif located in the GGDEF domain of Slr1143. This motif is involved in a feedback inhibition mechanism of DGC activity. They introduced the mutation R587A (R250 of Slr1143) and eliminated the feedback inhibition system. A schematic representation of this protein assemble is reported in Fig. 3.14 A. The mutated construct (named BphS) turned out to have a DGC activity in the light that was circa 2.2-fold higher than that of BphS1 and~5.5-fold higher compared to the original BphG. This modification hence resulted in an improvement of the DGC activity but, at the same time, caused also an unwanted increase in the dark activity of the protein. To circumvent this problem they co-expressed a constitutive PDE, which should maintain low levels of c-di-GMP in the dark: YhjH (Fig. 3.14 B).

The expression of YhjH needed to be adjusted to achieve degradation of the cyclic di-nucleotide in the dark without affecting (or affecting only minimally) the c-di-GMP synthesis in the light. To do this, they prepared different plasmids in which they inserted, upstream of YhjH, different ribosome binding sites (RBSs). They expressed the plasmid in *E. coli* cells and checked their motility. It was indeed known that c-di-GMP can bind a specific receptor that hampers the activity of the flagellum rotor. With this functional assay they were able to select the RBS, which offers the biggest difference in motility between light and dark (Fig. 3.14 C). To further verify that the co-expression of BphS and YhjH can be used to photo-modulate cellular phenomena, they tested the ability of the system to activate a c-di-GMP-dependent expression system. They were able to obtain a light-dependent expression of *lacZ*, monitored with the color of the colonies.

In further experiments the combined BphS-YhjH system could be used to increase the intracellular concentration of c-di-GMP in response to far red light and therefore to photo-modulate pathways activated by this second messenger. The construct has two important features. 1. It responds to red light e.g. a light that is able to penetrate tissues more deeply than blue or yellow light. 2. As mentioned in previous paragraphs, cyclic di-nucleotides are second messengers in bacteria, not in mammals. In humans, cGAMP can be found only in cells of the immune system under certain conditions, i.e. activation of the immune response, while c-di-GMP is totally absent in human cells. Since the bacterial and human system are orthogonal the c-di-GMP concentration in human cells can be manipulated without altering other

physiological signaling pathways, i.e. cascades which are activated by endogenous mammalian second messengers like cAMP. One target for the light-dependently produced c-di-GMP could be the HCN4 channel, as it can be directly regulated by cyclic di-nucleotides. The aim of this work was to examine the possibility of using the bacterial cyclases described in the previous paragraph to photo-modulate channel gating of HCN4 and as a result the pacemaker current I_f in the sinoadrinal node.

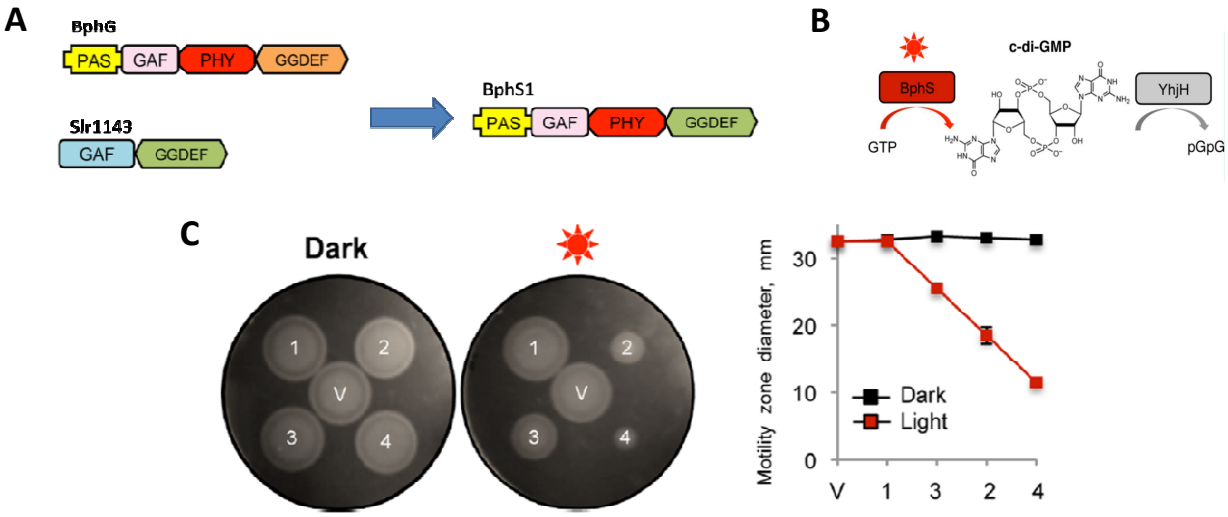

Fig 3.14 The synthetic BphS construct. (A) Construction of the Chimeric protein BphS by fusing BphG and Slr1143. (B) The dual regulation of c-di-GMP levels by BphS and YhjH. (C) Light regulation of c-di-GMP production reflects on the different motility in light and dark of bacterial cells expressing BphS and YhjH. The numbers indicates the different RBSs used. V indicates cells transformed with an empty vector.

3.4 Aim of the thesis

The current progress in optogenetics underscores that the regulation of cellular events with light is very useful for research and applications in many areas of biology. This has stimulated the development of new optogenetic tools in the past years. With the present project we wanted to examine the possibility of designing a potential new optogenetic tool for a remote regulation of the HCN4 channel by light. This channel is crucially involved in the generation of the spontaneous electrical activity in the pacemaker cells of the sinus node and its activity determines the frequency of the heart beat. Like in the case of all HCN channels also the gating of HCN4 is dually controlled by voltage and cAMP. The channel is activated by hyperpolarization and this voltage dependence is further modulated by cAMP. This second messenger binds the C-terminal domain of the channel in the cytoplasm, causing a positive shift in the channel voltage dependency. Upon binding of cAMP, the channel opens at less depolarized voltages as the binding of the cyclic nucleotide stabilizes the open state of the pore. The consequence of this cAMP mediated alosteric regulation of HCN4 channels, in the sinol adrial node, is a fine tuning of the beating frequency of the heart. It has been demonstrated that also cyclic di-nucleotides can bind the HCN4 channel, in an isoform specific manner, in a binding side upstream of the cAMP binding site. The effect of cyclic di-nucleotide binding to HCN4 is to counteract the effect of cAMP on the channel voltage dependence. The present project is inspired by the idea that the gating of HCN4 channels and consequently the frequency of heart beat can be influenced via a modulation of cyclic di-nucleotides concentration in the sinus node .

Cyclic di-nucleotides are ubiquitous second messengers in bacteria, where they regulate many different pathways. Among the cyclic di-nucleotides, c-di-GMP is completely absent in human cells. This implies that the synthesis and degradation of this molecule, by specific cyclases and phosphodiesterases, should not affect physiological pathways of human cells, in which cAMP or cGMP are used as second messengers. The idea of creating a light regulated system is based on the finding of a bacterial phytochrome, which catalyses the synthesis of c-di-GMP in a far red light dependent manner. It is important to mention that such a red light based optogenetic tool would favor applications over those triggered by blue light, since the former is able to penetrate tissues more deeply.

Given the present state of the art, we decided to test if it is possible to regulate the gating of HCN4 channel by using bacterial di-guanylate cyclases. For this purpose we co-expressed these enzymes in human cells together with HCN4 and tested if they were able to produce sufficient c-di-GMP in a light depednent manner for affecting the voltage dependence of the channel. In the case that the light-activated enzyme is able to generate an appreciable amount of c-di-GMP, it should counteract the effect of cAMP on channel gating. By interfering with the cAMP dependent modulation of the funny current, this tool could be suitable to achieve a remote regulation of the heart rate.

4

RESULTS AND DISCUSSION

4.1 A bacterial cyclase can modulate the voltage dependency of HCN4 channels

I reasoned that the best strategy for the construction of a light-regulated modulation of HCN4 channel activity would be to start with the constitutively active diguanylate cyclase Slr1143 from the cyanobacterium *Synechocystis* sp. This protein was extensively described in the Introduction. The GGDEF domain of this protein is identical to the catalytic part of the light-activated construct BphS (Ryu and Gomelsky, 2014). By expressing Slr1143 in HEK293T cells and measuring HCN4 channel activity, I wanted to learn whether this protein is able to synthesize enough c-di-GMP to affect the voltage dependency of HCN4 channels. These experiments should also provide information on the time which is required between transfection and the first measurable effect of c-di-GMP on HCN4 channel gating. The Slr1143 DNA for these experiements was provided by the laboratory of prof. Gomelsky. The gene was inserted in a pCAG expression vector that included a GFP tag (P_{CAG}-GFP; P_{SV40}-Slr1143). As mentioned in Matherials and Methods, for this work it was used rabbit HCN4 DNA (RbHCN4) that was included into a pCI vector (P_{CMV}-RbHCN4). From now on I will refer to this channel and its DNA simply as HCN4. GFP DNA was required to monitor the expression of the channel in control cells, given the lack of fluorescent tag in the pCI vector. The GFP gene was contained in a pMAX plasmid (P_{CMV}-GFP). Both these two plasmids had been previously proved to be suitable for transfection and expression of GFP and HCN4 in HEK293T cells. The HEK293T cells were then transfected, as described in Materials and Methods, with 1 µg of HCN4 + 1µg of GFP (as control) and 1 µg of HCN4 + 1 µg of Slr1143.

After 20 hours the activity of the heterologously expressed HCN4 channel was monitored by patch-clamp measurements in the whole-cell mode. Voltage-clamp protocols were applied and the corresponding currents were recorded as detailed in Materials and Methods. In the last step of each clamp cycle, the voltage was clamped to -40 mV. This step elicits the typical tail currents of HCN4 channels with a distinctive kinetics (Fig. 4.1 A). The tail currents, which are recorded immediately after a test pulse (second segment of a cycle), are a measure for the open probabaility of the channel at the test pulses. A plot of the tail currents as a function of the preceding test pulse can be used for an analysis of the voltage dependency of this channel. The amplitude of a tail current depends, indeed, on the number of channels that are open when the current reaches its plateau during the second phase of each cycle. In the latter, the voltage increases of +15 mV in each cycle and it is impossible to understand if the correspondent increases in current amplitudes are due to higher channel opening or just to the increased driving force. Since tail currents are all recorded at the same voltage but strongly depend on the voltages applied in the second segments of the protocol, they offer a better possibility to describe the voltage dependency.

Normalized tail current amplitudes were plotted as a function of the preceding test voltage. The sigmoidal transition of the closed channel at positive voltages to the open channel at negative voltages can be fitted with the Boltzman equation (Equation 1):

$$(Eq.1)\quad Y = \frac{A_2 + (A_1 - A_2)}{1 + e^{\frac{x - x_0}{dx}}} + A_2$$

where A_1 is the maximal tail current amplitude, A_2 is the minimum tail current value, x is the test pulse voltage, x_0 is the half-activation voltage ($V_{1/2}$) and dx is the slope factor. In this way it is possible to describe the relationship between channel opening and voltage (Fig. 4.1 C).

Fig. 4.1 A shows an example for a measurement of HCN4 in a HEK293T cell under control condition, i.e. without co-expression of Slr1143. The cell exhibited the typical currents of this inward rectifying channel, in which hyperpolarizing voltages elicit a slow activating inward current. The kinetics of activation of HCN4, as in this case, is typically accelerated the more negative is the imposed the voltage. The steady state I/V relation of this recording showed that the channel is closed at positive voltages and only opens at voltages more negative than approximately -70 mV (Fig. 4.1 B). The tail currents are shown in Fig. 4.1 A and data for the activation curve were collected in the region marked by the red dashed lines. A plot of the normalized tail currents as a function of the test voltages exhibited the typical shape of the activation curve of this inward rectifier. It could be well fitted with the Boltzmann function yielding, in the present example, a value for $V_{1/2}$ of -110 ± 0.7 mV (Fig. 4.1 C). The slope factors and other parameters for this and the rest of the figures are reported in Additional Information. The same measurements were repeated with 12 other control cells giving a mean half-activation voltage of -107.7 ± 1.6 mV (Fig. 4.2). HCN channels are known to display an high variability in the $V_{1/2}$ values: for the same channel different kinetics and $V_{1/2}$ have been found by different laboratories (Biel et al., 2016; Biel et al., 2009). For this reason, every set of experiments includes control measurements; when changes in the $V_{1/2}$ are shown, they always refer to the actual controls from the same set of experiments.

The same measurements were repeated with cells co-expressing HCN4 and Slr1143. Fig. 4.1 A shows a representative recording from such a HEK293T cell. Scrutiny of the current responses showed that the currents were overall similar to those in control cells. But a closer inspection of the dynamics of activation indicated that co-expression of Slr1143 caused a slight slowdown of channel activation. The steady state I/V curve showed indeed that the channel began to open at more negative voltages compared to the controls: -90 mV in the reported example (Fig. 4.1 B). A plot of the tail currents indicated that the activation curve of the HCN4 channel is negatively shifted in the cell, which co-expresses the Slr1143 protein. In the present example the fit of the data with the Boltzmann function showed a 8 mV left shift compared to the control cells (Fig.4.1 C).

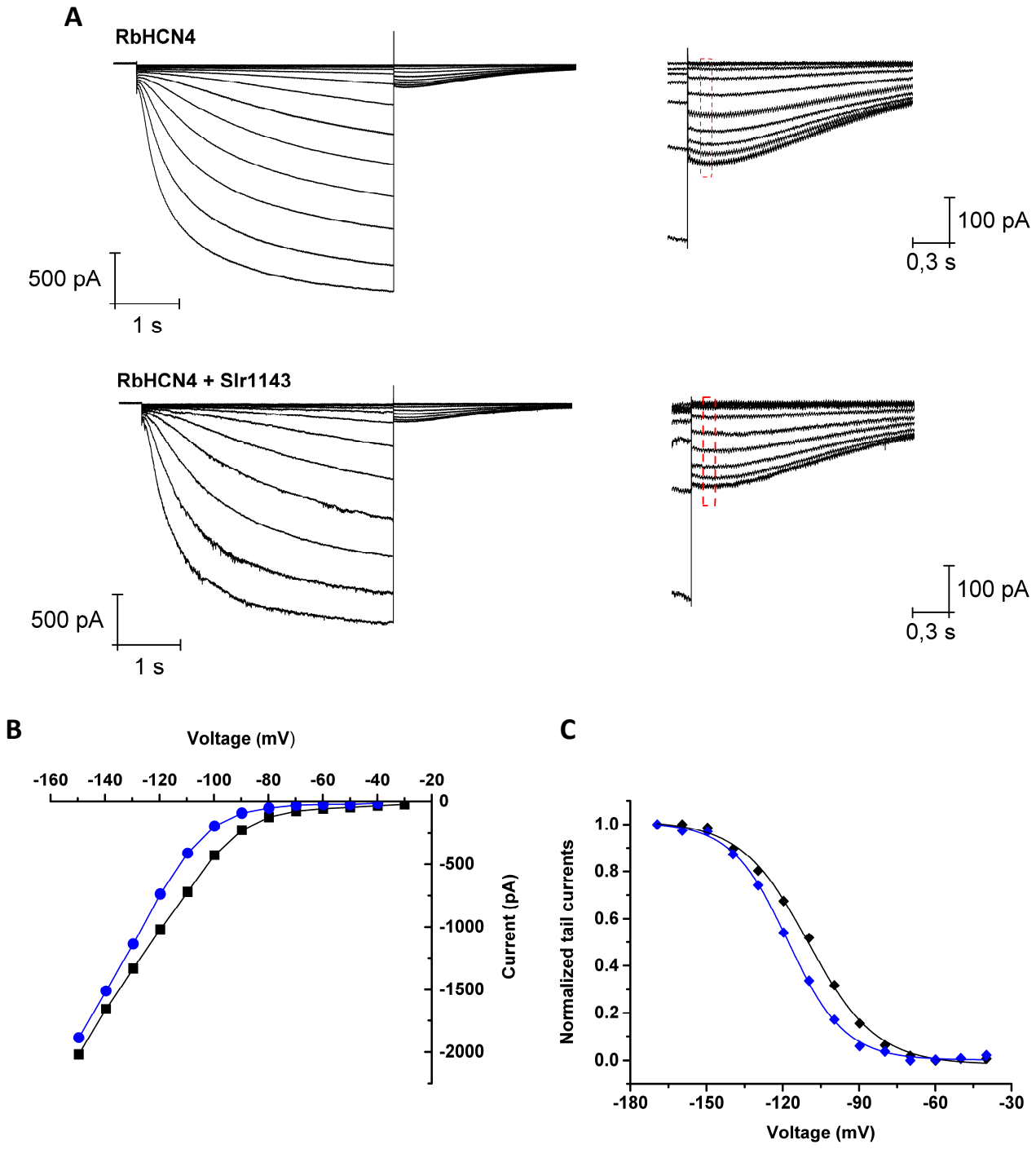

Figure 4.1 Co-expression of Slr1143 and HCN4 in HEK293T cells. (A) Exemplary current traces obtained by application of voltage protocols in control and Slr1143-expressing cells. Tail currents recorded at -40 mV of each current family are enlarged and reported on the right for each measurement. Amplitude values of the tail currents were taken in the region marked by the red dashed lines. (B) I/V curves from the measurements showed in (A), obtained by plotting the steady state current amplitudes as a function of the voltage. (C) Normalized tail current amplitudes plotted as a function of the preceding test voltage. Black dots: HCN4; Blue dots: HCN4 + Slr1143. Data points were fitted with the Boltzmann equation (equation 1). Color code for the fitting is the same used for the data points.

The same experiments were repeated in 25 other cells where it turned out that the $V_{1/2}$ values could be separated in two populations (Fig. 4.2). In 50% of the cells the $V_{1/2}$ value was identical to the control. In the other 50% of the cells co-trasfected with HCN4 and Slr1143 (N=13) the $V_{1/2}$ was -114.8 ± 0.9 mV. The comparison with control cells suggested that this negative shift, of about 7 mV, is related to the effect of the c-di-GMP on the endogenous cAMP binding to the CNBD. This result differed from what had been

observed by Lolicato and colleagues, which didn't see any effect of the c-di-GMP on the binding of basal level of cAMP to the CNBD (Lolicato et al., 2014).

To test the hypothesis that the synthesis of c-di-GMP affects the regulation of HCN4 by cAMP, the experiments in Fig. 4.1 were repeated by adding cAMP to the intracellualr solution (i.e. the pipette solution) at saturating concentration (15 µM). An analysis of the $V_{1/2}$ values from control cells showed that the presence of cAMP caused the expected right shift of the HCN4 activation curve (Fig. 4.2). The average $V_{1/2}$ of control cells was -93.5 ± 2 mV (N=4). This value is similar to the cAMP induced shift of the activation curve in other studies and supports the robustness of the measurements. In cells co-transfected with HCN4 + Slr1143 the average $V_{1/2}$ value was -95 ± 0.7 mV (N=6). The results of these experiments suggested that the enzyme was not synthesizing enough c-diGMP to counteract the effect of saturating concentrations of cAMP of the channel gating.

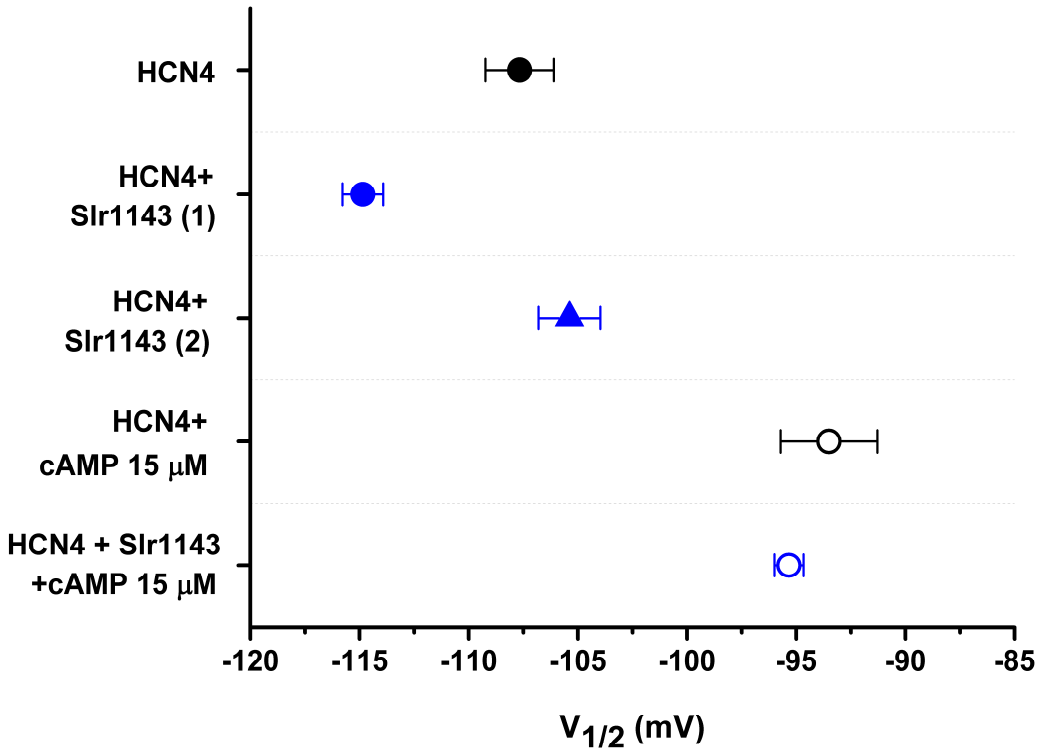

Fig. 4.2 $V_{1/2}$ values of control and Slr1143-expressing cells. Mean ± S.E. of the $V_{1/2}$ values of HEK293T cells expressing HCN4 or co-expressing HCN4 + Slr1143 in presence or absence of cAMP in the recording pipette. Black circle: HCN4 (N=13); Blue circle: HCN4 + Slr1143, shifted (N=13); Blue trangle: HCN4 + Slr1143, not shifted (N=12); Empty Black circle: HCN4 + 15uM cAMP (N=4); Empty blue circle: HCN4 + Slr1143 + 15uM cAMP (N=6).

The negative shift of the activation curve observed in cells expressing Slr1143 suggested that the c-di-GMP synthesized by Slr1143, could be potentially able to modulate the voltage dependency of HCN4. One mechanism by which it might do this is by interfering with the endogenous cAMP, which is present in the cells and affects channel gating. The fact that the expression of Slr1143 was however not able to counteract

saturating concentrations of cAMP, which were delivered via the pipette, might indicate that the enzyme was not synthesizing enough c-di-GMP to reverse the positive shift induced by this channel regulator when the concentration of the latter increased. This conclusion was consistent with the observation that the negative shift of the activation curve was only observed in 50% of the cells expressing Slr1143. It is reasonable to assume that the level of c-di-GMP synthesis was so low that it was only able to counteract the effect of the basal levels of cAMP on channel gating. In the light of these data we speculated that the activity of the Slr1143 enzyme was not as strong as it was expected to be.

An idea for improving the performance of Slr1143 came from the literature. When Ryu and Gomelsky developed BphS, they created a chimera by substituting the cyclase domain of the phytochrome BphG with Slr1143 (Ryu and Gomelsky, 2014). Although the first results were encouraging, they needed to further improve the c-di-GMP synthesis by introducing in Slr1143 a mutation known to augment the catalytic activity of the GGDEF domain. For this purpose they mutated the arginine in position 250 (587 in the whole BphS protein) into an alanine. Inspired by these data I decided to insert in Slr1143 the R250A mutation and, moreover, to move it under a CAG promoter. This operation should increase both the expression and the activity of the protein. I decided to move the construct in a plasmid that contained, in this order: a CAG promoter, the multiple cloning site and an IRES sequence followed by a TdTomato (P_{CAG}-IRES-Tdtomato) This pCAG plasmid was already available in the lab and successfully used for previous cloning by colleagues: for this reason was chosen to perform this cloning.

The mutated gene was transferred into the new plasmid with an enzyme-free cloning technique called AQUA cloning (detailed description in Materials and Methods). This method requires the preparation of an insert with flanking regions of homology to a linearized expression vector. The insert and the linearized plasmid should then be transformed into competent E.coli cells, which will integrate the insert in the plasmid via homologous recombination (Beyer at al., 2015). The Slr1143 R250A insert was prepared by overlapping-PCR in order to insert the mutation and the flanking sequences. The desired PCR product was gel-purified while the P_{CAG}-IRES-Tdtomato plasmid was linearized by digestion with a restriction enzyme and gel-purified as well. The insert and the linearized plasmid were then used to perform an AQUA cloning, after which colonies were obtained and subsequently screened by colony-PCR. A scheme of the procedure is reported in Fig. 4.3.

The new plasmid was tranfected into HEK293T cells using the same amount of DNA employed in the previous experiments: 1 µg HCN4 + 1 µg Slr1143 R250A. After 20 hours, an unexpected effect was observed: the cells were all dead and detached from the bottom of the petri. I reasoned that the combination of the mutation and the new promoter were causing an over-expression of the protein and therefore an excess of c-di-GMP in the cytoplasm. This high concentration of the signaling molecule might have been the cause of cell death. To overcome this problem, I decided to try different experimental

conditions in which I varied the amount of transfected DNA and the after-trasfection time. By a fine tuning of these parameters, I should find the best way to express Sl1134 R250A in HEK2393T cells without killing them.

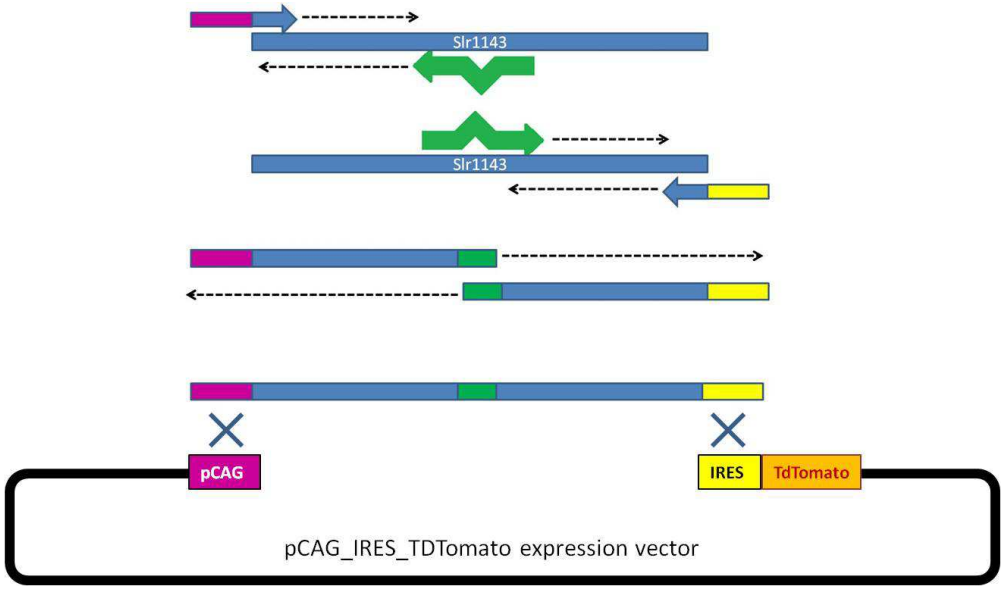

Fig. 4.3. Schematic representation of the cloning procedure. By overlapping-PCR the mutation and the flanking sequences required for AQUA cloning were inserted. The insert was mixed with the linearized expression vector and the DNA mixture was transformed into competent cells.

For the first set of experiments, HEK293T cells were transfected with only 0.5 µg of Slr1143RA + 1 µg of HCN4 and the time between the transfection and the measurements was reduced to 12 hours. The cells were alive and they looked morphologically good. However, only in few cells per day it was possible to measure currents with the amplitude and the typical features of HCN4 currents (Fig 4.5 A). Most of the cells showed currents with very low amplitudes, atypical activation kinetics and poor tail currents that were impossible to analyze. Fig. 4.4 shows a representative example of these measurements.

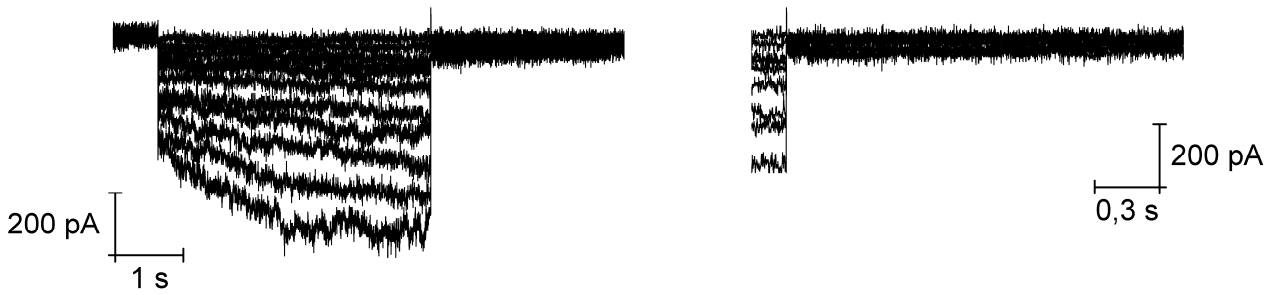

Fig. 4.4 12 hours are not enough for a good expression of both the HCN4 channel and the construct. Exemplary current traces from cells expressing 0.5 µg of Slr1143RA + 1 µg of HCN4 recorded 12 hours after transfection.

I concluded that 12 hours were not enough to obtain a good expression of both the channel and the enzyme (Fig. 4.5 A). Nevertheless, these experiments showed that the mutagenesis and the cloning were affecting and presumably improving the system. In the days in which I obtained a reasonable channel expression, I was able to observe a negative shift of the $V_{1/2}$ in 80% of the cells co-transfected with Slr1143 R250A and HCN4. The average $V_{1/2}$ of cells which co-expressed the channel and the mutated enzyme was -108.1 ± 1.36 mV (N=16). Control cells without Slr1143 measured in those days had a $V_{1/2}$ value of -102.0 ± 1.39 mV (N=14) (Fig. 4.5 C). The results of these experiments suggested that modifications in the protein and in the expression procedure, which should improve the synthesis and the activity of the contruct, are indeed effective: they improved the number of responsive cells.

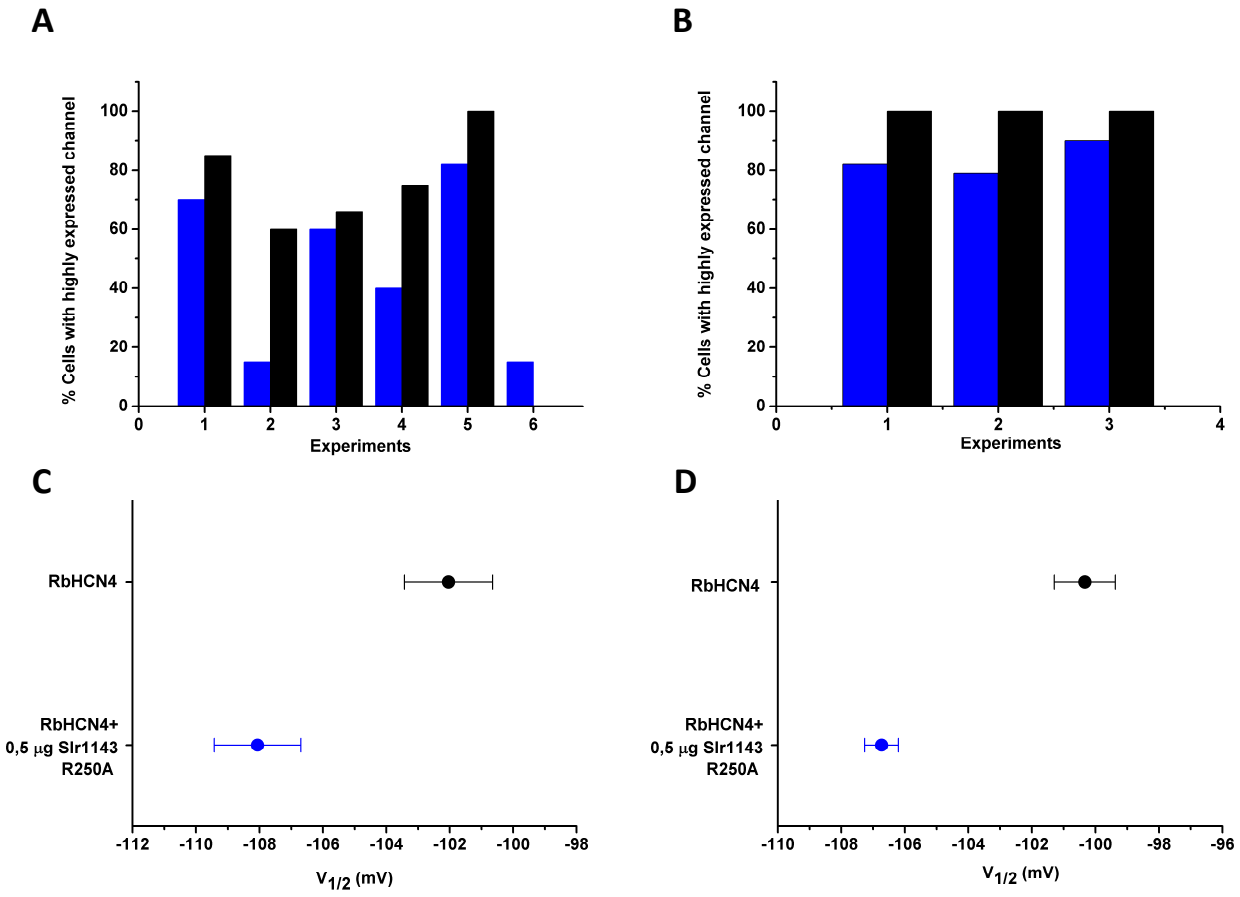

Fig. 4.5 Determining the proper conditions for expressing the mutated enzyme. (A) and (B) Estimation of the expression of HCN4 in HEK293T cells. Transfected cells were measured after 12 (A) or 18 (B) hours after transfection. For each experiments are reported the percentages of cells with the following features: high current intensity, clear HCN4 kinetics, presence of tail currents with closure kinetics. Black: HCN4 control cells; Blue: HCN4 + Slr1143 R250A co-transfected cells. C) Avarage $V_{1/2}$ values ± SE of cells in which HCN4 currents could be recorded in the expreiments reported in (A). Black dots: HCN4 control cells (N=14); Blue dots: HCN4 + Slr1143 R250A co-transfected cells (N=16). (D) Avarage $V_{1/2}$ values ± SE of cells in which HCN4 currents could be recorded in the expreiments reported in (B). Same color code as in (C), N=9 for both control and co-transfection.

To achieve an even better compromise between the amount of DNA to be transfected, the time after transfection and the channel expression, new experiments were performed. HEK293T cells were transfected again with 0.5 μg of Slr1143 R250A + 1 μg of HCN4 but the time between the transfection and the measurements was increased to 18 hours. In this way cells with a good expression of both HCN4 and Slr1143 R250A could be obtained (Fig.4.5 B). Measurements of HCN4 currents in these cells showed that it was possible to see again an effect of the c-di-GMP on the $V_{1/2}$ in 80% of the co-transfected cells (Fig. 4.5 D). The $V_{1/2}$ value of the latter cells was -106.7 mV ± 0.5 mV (N=9). This value is again more negative than that of control cells, which were measured in parallel ($V_{1/2}$= -100.3 mV ± 0.9 mV (N=9)).

In the next step we tested whether the endogenously synthesized cyclic di-nucleotide is now sufficient to counteract the effect of saturating concentrations of cAMP. The results of these experiments showed that cAMP at 10 uM in the pipette solution was able to cause a positive shift the activation curve of the control cells as expected (Fig 4.6 B). Measurements of HCN4 activity in cells co-expressing Slr1143 R250A exhibit a surprising response to cAMP. Fig. 4.6 B shows that cAMP shifted the activation curve of HCN4 to the same value irrespective of whether Slr1143 R250A was expressed or not. With cAMP the average $V_{1/2}$ values was - 90.7 ± 1.3 mV (N=6) in control cells and -91.4 ± 1.5 mV (N=5) in cells transfected with the mutated enzyme (Fig 4.6 C).

The effect of cAMP on channel opening could be noticed also in the current recordings (Fig 4.6 A), where it was possible to observe an acceleration of the current kinetics when the channel regulator was delivered in the cytoplasm. The cAMP-induced acceleration of the kinetics can be observed in both control and cells expressing Slr1143 R250A. The acceleration of the kinetics can be described with the $T_{1/2}$ value, that is the time it takes a current to reach half of its full activation (plateau). To describe quantitatively that the effect of cAMP is the same in the two conditions, the $T_{1/2}$ values for the currents elicited at -135 mV can be considered. For the current traces reported in Fig. 4.6 a, when no cAMP was present in the recording pipette, the $T_{1/2}$ values for the control and the co-transfected cell were 678 and 828 respectively. For the current traces in which cAMP was present in the pipette the values were 542 for control cell and 549.

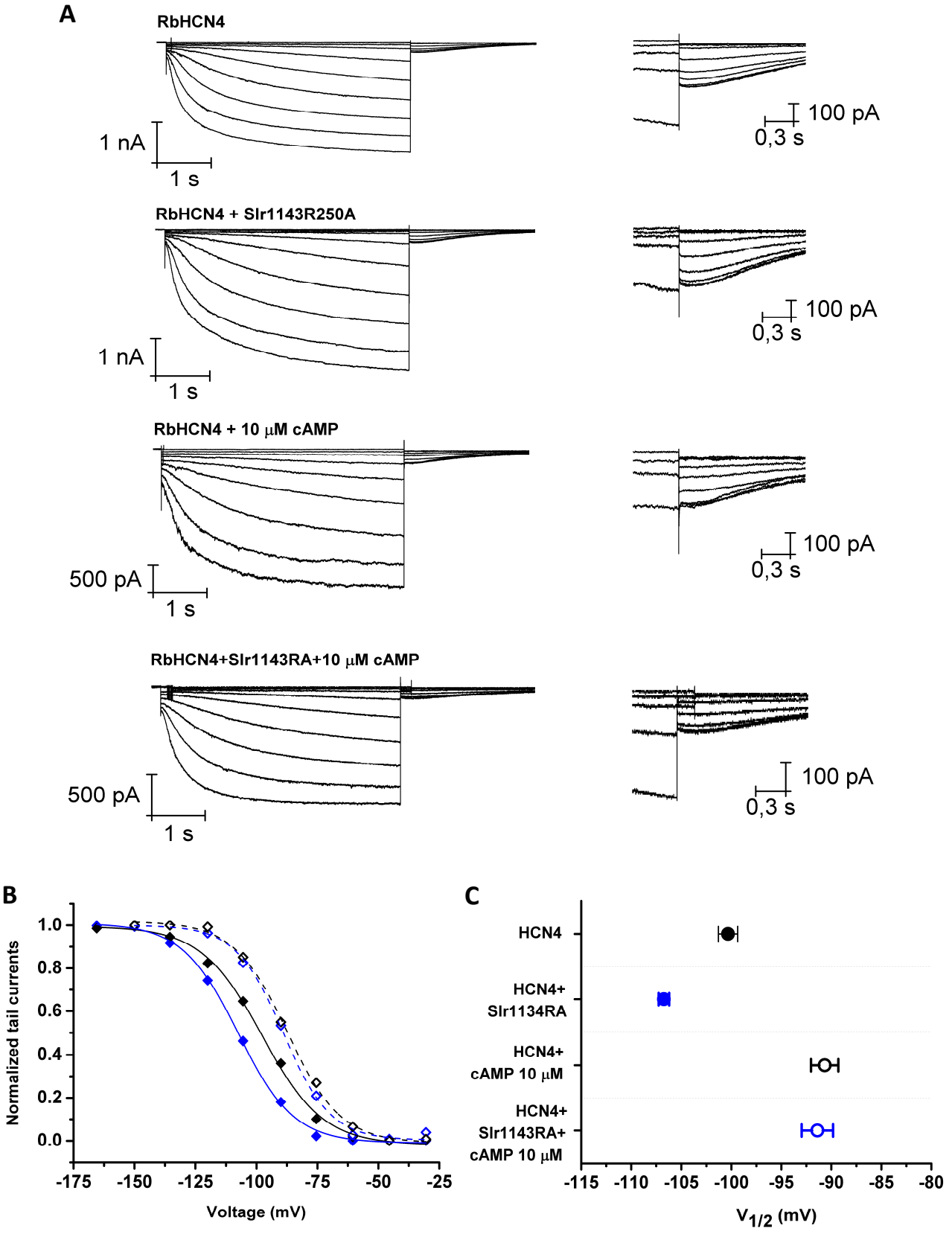

Figure 4.6 effect of cAMP in cells co-expressing Slr1143 R250A and HCN4. (A) Exemplary current traces obtained by application of voltage protocols in control and Slr1143-expressing cells. Tail currents (recorded at -40 mV) of each current family are enlarged and reported on the right for each measurement. (B) Normalized tail current amplitudes plotted as a function of the preceding test voltage. Black dots: HCN4; Blue dots: HCN4 + Slr1143 R250A; empty black dots: HCN4 + 10 uM cAMP; empty blue dots: HCN4 + Slr1143 R250A + 10 uM cAMP. Data points were fitted with the Boltzmann equation (equation 1). Color code for the fitting is the same used for the data points: continuous lines: no cAMP; dashed lines: cAMP. (C) Mean ± S.E. of the $V_{1/2}$ values extrapolated from the fitting of the activation curves. Same color code as in (B). HCN4 N=9; HCN4 + Slr1143 N=9; HCN4 + 10uM cAMP N=5; HCN4 + Slr1143 + 10uM cAMP N=6.

Since it was clear, at that point, that the enzyme was not able to reverse the effect of saturating concentrations of cAMP, the next step was to test the effect of the enzyme under conditions of non-saturating cAMP concentrations. To do this were performed other experiments, in which the cAMP concentration in the pipette was further reduced to 1uM (Fig. 4.7). In these experiments it was possible to see a trend for a small difference between the controls and cells expressing Slr1143 R250A. The mean $V_{1/2}$ values for this set of experiments were:

- -102.5 ± 2.9 mV (N=4) in control cells expressing RbHCN4
- -109.5 ± 1.7 mV (N=5) in cells expressing Slr1143 R250A
- -95.9 ± 2.6 mV (N=8) in control cells expressing RbHCN4 with 1 uM cAMP in the pipette solution
- -102 ± 2.2 mV (N=12) in cells co-expressing Slr1143 R250A with 1 uM cAMP in the pipette solution

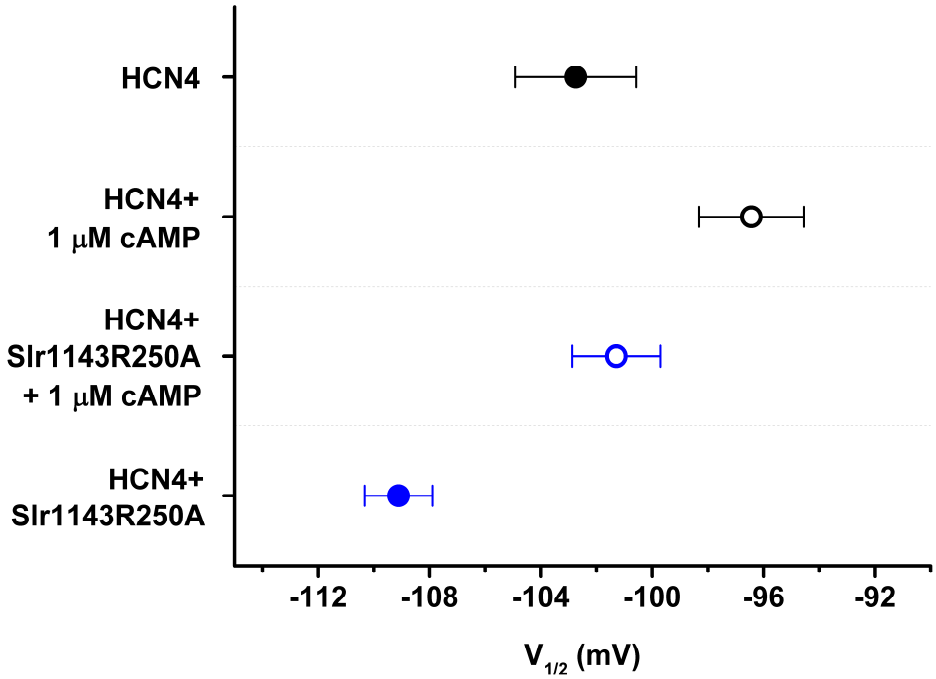

Fig. 4.7 Effect of 1uM cAMP on the half-activation voltage. Mean ± S.E. of the $V_{1/2}$ values from experiments with 1 uM cAMP. Black circle: HCN4 (N=4); Blue circle: HCN4 + Slr1143 (N=5); Empty Black circle: HCN4 + 1 uM cAMP (N=8); Empty blue circle: HCN4 + Slr1143 + 1 uM cAMP (N=12).

The results so far suggested that the critical point for seeing the antagonistic effect of c-di-GMP on cAMP mediated HCN channel gating was related to the concentration ratio of the two cyclic nucleotides in the cytoplasm. I assumed that what had been seen in these experiments was due to a diffusion problem. The pipette solution is prepared according to intracellular ion concentrations but when the membrane is broken, i.e. the pipette content is in direct contact with the cytoplasm, small molecules can diffuse from the latter into the pipette (Pusch and Neher, 1988). When no cAMP was added to the pipette solution, both

the c-di-GMP synthesized by Slr1143 R250A and the endogenous cAMP equally diffused into the pipette: in this case it was still possible to see an effect of the c-di-GMP binding to the CNBD. When extra cAMP was added to the pipette solution the second messenger diffused constantly from the pipette into the cytoplasm. Within minutes the cytoslolic cAMP concentration equilibrated with the concentration of cAMP in the pipette. The c-di-GMP messenger, in contrast, was diffusing from the cytoplasm to the pipette, which means that it was rapidly diluted in the cytosol.

To circumvent this problem I decided to continue with the photo-activated enzyme and search for conditions e.g. light intensity, wavelength, exposure time that might allow robust production of c-di-GMP. This should affect at least the binding of endogenous cAMP to the CNBD and modulate in this way cAMP gating.

4.2 Experiments with a light-activated bacterial diguanylate cyclase.

The BphS-1 DNA was a generous gift form Prof. Gomelsky, Wyoming University. This is a chimera composed by the photo-switch of the pytochrome BphG plus Slr1143 as the effector domain. The latter does not have the aforementioned R250A mutation. Given the results from Chapter 4.1, I decided to introduce the mutation in this construct (now called BphS) and to move it into the pCAG-IRES-TdTomato plasmid. The mutated construct was obtained in the same manner as that used for Slr1143: overlapping-PCR with primers for AQUA cloning and for mutagenesis. The insert was then integrated in the plasmid by AQUA cloning and positive colonies were screened via colony-PCR.

Since it was already known that BphS can have some dark activity (Ryu and Gomelsky, 2014), it was important to verify that this dark activity could not influence the voltage dependence of the channel in a light-independent manner. To estimate this dark effect, HEK293T cells were transfected with 1µg of HCN4 + 0.5 µg of BphS and 1µg of HCN4 + 0.5 µg of GFP as controls.

After 18 hours of cultivation, the HCN4 activity was estimated by patch clamp recordings. Cells were measured as in Fig. 4.8 A in the whole cell configuration: voltage-clamp protocols with negative voltage steps were applied to the cells to activate and measure HCN4 currents. Tail current values were used again to assess the voltage dependency of the channel. A comparison of the activation curves obtained from BphS-expressing cells and from control cells showed that the two voltage dependencies are almost indistinguishable (Fig. 4.8 B).

Consequently also the estimated $V_{1/2}$ values from Boltzmann fits were the same: -104 ± 1 mV for the controls (N=14) and -103 ± 0.8 mV for BphS-expressing cells (N=12) (Fig. 4.8 C). The results of these experiments showed that the dark activity of the enzyme did not affect the channel opening in any way.

After this important control, current measurements were performed on cells which were exposed to red light. For these experiments, cells were grown and transfected in a medium that did not contain phenol red. This should prevent any kind of interference between the medium and the light. As an irradiation tool, I used a custom made array of LEDs (10x15 cm, c.a. 300 LEDs) with an emission maximum at 660 nm; six petri dishes could be positioned on this array. The LED array was connected to a timer, which allowed a regulation of the light/dark cycles (Fig. 4.9). In the present case a continuous cycle of 20 seconds of light and 90 seconds of dark was used for stimulation. The light/dark cycle was recommended by prof. Gomelsky.

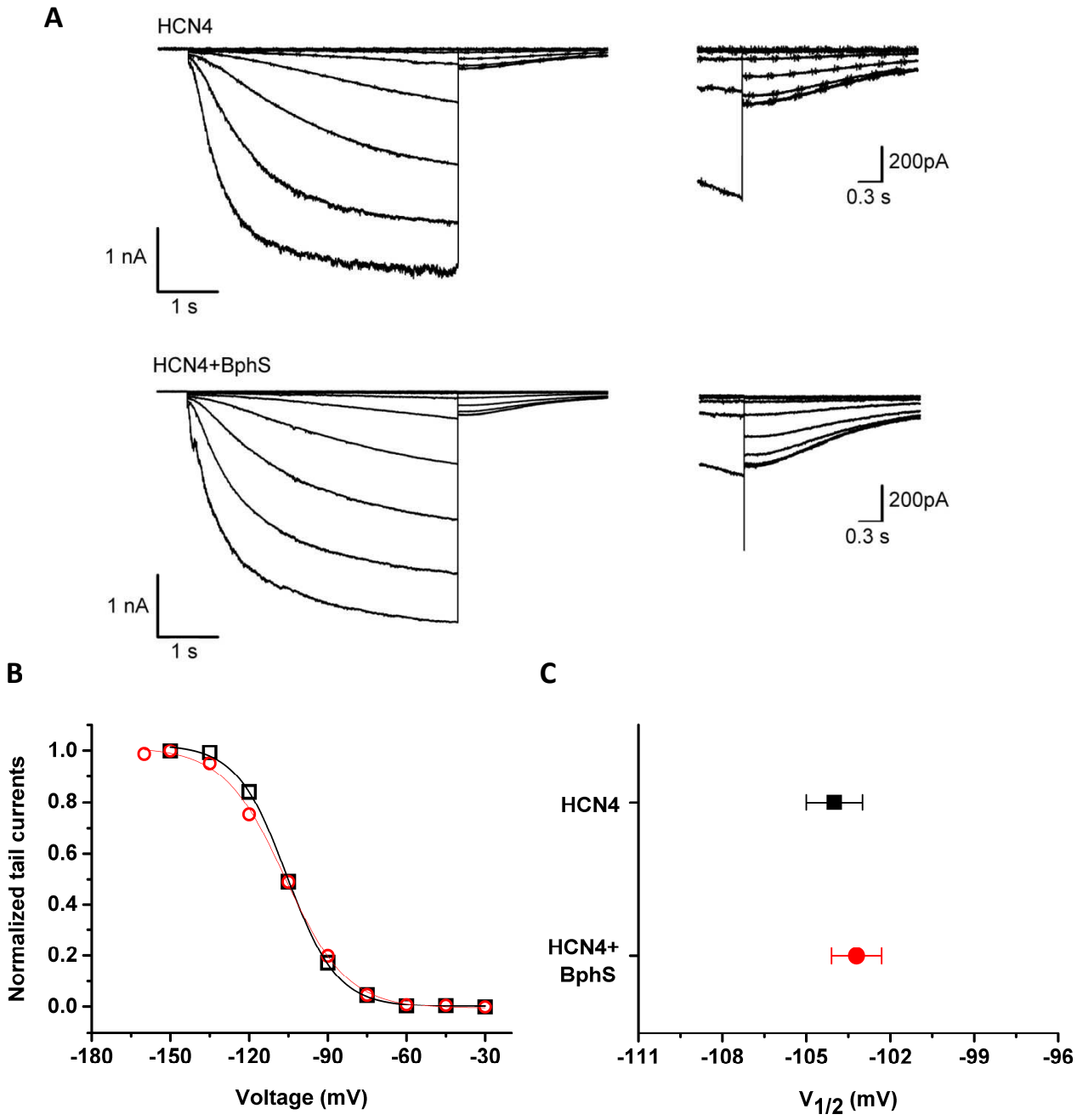

Fig. 4.8 Monitoring the dark activity of BphS. (A) Exemplary current traces obtained by application of voltage protocols in control and BphS-expressing cells. Tail currents (recorded at -40 mV) of each current family are enlarged and reported on the right for each measurement. (B) Normalized tail current amplitudes plotted as a function of the preceding test voltage. Black empty squares: HCN4; Red empty squares: HCN4 + BphS. Data points were fitted with the Boltzmann equation (equation 1). Color code for the fitting is the same used for the data points. (C) Mean ± S.E. of the $V_{1/2}$ values of HEK293T cells expressing HCN4 or co-expressing HCN4 + BphS. Black squares: HCN4 (N=14); Red squares: HCN4 + BphS (N=12).

The set up was constructed in such a way that the cells were not in direct contact with the LEDs: empty petri dishes were used as a “spacer” between the dishes with cells and the light source. In addition to the timing, also the light intensity of the LED array could be regulated. The initial experiments were planned with a long light exposure (hours). This extreme exposure should provide information on whether the system results at all in a measurable response of the HCN4 currents. In the next step the treatment should then be adapted with respect to light intensity and exposure.

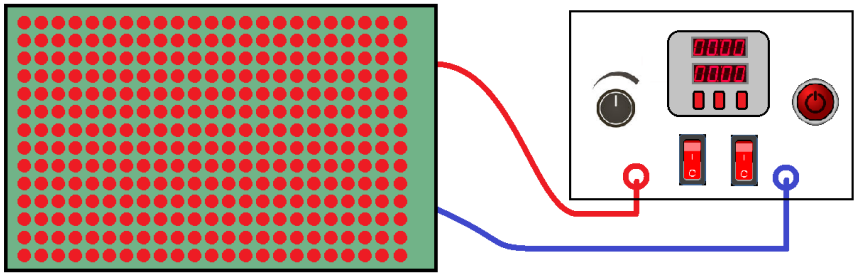

Fig 4.9 Scheme of the LED apparatus. The LED array was connected to a timer to regulate light/dark cycles. With a knob it was possible to regulate the light intensity. On/off button allowed to use continuous light when needed.

The light produced by the LED array turned out to have a much lower intensity than the one used to activate the protein in previous studies (Ryu and Gomelsky, 2014). However we found that the light exposure of HEK293T cells resulted, after an overnight incubation (15 hours), always in cell death. This occurred regardless of the distance, created by the aforementioned spacer, between the cells and the LED plate; cells died with one, two or four empty petri dishes as a spacer. To avoid cell death and to obtain living cells for some measurements, I decided to leave the cells on the LED plate for shorter periods of time; two empy petri dishes were employed as spacer.

As a first short irradiation time, a period of 1 hour was tested. Worth mentioning is that this time describes the length of exposure over which the cells were treated with the aforementioned alternating light/dark cycles. Cells treated in this manner turned out to be difficult for obtaining good seals for patch clamp recordings. Only a small number of cells were suitable for good whole-cell measurements. In those cells it was possible to measure HCN4 type currents slowly activating at negative voltages (Fig. 4.10 A). The respective tail currents were used as in Fig. 4.10 B for construction of activation curves. A scrutiny of the activation curves implied that light exposure did not affect the voltage dependency of the channel. This visual impression was confirmed by the $V_{1/2}$ values, which were obtained from fitting of data with the Boltzmann function (Fig. 4.10 C). For control cells the average $V_{1/2}$ was -100.1 ± 0.9 mV (N=16) and for irradiated BphS-expressing cells it was -102.1 ± 1.1 (N=8).

In subsequent experiments it was intended to improve the expression of the light sensitive protein by increasing the amount of transfected BphS DNA (from 0.5 µg to 0.75 µg). Additionally, the activity of the protein was increased by lengthening the exposure time of up to two hours. An analysis of HNC4 currents in cells, which were treated in this manner, showed no effect of light exposure (Fig4.10 A, B and C). The average $V_{1/2}$ value of HCN4 currents in cells transfected with 0.75µg of BphS and kept in pulsed light for one hour was -97.8 ± 0.7 mV (N=5). Also extending the light exposure to two hours caused no significant shift in the $V_{1/2}$; the mean $V_{1/2}$ value in these cells was -98.9 ± 1.1 mV (N= 4). $V_{1/2}$ values for control cells of these experiments are included in the aforementioned mean value for control cells: -100.1 ± 0.9 mV (N=16). Cells kept on the LED plate for more than two hours were impossible to be measured.

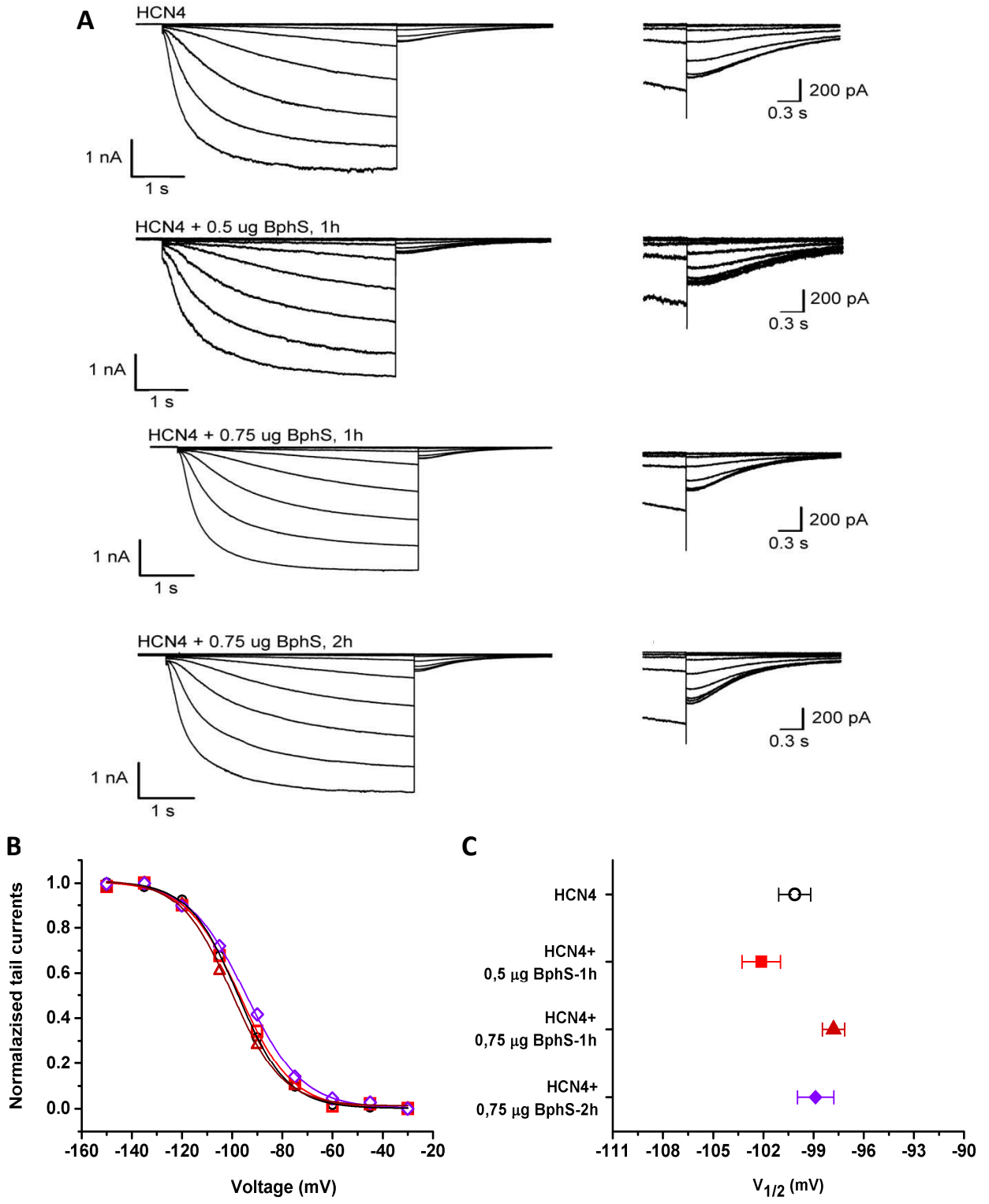

Figure 4.10. Expreiments with 660 nm light. (A) Exemplary currents elicited by voltage protocols in different cells (transfection and treatment reported on each). Tail currents (recorded at -40 mV) of each current family are enlarged and reported on the right for each measurement. (B) Normalized tail current amplitudes plotted as a function of the preceding test voltage. Black empty circles: HCN4; Red empty squares: HCN4 + 0.5 µg BphS-1hour irradiation; Brown empty triangle: HCN4 + 0.75 µg BphS-1hour irradiation; Violet empty diamonds, HCN4 + 0.75 µg BphS-2hours irradiation. Data points were fitted with the Boltzmann equation (equation 1). Color code for the fitting is the same used for data points. (C) Mean ± S.E. of the $V_{1/2}$ values extrapolated from the fitting of the activation curves. Same color code used in (B); HCN4 N=16; HCN4 + 0.5 µg BphS-1hour irradiation N=8; HCN4 + 0.75 µg BphS-1hour irradiation N=5; HCN4 + 0.75 µg BphS-2hours irradiation N=4.

At this point I decided to design a new irradiation device. This LED array should provide a higher irradiance without killing the cells. In a first step I tested the possibility to increase the LEDs irradiance by increasing the applied voltage. This strategy was not successful because the voltage used for experiments in Fig. 4.10 was already close to the tolerance level of the LEDs. Moreover, it turned out that the array of many parallel LEDs was producing a lot of heat. The heat was presumably the reason why the cells where dying after some hours on the LED array, even if they were not directly in contact with the LEDs.

To increase the light irradiance, new and, more powerful LEDs (1W) were purchased (660 nm LEDs from LumenLaden). To reduce heat exposure of the cells a plastic support with holes in which 35 mm petri could fit was designed. The LEDs were fixed with a specific glue on an aluminum plate, which improved the heat dissipation. The plastic support was located above the LED array and the distance between the two could be adjusted and modified with four screws. The whole structure was organized in such a way that each LED was located under the center of a petri dish (Fig. 4.11). The new device was able to generate a maximal light at an higher irradiance of up to 2 W/m^2 (with the previous device was only 0.2 W/m^2).

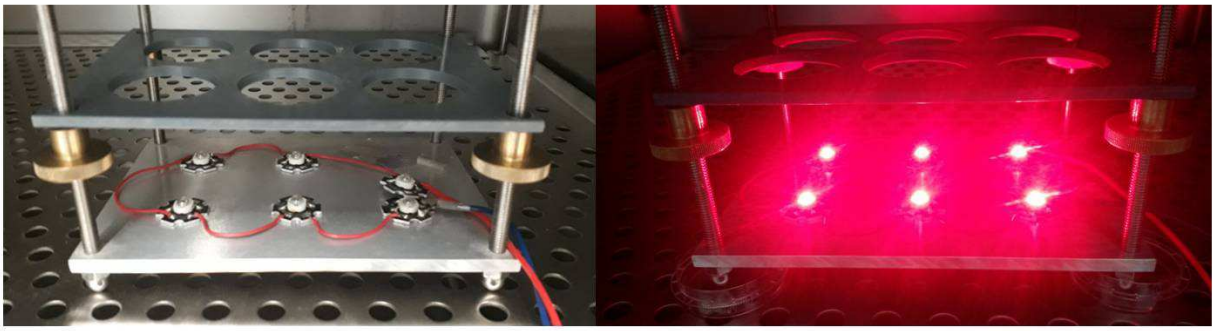

Fig. 4.11 New irradiation device. With this irradiation device it was possible to achieve an higher irradiance and much better heat dissipation.

Once the new device was ready, also a newer version of BphS became available: the construct had been codon-optimized for expression in mammalian cells by prof. Gomelsky's group. The new BphS DNA was inserted into a pCDNA plasmid, under the control of a CMV promoter and was followed by an auto-cleavage sequence of the 2A family (Wang et al., 2015). The 2A self-cleaving peptides are a family of oligopeptides located between two proteins that can undergo self-cleavage to generate mature proteins. The cleavage site is located between the last two amino acid of the oligopeptide: a glycine, that will become the last amino acid of the first protein, and a proline that will be the first residue of the second protein (Wang et al., 2015). The 2A sequence separated BphS from a c-di-GMP phosphodiesterase called YhjH that should maintain a low concentration of c-di-GMP in the dark. It was expected that the codon optimization should allow a much higher expression of the BphS gene so also the dark activity of this construct should be improved. It was already known that the YhjH protein is able to lower, as a counter-

player of the cyclase, the problem of unwanted dark activity (Ryu et al., 2017 and 2014). The multi-genes expression system Bphs-2A-Yhjh from now on will be called BphSOpti.

During the course of the experiments, other groups had already tried to express the BphSOpti multi-genes in mammalian cells. Publications from these laboratories provided useful information for the present endeavor. Shao and colleagues published a study in which they expressed BphSOpti in HEK293T cells to try to regulate the expression of a gene of interest (Shao et al., 2017). The cyclic di-nucletide produced in a light dependent manner bound the STING protein, which then activated a signaling cascade resulting in activation and nuclear traslocation of the transcription factor IF3. The gene of interest was under the control of a promoter engineered to contain IF3 binding site. They were able to see a light-driven expression of the desired protein within 2-4 hours. Moreover they showed that the presence of the Yhjh phopshodiesterase was actually necessary to keep a low concentration of c-di-GMP in the dark.

The new plasmid containing the multi-genes expression system BphSOpti was therefore used to transfect HEK293T cells, taking advantage of the new information in terms of irradiation time and intensity. Since the new plasmid did not contain any fluorescent protein, I prepared the following co-transfection protocol: 1 µg of HCN4 + 0.75 µg of BphSOpti + 0.3 µg of GFP/µg other DNAs. The latter was an amount of GFP, which already proved to be good for triple transfections; these experiments had been performed by colleagues in the lab. In this case I preferred to use the GFP because it is a bit brighter than the TdTomato. Irradiance was set to 2 W/m^2 and 24 hours after transfection cells were exposed for 2.5 hours to pulsed red light.

The first measurements with cells, which expressed the new codon-optimized enzyme and which were exposed to the new light device, exhibited no perceivable response to red light. Tri-transfected cells showed weaker membranes and were therefore hard to measure. Recordings from cells suitable for patch clamp recordings, showed HCN4 type currents that were used for further analysis (Fig 4.12 A). An analysis of the activation curves, which were as in Fig. 4.12 B constructed from the tail currents, showed no appreciable difference between the control cells and tri-transfected cells exposed to red light. Also in this case the fitting of the data reveled no difference in the average $V_{1/2}$ values between the control cells expressing HCN4 and the BphSOpti-RbHCN4 co-transfected cells (Fig 4.12 C). The $V_{1/2}$ value was -102.1 ± 1.2 mV (N=3) in control cells and -103 ± 2.5 mV (N=4) in the BphSOpti-RbHCN4 expressing cells. Notably the number of tested cells was, because of the problems of obtaining robust measurements, rather low. But the data indicated already that an effect of a light regulated modulation of HCN4 channels by BphS would be, if any, very small.

The first results were not encouraging and asked for additional experiments in which other experimental parameters are tested. One critical parameter could be the exposure. According to Shao et al. exposure time between 2 and 48 hours could be suitable for testing (Shao et al., 2017). But since these experiments

are very time consuming and the electrical recordings of light treated cells are difficult, I decided to change the strategy. Notable the recording of HCN4 currents is an indirect assay system for the production of c-di-GMP. Hence it is not clear whether the absence of response of HCN4 gating in HEK293T cells exposed to light is caused by an insensitivity of the channel to the signaling molecule or whether light is not stimulating the synthesis of c-di-GMP. Under these circumstances, it would be more useful to find a way of quantifying the concentration of c-di-GMP in the cytosol of transfected HEK293 cells after red light irradiation. The quantification of the c-di-GMP will be explained in the following chapters.

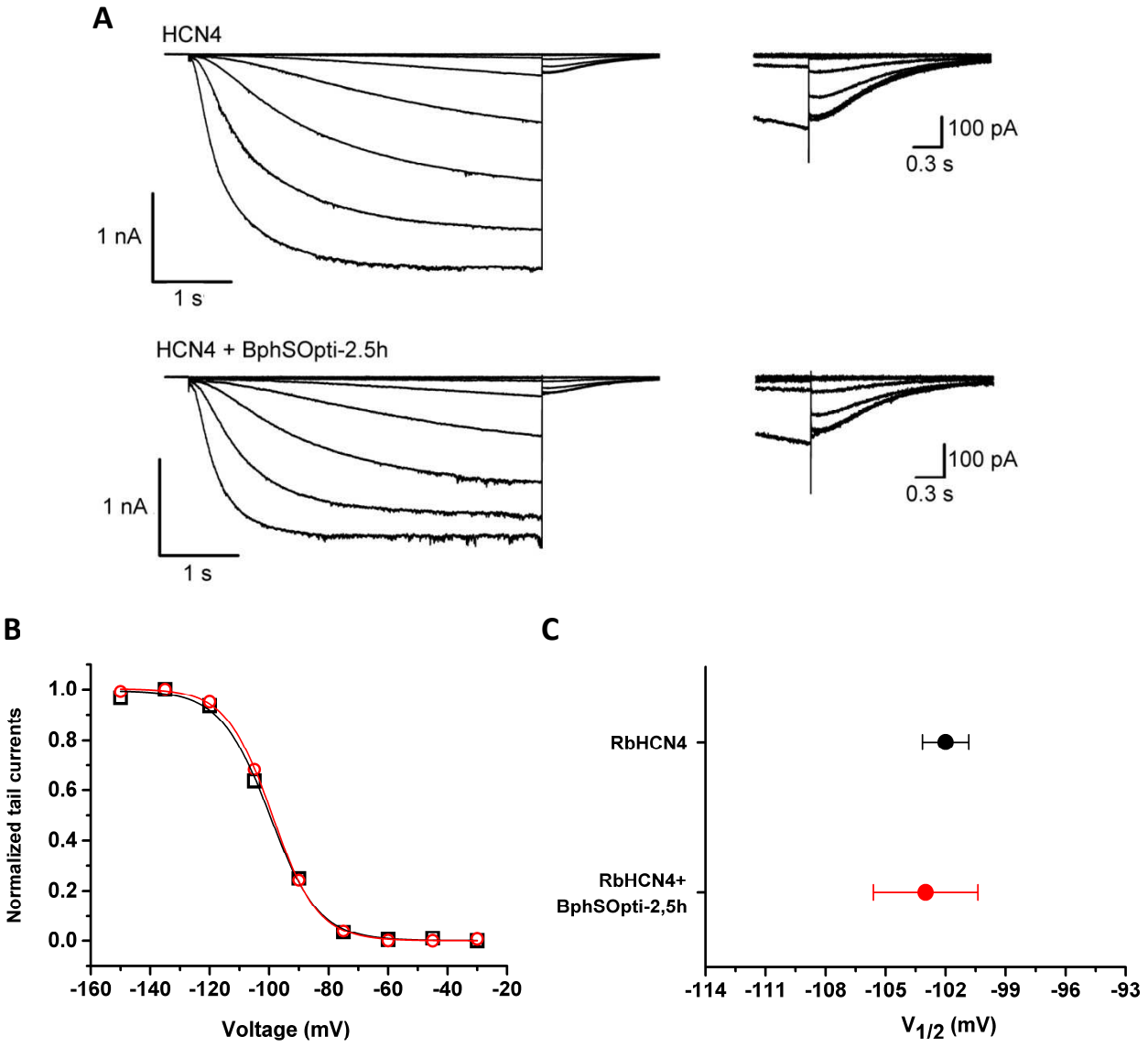

Fig. 4.12 Expression of BphSOpti. (A) Exemplary current traces obtained by application of voltage protocols in control and BphSOpti-expressing cells. Tail currents (recorded at -40 mV) of each current family are enlarged and reported on the right for each measurement. (B) Normalized tail current amplitudes plotted as a function of the preceding test voltage. Black empty squares: HCN4; Red empty squares: HCN4 + BphSOpti-2.5h irradiation. Data points were fitted with the Boltzmann equation (equation 1). Color code for the fitting is the same used for the data points. (C) Mean ± S.E. of the $V_{1/2}$ values of HEK293T cells expressing HCN4 or HCN4 + BphSOpti. Black dots: HCN4 (N=3); Red dots: HCN4 + BphSOpti-2.5 h irrdiation (N=4).

4.3 Quantification of the synthesis of c-di-GMP by ELISA assay.

As previously mentioned, I decided that it was necessary to quantify the c-di-GMP produced by the BphS-construct after different times of light exposure. By doing this it should be possible to understand the relationship between the irradiation period and the concentration of c-di-GMP in the cytoplasm of a BphS-expressing cell. From the results obtained in Chapter 4.1 with the constitutively active enzyme Slr1143 R250A, it was already anticipated that the latter was able to generate sufficient cyclic di-nucleotide for affecting the HCN4 voltage dependency. For this reason the constitutively active enzyme can be considered as a very good positive control. At the same time the cyclic di-nucleotide produced by this construct serves as an internal reference for the desired minimum amount of c-di-GMP. I decided to quantify the enzyme activity by performing an ELISA assay, which is a test commonly used to detect the presence of a molecule of interest and to quantify its concentration in biological samples like cell culture supernatants, tissue homogenates, plasma etc.

An ELISA kit specific for quantification of c-di-GMP is available from EIAab and is based on the competitive immunoassay technique. In this type of ELISA the sample containing the substance of interest is mixed with a fixed amount of the same molecule whereby the latter carries a label. To calibrate the system, samples with known concentration of the analyte are prepared by diluting a stock solution provided with the kit. One of these standard solutions contains only the dilution buffer, which serves as the “blank” of the assay. The standards are mixed with the labeled molecule as well. The standards and the samples are loaded into a special multi-well plate in which the wells have been pre-coated with an antibody able to bind the analyte. In this manner, the molecules from the samples/standards and the labeled cyclic di-nucleotides will compete for binding sites on the antibodies located on the bottom of each well. The binding of the marked antigen to the antibody can be monitored optically as it will react with the buffers subsequently added to each well, changing their color to yellow. So the concentration of the molecule of interest in the samples is inversely proportional to the color change: the less colored a well, the higher the concentration of the analyte in the sample loaded in that well. The absorbance in the yellow range of the spectrum is measured for each well using a special spectrophotometer, designed for multi-well plates. The absorbance value of the blank has to be subtracted from all the others to apply the blank correction. The standards are used to create a concentration/absorbance calibration curve from which the unknown concentrations of the samples can be extrapolated. This type of ELISA was successfully used by Shao and colleagues to quantify c-di-GMP synthesis in HEK293T cells (Shao et al., 2017, Fig. 4.13 A). I used this paper as a reference for expression of BphS in HEK293T cells.

HEK293T cells were transfected with the same amount of DNA used for experiments in chapter 4.2: 1µg HCN4 + 0.75 µg BphSOpti +0.3 µg of GFP/µg other DNAs. Slr1143 R250A was used as a positive control: the respective cells were transfected with 1 µg of HCN4 + 0.5 µg of Slr1143 R250A. The transfections presented

in this chapter were performed with the calcium phosphate protocol (see Materials and Methods). Here are reported the ratios between the different plasmids, which are the same described in chapter 4.2, but the amount of DNA was scaled up for this type of transfection (1µg = 6µg). 24 hours after transfections, the transfection efficiency was checked under a microscope. The transfection efficiency was generally 30-40%. Half of the petri dishes containing the cells expressing BphSOpti were brought in a different incubator and exposed to pulsed red light (2 W/m^2) for different periods, namely 3, 6 or 9 hours. The other petri dishes were kept in the dark for the same amount of time. Slr1143-transfected cells were used for the preparation of cell extract samples right after post-transfection at 24 hours. One dish containing BphSOpti-transfected cells was used to prepare a sample right after the post-transfection at 24 hours: the t=0 of the experimental timeline. Samples of cytoplasm content of transfected HEK293T cells were prepared as described in Matherials and Methods. Briefly, cells were collected and centrifuged to obtain a pellet, which was re-suspended in 500 uL of PBS. The cell concentration of this suspension was determined with a cell counter and this information was used to further dilute the cells to a final concentration of $1x10^6$ cells/mL. Each cell suspension underwent three freeze-thaw cycles (-20°C to room temperature (RT)) to break the membranes and make the cells release their intracellular component. Samples were centrifuged and the supernatant was transferred into a new tube and kept at -20 °C. A scheme of the procedure is reported in fig. 4.13 B.

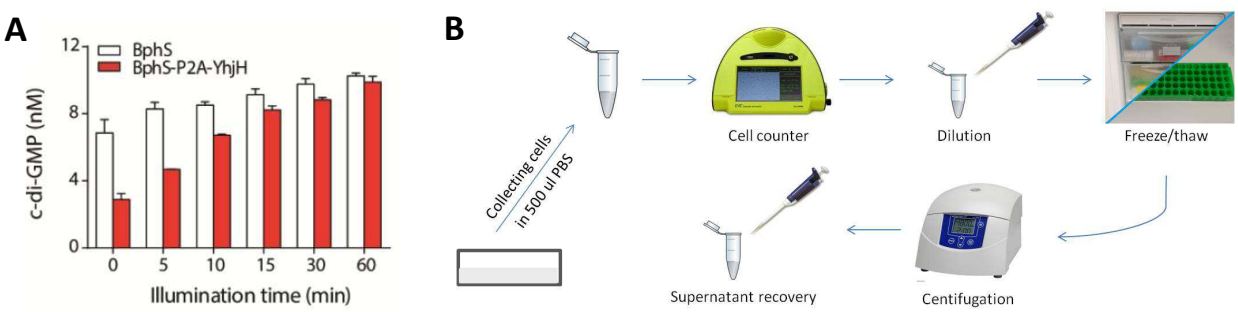

Fig. 4.13 Scheme of Elisa preparation protocol. (A) Results obtained by Shao and colleagues using the same kit that I used in this work. Shao and coworkers showed the concentration values of c-di-GMP in cytosol extracts of cells expressing BphS or the BphSOpti multi-gene system (Shao eta al., 2017) (B) Schematic representation of the preparation of the cell extract samples.

In the next step the samples and the standards were loaded in the multi-well plate together with biotin-labeled c-di-GMP (two wells for each sample/standard). Like mentioned before, the latter competes with the cyclic di-nucleotide from the samples for binding to the antibody coating during an incubation at 37°C. After washing away the unbound molecules, avidin conjugated to Horseradish Peroxidase (HRP) was added to each well. Avidin is known to strongly bind the biotin so, after another incubation at 37°C, the enzyme HRP would be bound to the biotin-labeled c-di-GMP. The substrate for HRP (3,3',5,5'-tetramethylbenzidine or TMB) was added, together with hydrogen peroxide (H_2O_2), in each well and the reaction with peroxidase developed an intense blue color. The enzyme-substrate reaction was terminated by the addition of a sulphuric acid solution that also changed the color from blue to yellow. The color change was measured

spectro-photometrically at a wavelength of 450 nm. Absorbance values of the standards were averaged, plotted as a function of the Log_{10} of the c-di-GMP concentrations and fitted with a four parameter logistic curve (4PL) (Equation 2):

$$(Eq.2)\ y = A_2 + \frac{(A_1 - A_2)}{1 + \left(\frac{x}{x_0}\right)^p}$$

where A_1 is the maximum value and A_2 is the minimum value that can be obtained. X_0 gives the point of inflection (i.e. the point on the S shaped curve halfway between A_1 and A_2) and *p* the slope of the curve (related to the steepness of the curve at point c) (Fig. 4.14 A). The unknown concentration of c-di-GMP in the samples was then determined with this curve.

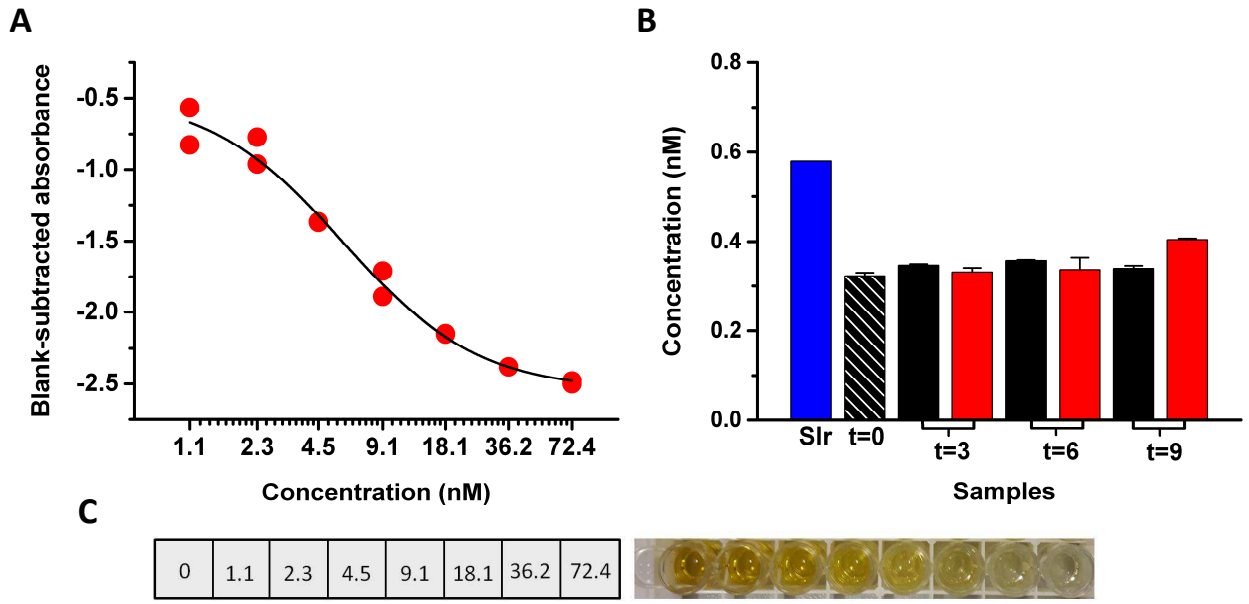

Fig 4.14 First quantification of c-di-GMP content in HEK293T cells. (A) Blank-subtracted absorbance values of the standards (red dots) measured at 450 nm plotted as a function of their known concentrations (in logarithmic scale). Data points were fitted with a 4PL function (Eq. 2). (B) Concentration values of different cell extracts extrapolated from the calibration curve in (A). Each sample was loaded in two wells of the plate to obtain double absorbance measurements and therefore two concentration values for each sample: in the graph are reported mean values ± SE. An extract of cells expressing Slr 1143 R250A was prepared as a positive control of the test (blue) 24 hours after transfection. At the same time, an extract of cells expressing BphSOpti was prepared to serve as the t=0 (black and white) of the experimental timeline. From that moment, two extracts of BphSOpti-expressing cells were prepared every 3 hours: one using cells kept in the dark (black) and one using cells exposed to light (red). (C) Exemplary standard column for competitive ELISA test. Left, loading scheme; right, color change gradient.

The results of the assay were negative in the sense that they did not reveal any effect of red light exposure on the c-di-GMP concentration (Fig 4.14 B). The c-di-GMP concentration in each sample was lower than the lowest standard concentration (1.1 nM). This means that all the concentration values were below the detection level of the assay. Different from what was expected from the experiments in Chapter 4.1, also the positive controls with the constitutively active Slr1143 R250A revealed c-di-GMP concentrations below the detection level. From this result we reasoned that the assay system may have not been appropriate for measuring the expected elevation of c-di-GMP in the cells. It has been already mentioned that each of the eight standards was loaded into two wells, one in the first column of the plate and one in the last after all

the samples. This procedure provides two values for each concentration and offers an internal check for the precision of the performance of the assay. A comparison of these internal standards showed that both gave about the same color gradient as the one reported if Fig. 4.14 C: a very pale yellow turned into orange according to the decrease in concentration of the standards (from 72.4 to 1.1 nM). This means that the procedure of the assay is sufficiently robust; even some pipetting error between individual samples should not compromise the whole test. Based on the results of these experiments and on the considerations on the assay system, we reasoned that the problem could have been an un-sufficient cell lysis. An inefficient membrane disruption may have prevented the release of cytosolic c-di-GMP from the cells into the supernatant.

To improve the assay I contacted prof. Haifeng Ye, the corresponding author of the paper by Shao et al. (Shao et al., 2017), to ask for advice on experimental details of the ELISA assay, which were not spelled out in the paper. It turned out that, despite of what they wrote in the paper, they did not follow the instructions in the manual. Instead they used a lysis buffer from another ELISA kit to break the cell membranes. I then decided to perform a chemical lysis as well. I prepared two types of lysis buffer. For the first one I took advantage of the knowledge of my colleagues that lysed human cells with the detergent Triton (1%) to analyze their protein content. The second buffer was kindly suggested by prof. Haifeng Ye. He recommended a buffer used in another paper, in which the authors were trying to extract cytosolic c-di-GMP from HEK cells (Folcher et al., 2014). This buffer contained acetonitrile, methanol and H_2O (2:2:1).

Three sets of samples were prepared in order to achieve a sufficient cell lysis. The preparation of the first set of samples followed the instruction manual of the kit, i.e. including a re-suspension of the cells in PBS. But unlike in the experiments in Fig. 4.14 the freeze-thaw cycles were performed from -80°C to RT. The second set of sample was prepared by lysing the cell with Triton buffer. In the third attempt an Acetonitrile-Methanol buffer was used to prepare the cells. Detailed protocols and buffer contents can be found in Materials and Methods. In this round of experiments also samples of un-transfected cells were prepared as an additional negative control. Each sample, as well as the standards, were loaded two times on an ELISA plate. Also in this assay, the color gradient of the standards was the expected one with little variations between the values of the two dual recordings. The absorbance data points of the standards were well fitted with a 4PL function (Equation 2) providing the calibration curve. Unlike in the experiments reported in Fig. 4.14, modified lysis procedure provided some interesting differences between the experimental samples (Fig. 4.15).

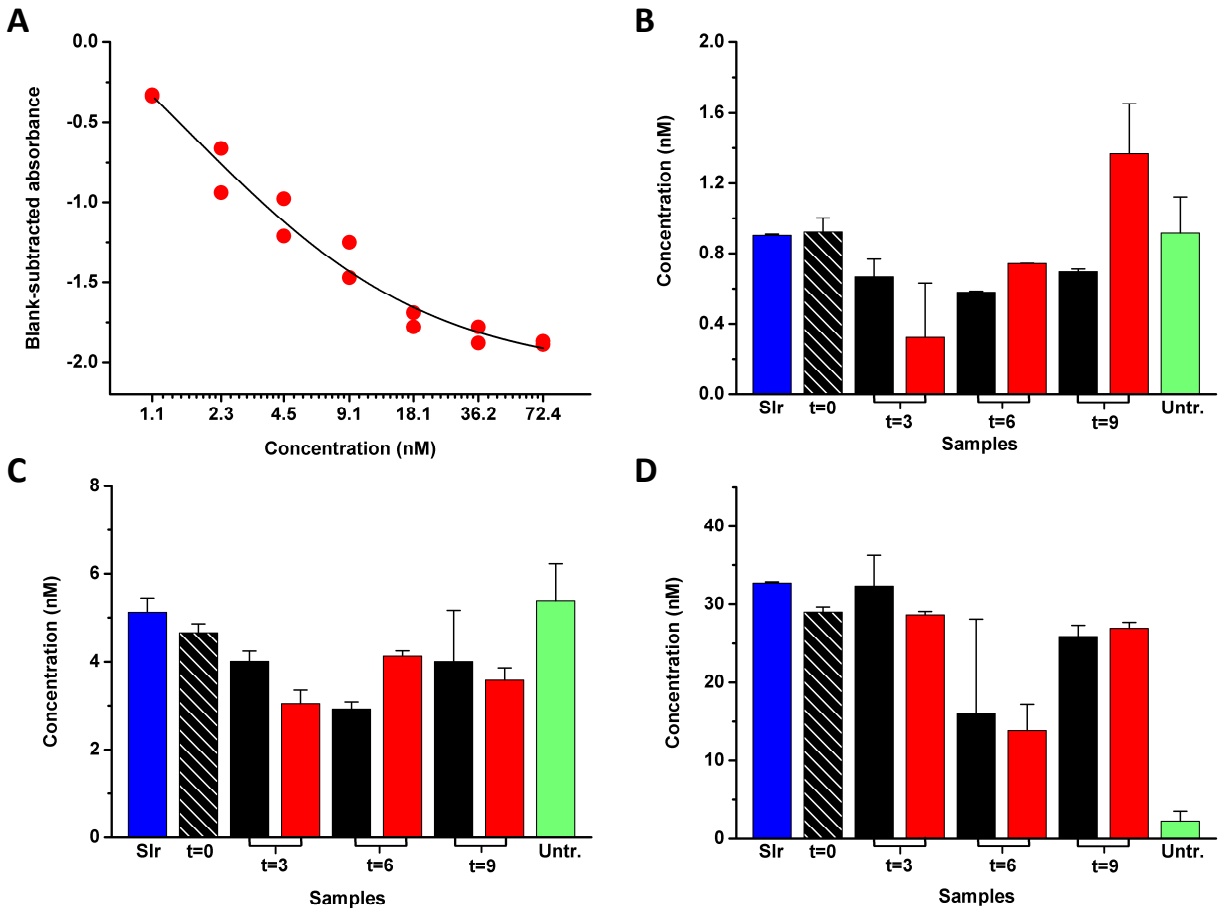

Fig 4.15 Assay of c-di-GMP concentration in HEK293T cells after lysis with different buffers. (A) Blank-subtracted absorbance values of the standards (red dots) measured at 450 nm plotted as a function of their known concentrations (in logarithmic scale). Data points were fitted with a 4PL function (Eq. 2). (B), (C) and (D) In these three graphs are grouped the concentration values of cell extracts obtained by performing the lysis in PBS (B), in 1% Triton buffer (C) and in Acetotintrile-Methanol buffer (D). Each sample was loaded in two wells of the plate to obtain double absorbance measurements and therefore two concentration values for each sample: in the graph are reported mean values ± SE. In each graph the samples are identified by the same colors and names used in Fig. 4.14 with the addition of untransfected cell extracts (green).

The first set of samples provided once again a c-di-GMP concentration for almost every sample less than 1.1, i.e. below the detection range (Fig. 4.15 B). This seemed to confirm again that, despite what is reported in the instruction manual, freeze-thaw cycles in PBS are not sufficient for a good membrane disruption. The samples from cells lysed with the Triton buffer turned out to have c-di-GMP concentrations appreciably above the background value (Fig. 4.15 C). As mentioned before, the amount of c-di-GMP synthesized by Slr1143 R250A should be taken as a reference for the desired synthesis activity. The concentration values obtained with BphSOpti-expressing cells were very similar to that of cells transfected with Slr1143 R250A: this suggested that the two constructs were synthesizing the same amount of c-di-GMP. An comparison of the concentration of different extracts of BphSopti-expressing cells, could give information about light dependency of the c-di-GMP production. The measurements provided concentration values between c.a. 3 and 5 nM for all the samples irrespective of whether the cells had been exposed to the light or not. Notably the estimated concentration value for the samples prepared from untransfected cells was in the same range: this may suggest that the light regulated enzyme was not generating c-di-GMP above the resting

concentration of cells. However, the instruction manual of the kit reports that a chemical lysis may cause unexpected ELISA results by a cross reaction between the lysis agent and the assay system. For this reason it was assumed that the measured values might be affected by an interaction between the buffer and the rest of the ELISA components.

With the third lysis buffer I was able to obtain the best results (Fig. 4.15 D). First of all the concentration values were on average 6 and 30 times bigger than the previous approaches with Triton and PBS respectively. This indicated that the cell lysis was more efficient and that the lysis buffer did presumably not interfere in a negative manner with the assay. The estimated c-di-GMP concenatrations were in the range of 15 and 32 nM. An overlook of the results obtained with different types of samples indicated that there was no significant difference between the concentration of the second messenger in the cells transfected with Slr 1143 R250A and its light-dependent counterpart. The cytoplasm sample from cells transfected with BphSOpti, 24 hours after transfection, turned out to have the same c-di-GMP concentration as the positive control. The lack of light regulation could be confirmed also by comparing the BphSOpti samples: there was no concentration difference on whether cells were exposed to the light or not. In this assay, the concentration value obtained from the untransfected cells was very close to the minimum value of the calibration curve. This result is reasonable for cells that do not express any digaunylate cyclase; together with the expected behavior of the standards, this is a proof of the robustness of the assay.

The results of the experiments suggested that the concentration values obtained with the third lysis method were the most reliable because they were all in the detection range of the assay, which did not seem affected by the buffer (as indicated by the negative control). This assay showed that the c-di-GMP levels produced by cells expressing Slr1143 R250A and BphSOpti are basically the same. Notably also the samples prepared at t=0, i.e. without any light stimulation, contained c-di-GMP at a concentration similar to that of the positive control (Fig 4.15 D). These results suggested the following interpretation: the BphSOpti system was actually able to synthesize c-di-GMP in a similar manner to the Slr1143 R250A enzyme. This synthesis however did not exhibit any light-regulation: between paired samples, which were exposed for the same length of time to light or dark, the assay showed no appreciable difference in terms of concentration of the second messenger. The data seemed to describe a homeostatic system in which c-di-GMP synthesis by BphS in the dark is not antagonized by the activity of Yhjh, which degrades the second messenger. The system presumably reaches an equilibrium in which the phosphodiesterase is not able to counteract the construct activity.

The assay of Fig. 4.15 D with the lysis in Acetonitrile-Methanol was repeated a second time to confirm the results. In this experiment the samples were loaded three times on the multi well plate in order to have more absorbance measurements. Moreover, the first sample from light-exposed cells was collected at 1.5 hours to test whether a shorter exposure time could beneficial for detecting a difference between light and

dark. The calibration curve from this experiments looked better, i.e. more S-shaped, compared to that from the previous assay (Fig. 4.16 A). The c-di-GMP concentration values obtained from this second test were more similar to data from Shao et al. (reported in Fig 4.13). All the samples had a concentration between 8 and 1 nM (Fig. 4.16 B). The sample taken from untransfected cells showed a concentration correspondent to the curve minimum, consistent with the fact that no c-di-GMP molecules are supposed to be synthesized in those cells. Also in this assay the c-di-GMP levels in the cell extracts of BphSOpti-expressing cells were very close to the positive control.

A comparison between the results obtained in this experiment and those from the previous quantification in 4.14 D indicated a considerable variability between the two assays, even though the conditions were the same in terms of transfection protocol, lysis buffer and assay protocol. In this second experiment the concentrations were lower and the shape of the calibration curved was different. This variability between two assays performed in the same conditions may indicate that this quantification system is very sensitive to indiscernible variations in the procedure. Nevertheless, in both the experiments the concentration of the positive control was always in between the detection range while that of untransfected cells sample corresponded to the minimum of the calibration curve. For this reasons the test was considered robust enough to get general information about the behavior of the enzymes. The important conclusion was the lack of light regulation. Cells kept in the dark or exposed to the light were synthesizing the same amount of c-di-GMP, that was similar to that of cells expressing Slr1143 R250A.

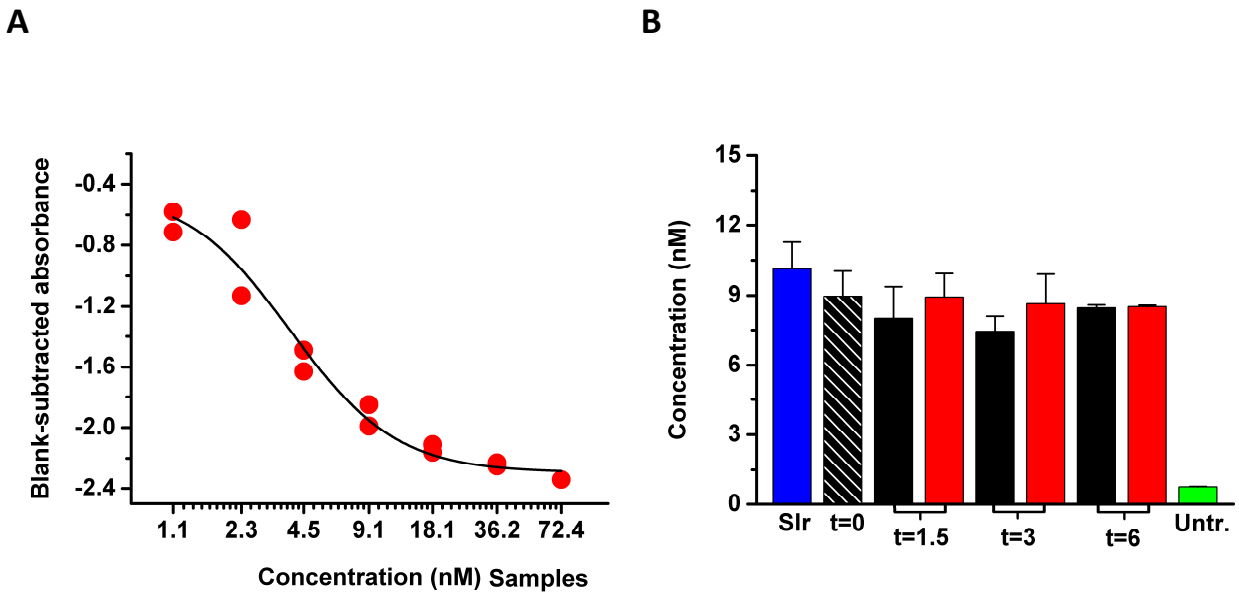

Fig 4.16 Assay of c-di-GMP concentration in HEK293T cells after lysis with Acetonitrile. (A) Blank-subtracted absorbance values of the standards (red dots) measured at 450 nm plotted as a function of their known concentrations (in logarithmic scale). Data points were fitted with a 4PL function (Eq. 2). (B) Concentration values of different cell extracts extrapolated from the calibration curve in (A). Each sample was loaded in three wells of the plate this time: in the graph are reported mean values ± SE. Samples are identified by the same colors and names used in Fig. 4.15 D.

The results of the ELISA assay seemed to contradict the data collected with the electrophysiological experiments and reported in Chapter 4.2, in which no effect on the voltage dependency of the HCN4 channel was observed in cells co-expressing the channel and the construct. If the optimized BphS protein is, according to the results from the ELISA assays, able to synthesize as much c-di-GMP as Slr1143 R250A one would expect an effect on the HCN4 currents in HEK293T cells co-rasfected with the channel and the construct.

In the light of these results I decided to repeat the electrophysiological measurements with BphSOpti transfected HEK293 cells. By repeating these experiments I wanted to exclude the possibility that the previous measurements were affected by some external factors, such as the number of culture passage, temperature in the room etc. HEK293T cells were transfected as for the ELISA assays and the experiments reported in chapter 4.2 in petri dishes. 24 hours after the transfection half of them were exposed to the light for 1.5 hours in order to be able to compare the results from electrophysiology with those from the ELISAs. The control cells transfected with HCN4 displayed the typical slowly activated inward currents previously described (fig.4.17 A). Tail currents amplitudes were plotted as a function of the voltage of the test pulse to construct the activation curves. The $V_{1/2}$ values were obtained from a fit of the activation curves with the Boltzmann equation (Equation 1). Representative activation curves from cells expressing different constructs of interest are shown in Fig 4.17 B. The average $V_{1/2}$ value of the control cells in this set of experiments was -103 ± 0.7 mV. No significant difference, neither in the currents kinetics or in the voltage dependency of the channel, was observed between the controls and the cells expressing the BphSOpti enzyme after incubation in the dark or in red light. As a consequence, also the $V_{1/2}$ values found in these two cell populations were not significantly different from the control cells. For cells kept in the dark the average $V_{1/2}$ was -102.6 ± 0.9 mV, while for their counterpart exposed to light it was -100 ± 1 mV (Fig. 4.17 C).

Data from the electrophysiological recordings and the ELISA remained contradictory. To have a better understanding on whether BphSOpti was actually producing some cytosolic c-di-GMP, which is sufficient to affect HCN4 gating, I developed an alternative manner to quantify the cyclic di-nucleotide. I reasoned that the large variability of the results between different ELISA assays of c-di-GMP (Fig. 4.15 D and 4.16 B) may indicate that this assay system is not sufficiently robust for uncovering small changes in c-di-GMP concentration. As an alternative method for measuring c-di-GMP concentrations in cells, I developed an immune-fluorescence based assay. With this new method it should be possible to monitor the production of c-di-GMP within a single cell. The main advantage of this new method is that no cell lysis is required and that the cell would act as a closed and unmodified entity in which the synthesis occurs. In the next chapter I will present the technique and the results obtained with it.

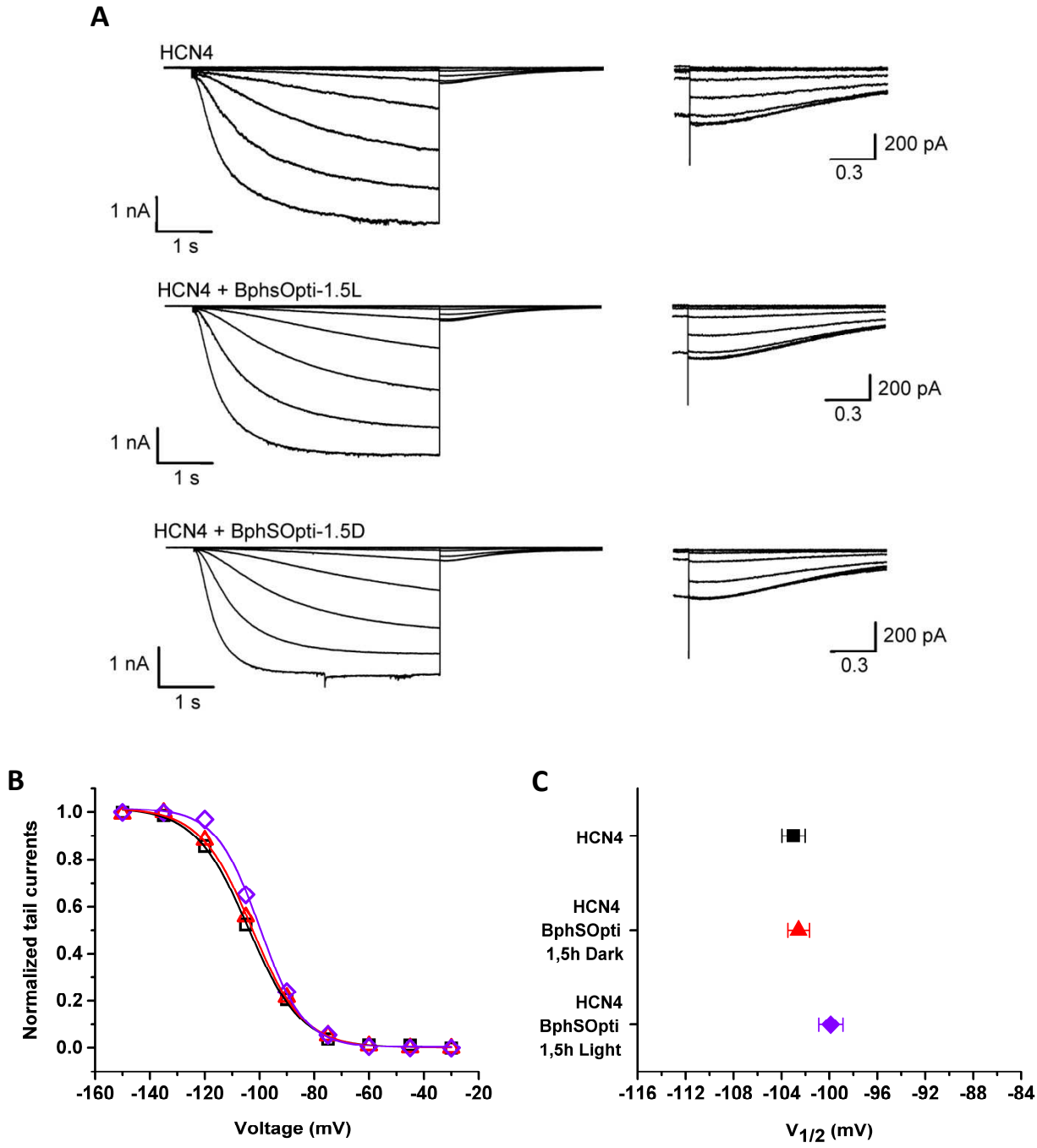

Figure 4.17. Additional electrophysiological data on HCN4 gating. (A) Exemplary currents elicited by voltage protocols in different cells (transfection and treatment reported on each). Tail currents (recorded at -40 mV) of each current family are enlarged and reported on the right for each measurement. (B) Normalized tail current amplitudes plotted as a function of the preceding test voltage. Black empty squares: HCN4; Red empty triangles: HCN4 + 0.75 µg BphSOpti-1.5 hours of dark; Violet empty diamonds, HCN4 + 0.75 µg BphS-1.5 hours irradiation. Data points were fitted with the Boltzmann equation (equation 1). Color code for the fitting is the same used for data points. (C) Mean ± S.E. of the $V_{1/2}$ values extrapolated from the fitting of the activation curves. Same color code used in (B); HCN4 N=6; HCN4 + 0.75 µg BphSOpti-1.5 hours of dark N=7; HCN4 + 0.75 µg BphS-1.5 hours irradiation N=5.

4.4 Quantification of the c-di-GMP via immuno-fluorescence.

It had been mentioned in the previous chapter that the measurements of the c-di-GMP concentration in HEK293 cells with the ELISA assays were contradictory to the data from electrophysiological experiments. In order to better understand if the optimized BphS enzyme can really synthesize sufficient c-di-GMP for shifting the activation curve of the HCN4 channel and if this synthesis is light sensitive, I developed another system to quantify the concentration of the molecule in human cells. The latter is based on the fact that cyclic di-nucleotides can induce the synthesis of Interferon Beta (IFN-β) in cells of the immune system (McWhirter et al., 2009; Burdette et al., 2011; Burdette and Vance, 2013). Cyclic di-nucleotides are indeed able to bind STING (Stimulator of Interferon Gene), a protein of the Endoplasmic Reticulum (ER) (Burdette et al., 2011). STING recruits and activates the TANK binding kinase 1 (TBK1), which, in turn, phosphorylates its downstream transcription factor: IFN regulatory factor 3 (IRF3); the latter is a key transcription factor required for the induction of IFN-β expression (Burdette and Vance, 2013). A scheme of the pathway is reported in Fig. 4.18.

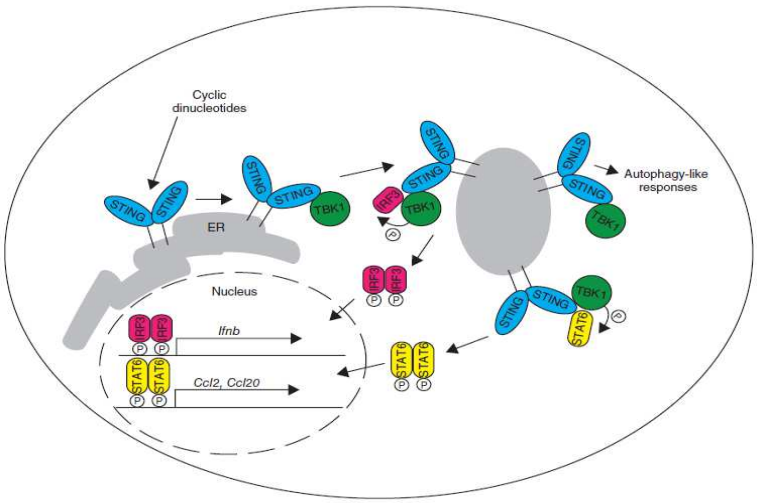

Fig 4.18 Schematic overview of the STING pathway. STING binds cyclic dinucleotides and recruits TBK1. TBK1 interacts with and phosphorylates IRF3, which induces its dimerization and translocation to the nucleus. IRF3 binds to promoter elements to induce transcription of INF-β (Burdette et al., 2011).

On the basis of this knowledge, the idea was to estimate the activity of BphSOpti and Slr1143 R250A by transfecting them into T cells and monitoring the synthesis of IFN-β induced by the c-di-GMP. The presence of the interferon in the cytoplasm of the cells can be detected optically in individual cells by using a specific couple of primary and secondary antibodies. A secondary antibody with absorbance/emission peaks equal to those of GFP was already present in the lab and successfully used for immune-fluorescence analysis, so a compatible primary antibody specific for IFN-β was purchased. Jurkat cells were chosen for these imaging experiments because they are an immortalized line of human T lymphocytes commonly used to study T cells signaling.

Before expressing the heterologous enzymes in Jurkat, we wanted to observe the ability of these cells to synthesize IFN-β when immune response is activated. To do this, a sample of Jurkat cells (1.5 x 10^6 cells) was exposed overnight to ImmunoCult, a mix of T cells activators. It was also prepared a similar sample of untreated cells that served as negative control, to monitor the basal levels of IFN-β in Jurkat cells. The following day, cells were fixated and permeabilized as described in Matherial and Methods. Afterwards, they were incubated overnight with the primary antibody and then exposed to the secondary antibody. After this preparation, the cells were ready to be imaged on a confocal microscope with light and filters suitable for observation of GFP-like signal. Pictures of the two samples were taken for further analysis of the fluorescence. In Fig. 4.19 are reported two exemplary images of the treated cells (A) and the negative controls (B). The sample of ImmunoCult-treated cells appeared to be heterogeneous. Most of the cells were brighter than the control cells, in which the fluorescence was weak and seemed to be localized close the membrane. In few treated cells the fluorescence was not so far from that of the controls, which means that the immune response was not the same for every cell. The fluorescence intensities of the cells were measured with an image analysis software (FIJI), in which the user can define a region of interest (ROI) in an image and quantify the brightness in the selected ROI. The software calculates the mean brightness of the pixels in the selected ROI giving a value for the Integrated Density (I.D.). ROIs were defined by following the borders of each individual cell, obtaining the correspondent I.D. values. The average I.D. for the control cells was 2613.3 ± 259.4 (N=36). This value was used as a reference value for the basal level of IFN-β in Jurkat cells. The treated cells showed a significantly higher green fluorescence compared to the negative controls: the average I.D. was 4753.8 ± 293.8 (N=68) (Fig. 4.19 C). This result suggested that an appreciable increase of the IFN-β in the cytoplasm can be detected with this method when the pathway is activated.

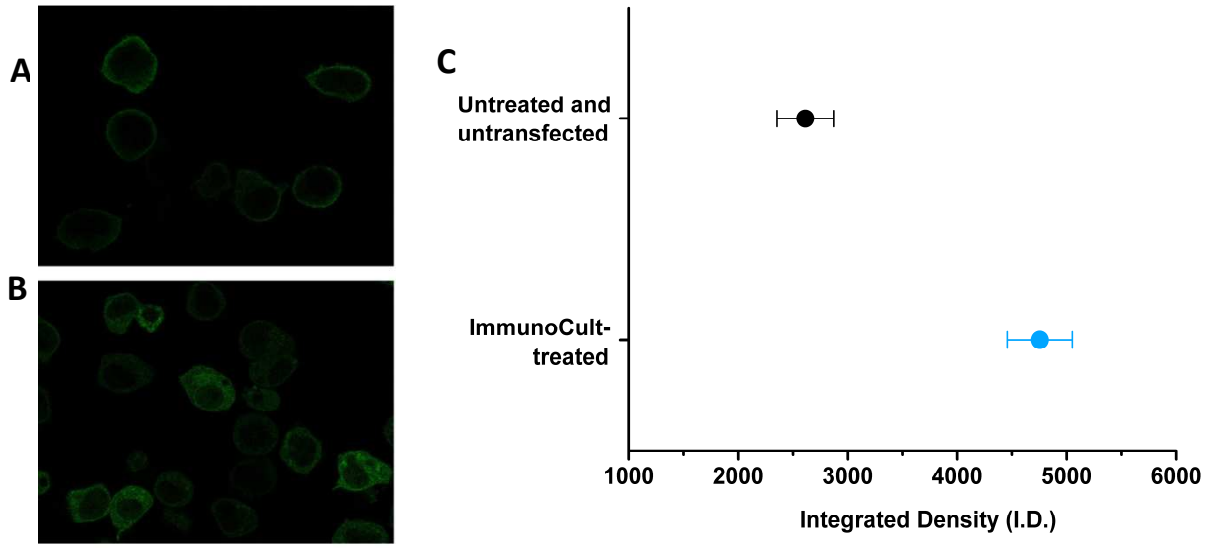

Fig. 4.19 Synthesis of INF-β in Jurkat T-cells. (A) Picture of a group of jurkat cells untreated and untransfected. (B) Picture of a group of Jurkat cells treated with ImmunoCult overnight. (C) Mean ± SE of I.D. values from control cells (black circles, N=36) and from activated cells (blue circles, N=68).

At this point I moved on with the estimation of the activity of the constructs. For this experiments the presence of IFN-β could again be detected with the fluorescent tag on the secondary antibody, while the transient expression of a construct could be verified by co-transfection with a fluorescent protein. The fluorescent tag on the secondary antibody and the co-transfected fluorescent protein should have different absorption/emission peaks. In this way it is possible to detect two different signals: the signal emitted by the fluorescent protein is an indirect measure of the expression level of the enzyme, while the signal emitted by the antibody detects the abundance of interferon in the cytoplasm. It can be assumed that the expression of the proteins of interest after transfection with exogenous DNA can vary from one transfection to another. Hence also the number of enzymes will vary from cell to cell. For this reason the data from each cell can be expressed in a ratiometric manner as the ratio "expression signal/IFN-β signal". A quantitative comparison of the "expression signal/IFN-β signal" ratio from cells expressing Slr1143 R250A and BphSOpti can tell whether the light sensitive synthetic protein synthesizes the same ammount of c-di-GMP as the constitutively active enzyme. The latter hypothesis was suggested from the ELISA measurements. In the case of the BphSOpti system, it must be kept in mind that the final concentration of c-di-GMP depends on the concerted activity of the cyclase BphS and the phosphodiesterase YhjH.

I decided to use the TdTomato as a fluorescent protein to monitor the expression of the enzymes since it absorbs and emits light at different wavelengths than those of GFP. In a first set of experiments the performance of the system was tested with the Slr1143 R250A construct as a positive control. Jurkat cells were therefore transfected, using the Lipofectamine, with 0.5 µg of HCN4 + 0.5 µg of Slr1143 R250A. Jurkat cells require a transfection protocol different from that used for HEK293T cells (details are found in Matherials and Methods). It turned out that a double transfection of the Jurkat cells was very difficult as there was no detectable fluorescence in the cytoplasm of the transfected cells. This is a well know phenomena in these cells which often exhibit a transfection frequency of ~10% when transfected with a single plasmid. Since these cells are already harder to transfect with a single plasmid, they may not be suitable for a double or triple transfection. To circumvent this problem, the cells were transfected with only the plasmid containing the construct and the fluorescent protein, without HCN4. 24 hours after the transfection the cells were fixated, permeabilized and exposed to the two antibodies. Single Jurkat cells were then imaged on a confocal microscope, where the two emission signals (red from the TdTomato and green from the antibody) could be observed by using different excitation wavelengths and appropriate filter sets. Bright light images were used to check the morphology of the cells. For each cell or group of cells, three pictures were taken: one with the light and the filters to see the antibody green signal, one with those necessary for the detection of the TdTomato fluorescence and one with unfiltered light.

Fig. 4.20 A reports an exemplary set of images from a group of Jurkat cells. The image contains cells that emit the red TdTomato signal as well as a strong green fluorescence from IFN-β. The latter was generally more intense than the emission in the red signal (blue arrows in the figure). Only a few cells showed a different behavior: they emitted a strong red signal from TdTomato and only a poor green signal from IFN-β. A closer examination of these cells showed that they displayed peculiar features: the red signal was diffused throughout the whole cell and the nucleus was undistinguishable from the cytoplasm (like the one indicated by the yellow arrow). When examined with the white light, the respective cells exhibited a more irregular morphology than other cells; notably Jurkat cells are suspension cells, which are generally perfectly round with a very similar size. In some cases, the membranes of the abnormal fluorescent cells occurred wrinkled. On the basis of these considerations I assumed that the Jurkat cells, which are displaying these feature are unhealthy; for this reason they were not included in the statistical analysis.

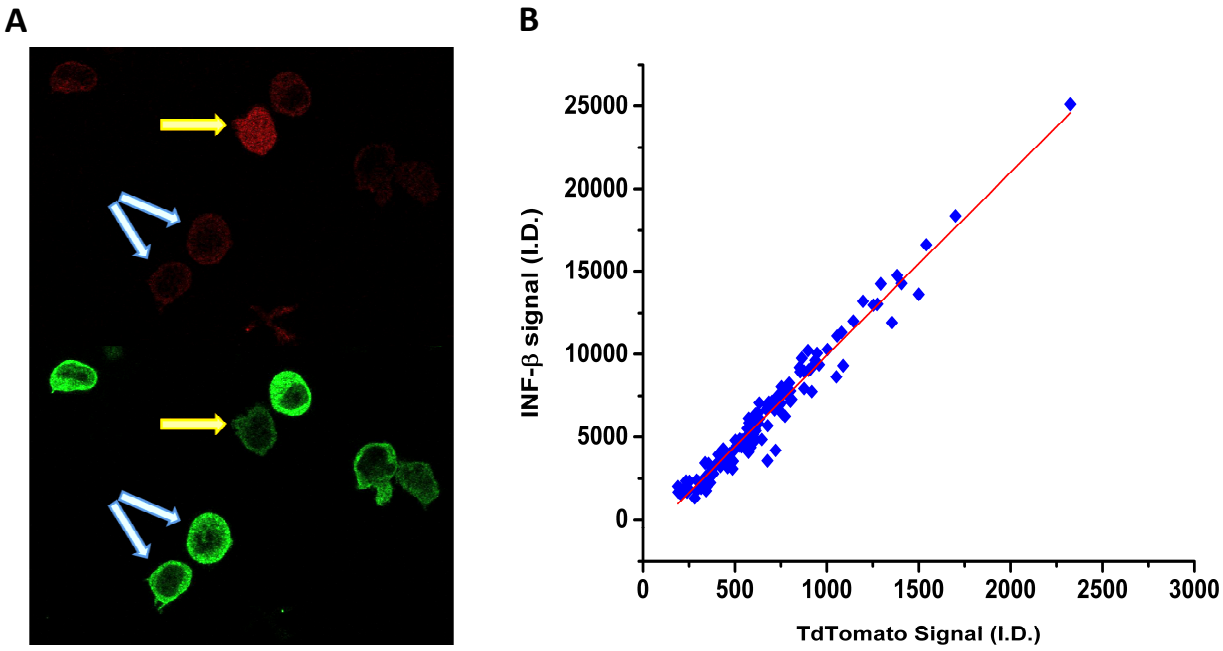

Fig. 4.20 The activity of Slr1143 R250A triggers the expression of IFN-β. (A) Exemplary set of pictures taken at the confocal microscope for a group of Jurkat cells transfected with Slr1143 R250A. The cells indicated by the blue arrows are a good example of what has been observed in most of the cells. They emits a read signal from the TdTomato and a much stronger green signal from the IFN-β. The yellow arrow indicates a cell in which the red signal is stronger than the green one. As explained in the text, this type of cells were discarded. (B) I.D. values for the green signal (IFN-β) measured in cells transfected with Slr1143 R250A plotted as a function of the I.D. values for red signal (TdTomato) (N=126). To better describe the relationship between the two fluorescence intensities, data points were fitted with a linear function (red line).

The fluorescence intensities were again measured with FIJI. To describe the relationship between the concentration of the BphS enzyme in a cell and the IFN-β concentration, as an indirect estimation for the c-di-GMP concentration, the two fluorescent values were plotted in a scatter plot (Fig. 4.20 B) with the red signal I.D. values on the x axis and the green I.D. values on the y-axis. The data from this plot show that the two values from individual 126 cells exhibit a striking linear relation with a correlation coefficient of +0.98

and a slope of 11 ± 0.2. It is noteworthy that the average I.D. value of the untransfected cells (Fig. 4.19 C) corresponds to the smallest values of the curve in Fig. 4.20 B. I reasoned that the higher green fluorescence in Slr1143 R250A sample, compared to negative controls, was due to the presence of the exogenous enzyme. The results of these experiments suggested indeed that an expression of Slr1143 R250A in Jurkat cells triggers the synthesis of IFN-β presumably via an increase in c-di-GMP concentration. The data furthermore suggest that the increase in the concentration of IFN-β is a function of the concentration of the BphS enzyme.

In the following set of experiments the same measurements were repeated with the light-regulated enzyme. As described in previous chapters, the multi-gene sequence BphSOpti was inserted in a plasmid that lacked a fluorescent tag. I then designed an AQUA cloning procedure to introduce after YhjH another 2A sequence and a Tdtomato, obtaining in this way a single suitable for single transfections of the Jurkat cells. Three dishes of cells were transfected: the first one with 1 µg of Slr1143 R250A (to have a positive control) and the other two with 1 µg of the new plasmid. 24 hours after the transfection, one of these two dishes was exposed to pulsed light for 1.5 hours. After this time, Jurkat cells from the three petri dishes were separately collected and prepared for the staining. The cell samples were then imaged on the confocal microscope, where it was possible to observe a high number of cells emitting the TdTomato signal in each of the three dishes. Like in the previous assay, these cells also emitted in the green spectrum. Pictures were taken at the microscope and analyzed with FIJI to investigate the fluorescence intensities.

First, I analyzed the fluorescence of the cells transfected with the positive control Slr1143 R250A. Red fluorescence from the TdTomato was linearly correlated with the green fluorescence from IFN-β (correlation coefficient +0.99; m = 14 ± 0.2; N=40) (Fig. 4.21 A). The vast majority of the I.D. values were larger than the average value of the negative control. In cells, which were expressing BphSOpti but kept in the dark the two fluorescent intensities exhibited the same linear relationship (fig 4.21 B) with a correlation coefficient of +0.96 and a slope of 15.6 ± 0.8 (N=27). These data seemed to indicate that the enzyme activity in the dark is already comparable to that of the positive control Slr1143 R250A. The same analysis was done for the cells expressing BphSOpti and treated with pulsed light. The two fluorescence intensities showed also in this case a linar relationship (Fig 4.21 C). Even if data points were more dispersed, a linear equation was perfectly able to follow the trend of their distribution: the correlation coefficient was +0.86 and the m value was 17.6 ± 2 (N=28). For this cell population the activity of the enzyme seems to be similar to that observed in cells kept in the dark: the slopes of the two lines were not too different (Fig. 4.21 D). The results of this analysis indicated that light had no positive effect on the production of IFN-β and hence on the underlying production of c-di-GMP.

If we take the correlation between the concentration of the enzyme and the synthesis of IFN-β as an indirect estimate for the BphS enzymatic activity, the data confirm the results from the ELISA assay. First, BphS is able to synthesize as much c-di-GMP as its constitutively active counterpart even if its effect on the HCN4 channel could not be observed in HEK293T cells. Second, the activity of BphS does not seem to be affected by red light.

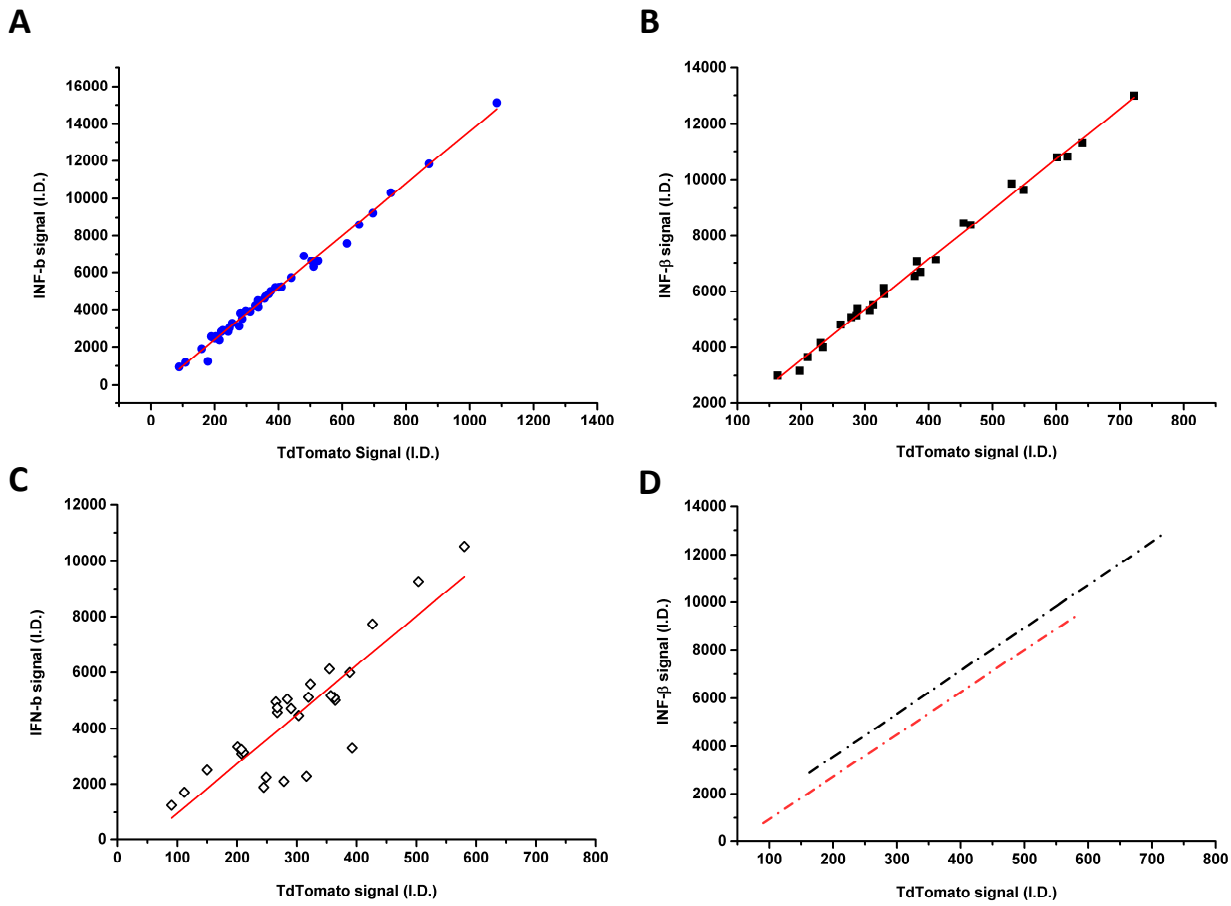

Fig. 4.21 Estimation of the BphS activity in light and dark. (A) I.D. values for the green signal (IFN-β) measured in cells transfected with Slr1143 R250A plotted as a function of the I.D. values for red signal (TdTomato) (N=40). (B) I.D. values for the green signal (IFN-β) measured in cells transfected with BphSOpti and kept in the dark, plotted as a function of the I.D. values for the red signal (TdTomato) (N=27). (C) I.D. values for the green signal (IFN-β) measured in cells transfected with BphSOpti and exposed to light for 1.5 hours, plotted as a function of the I.D. values for the red signal (TdTomato) (N=28). Data points in (A), (B) and (C) are fitted with a linear equation. (D) Linear equations used to fit the data points in (B) (grey) and (C) (red).

It has been mentioned that the final concentration of c-di-GMP in a cell with BphSOpti is determined by the combined and antagonistic action of the cyclase and the phosphodiesterase. The latter is required to maintain low levels of c-di-GMP in the dark. So one possible explanation for the lack of light regulation could be that the dark activity of the enzyme is not compensated by the phosphodiesterase. The capacity of this enzyme might be overloaded already by the dark activity of the enzyme. In this case it may not be able

to keep up with the activity of the BphS enzyme with the effect that a difference in c-di-GMP between light and dark may be masked. To understand the contribution of the phosphodiesterase to the final concentration of c-di-GMP, the experiments were repeated with a construct which lacked the phosphodiesterase. If the aforementioned hypothesis is correct elimination of the phosphodiesterase should generate a positive bias for an increase in c-di-GMP concentration as a result of BphS activity. In this case it might be possible to detect a small amount of un-cleaved nucleotide.

To eliminate YhjH from the construct, the plasmid was double-digested with two restriction enzymes cutting right before YhjH and after the stop codon of the TdTomato. The linearized plasmid was separated from the other fragment by gel electrophoresis and purified. A TdTomato was then inserted in the plasmid via AQUA cloning after the 2A of BphS. The new plasmid was transfected into Jurkat cells, which were then treated and analyzed as in Fig. 4.20. The analysis of the fluorescence intensities is reported in Fig 4.22. In both experimental conditions namely with cells kept in the dark (A) or exposed to light (B) the red and green fluorescent signals were again linearly correlated. In cells kept in the dark or exposed to light the slope of the curve was 14.2 ± 0.2 (N=19) and 14.8 ± 2 (N=20), respectively. Notably there is no difference between the two values indicating again an absence of light sensitivity of the BphS enzyme. Moreover, the slope values are not bigger than that calculated for the experiments in which the YhjH was present and are indeed similar to that of Slr1143 R250A from the same set of measurements. This suggested that the presence/absence of the phosphodiesterase has no impact on the synthesis of the IFN-β reporter and hence on c-di-GMP production.

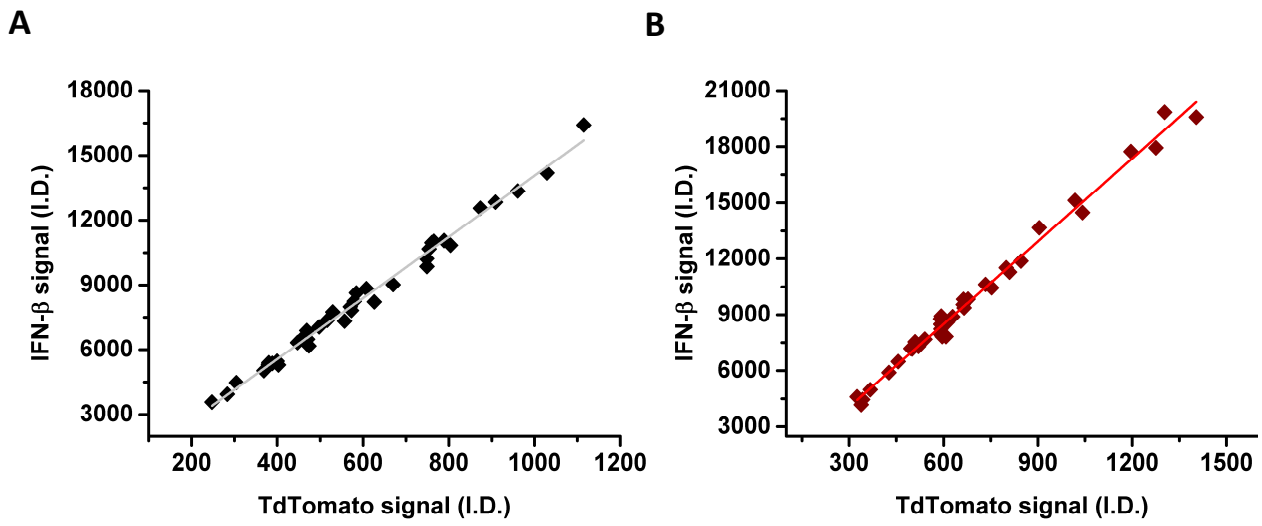

Fig 4.22 Estimation of the impact of YhjH on the BphSOpti system. (A) I.D. values for the green signal (IFN-β) measured in cells transfected with only BphS and kept in the dark, plotted as a function of the I.D. values for the red signal (TdTomato). (B) I.D. values for the green signal (IFN-β) measured in cells transfected with only BphS and exposed to light for 1.5 hours, plotted as a function of the I.D. values for the red signal (TdTomato). Data points in (A) and (B) are fitted with a linear equation (grey and red).

4.5 Additional information

In the following tables are reported the parameters of the non-linear curve fitting showed in the figures.

Fig. 4.1 c – black	A1	1,0147 ± 0,01378	Fig. 4.14 A	A1	-0.47379 ± 0.16305
	A2	-0,01693 ± 0,01138		A2	-2.54816 ± 0.09327
	x0	-109,97454 ± 0,75614		x0	5.91888 ± 0.82498
	dx	13,28941 ± 0,71979		p	1.34424 ± 0.26839
Fig. 4.1 c – blue	A1	1,00847 ± 0,00995	Fig. 4.15 A	A1	0.73049 ± 1.61478
	A2	0,00136 ± 0,00646		A2	-2.05559 ± 0.23558
	x0	-117,97529 ± 0,48109		x0	1.95145 ± 2.61152
	dx	11,21268 ± 0,43482		p	0.80597 ± 0.46069
Fig. 4.6 c – black	A1	0,99509 ± 0,01594	Fig. 4.16 A	A1	-0.43861 ± 0.2363
	A2	-0,01931 ± 0,01603		A2	-2.29407 ± 0.08261
	x0	-97,68674 ± 1,03118		x0	3.9242 ± 0.76701
	dx	12,54811 ± 0,94175		p	1.76725 ± 0.51808
Fig. 4.6 c – blue	A1	1,00928 ± 0,01307	Fig. 4.17 B black	A1	1.01795 ± 0.01017
	A2	-0,01016 ± 0,00994		A2	0.00257 ± 0.00657
	x0	-107,53026 ± 0,71036		x0	-104.13818 ± 0.45094
	dx	11,4975 ± 0,64951		dx	9.66888 ± 0.40686
Fig. 4.6 c – black dashed	A1	1,01745 ± 0,01367	Fig. 4.17 B red	A1	1.01674 ± 0.01044
	A2	-0,00936 ± 0,01505		A2	0.00115 ± 0.00712
	x0	-87,35274 ± 0,80934		x0	-102.81618 ± 0.47116
	dx	10,99424 ± 0,75135		dx	9.41143 ± 0.42393
Fig. 4.6 c – blue dashed	A1	0,99993 ± 0,01539	Fig. 4.17 B violet	A1	1.01632 ± 0.01257
	A2	0,00318 ± 0,01593		A2	0.00329 ± 0.00978
	x0	-89,06617 ± 0,88237		x0	-99.88526 ± 0.58078
	dx	9,78787 ± 0,80604		dx	8.03066 ± 0.49958
Fig. 4.8 - black	A1	1,02227 ± 0,00941			
	A2	0,00209 ± 0,00581			
	x0	-105,57471 ± 0,40269			
	dx	9,45922 ± 0,36278			
Fig. 4.8 - red	A1	1,01238 ± 0,0132			
	A2	-0,00611 ± 0,01004			
	x0	-106,18536 ± 0,71841			
	dx	11,6219 ± 0,66027			
Fig. 4.10- black	A1	1,00937 ± 0,00589			
	A2	0,00155 ± 0,00465			
	x0	-97,83592 ± 0,29465			
	dx	9,80697 ± 0,26261			
Fig. 4.10- red	A1	1,00826 ± 0,01326			
	A2	1,74859E-4 ± 0,0105			
	x0	-97,19258 ± 0,67851			
	dx	10,63125 ± 0,61575			
Fig. 4.10- brown	A1	1,01414 ± 0,01697			
	A2	0,01193 ± 0,01229			
	x0	-100,27211 ± 0,82441			
	dx	10,16516 ± 0,74177			
Fig. 4.10- violet	A1	1,01048 ± 0,01215			
	A2	0,00112 ± 0,01037			
	x0	-94,63032 ± 0,65408			
	dx	11,38391 ± 0,60538			
Fig. 4.12- black	A1	0,99623 ± 0,01526			
	A2	6,90877E-4 ± 0,01184			
	x0	-99,75144 ± 0,72334			
	dx	8,24174 ± 0,62471			
Fig. 4.12- red	A1	1,00374 ± 0,00615			
	A2	4,02983E-5 ± 0,00493			
	x0	-99,00137 ± 0,28881			
	dx	7,69234 ± 0,24222			

5

CONCLUSIONS AND FUTURE PROSPECTIVES

From the results obtained so far it is possible to draw some conclusions about the functionality of the tested constructs. The experiments in which the HCN4 channel and the constitutive Slr1143 enzyme were co-expressed in HEK239T cells clearly show that the latter results in a measurable increase in c-di-GMP in these cells an that this elevated levels of the ligand affect the voltage dependence of the HCN4 channel. The increase in c-di-GMP concentration in Slr1143 expressing cells was confirmed by two independent methods and the left shift of the activation curve of HCN4 between Slr1143 expressing cells and control cells is significant. The coincidence between an elevated concentration in c-di-GMP and a modulation of HCN4 gating strongly supports previous reports, which advocated cyclic di nucleotides binding to HCN4 and a consequence on channel gating (Lolicato et al. 2014). The present data further advocate a correlation between the catalytic activity of the enzyme and a shift of the voltage dependence of HCN4. The data show that an improvement in the synthesis of c-di-GMP by the mutation R250A in the Slr1143 enzyme, causes an increase in the number of measurements in which the activation voltage of HCN4 is negative shifted with respect to the control. All this contradicts the results from an other publication in which no binding of cyclic di-nucleotides to the channel was observed (Hayoz et al., 2017).

While the present data confirm a previous report on an interaction of c-di-GMP with the HCN4 channel (Lolicato et al. 2014) they reveal also some differences to the latter study. The aforementioned study reported that c-di-GMP did not modulate the channel at endogenous physiological concentration of cAMP in HEK293T cells; in their measurements c-di-GMP was only effective in reverting the effect of additionally added cAMP. In contrast to these data the present recordings show already an effect of c-di-GMP on HCN4 gating with basal physiological cAMP concentrations. The reason for the different results of the two studies might be related to the different type of experiments. While c-di-GMP was continuously synthesized in the present study it was added together with or without cAMP via the patch pipette in the study by Lolicato and coworkers (Lolicato et al. 2014). Based on the two different experimental systems, the following hypothesis could be formulated. Cells have a basic level of cAMP, which determines the position of the activation curve of HCN4 channels. With a continuous synthesis of c-di-GMP -as in the present study- the $V_{1/2}$ value is left shifted with respect to control cells, which do not synthesize the cyclic dinucleotide. During a whole-cell recording the concentration of cAMP and of c-di-GMP presumably decrease together as a result of a perfusion from the patch pipette. The $V_{1/2}$ value is, at any time, reflected by the concerted activity of both agents. The situation is different in the setting used by Lolicato and co workers (Lolicato et al. 2014). In their case c-di-GMP was dyalized into the cell while cAMP was already diluted out. It is reasonable to assume that the delayed arrival of c-di-GMP at its binding site with the concomitant decrease in cAMP concentration masks any effect of the cyclic dinucleotide on HCN4 gating. One aspect of this hypothesis deserves further thinking. In a recent paper, the HCN4 channel was exposed to a synthetic peptide that stabilizes the unbound conformation of the CNBD (Saponaro et al., 2018). In the presence of the peptide and 10 uM cAMP, they observed that the $V_{1/2}$ was exactly the same as the control cells, i.e.

without the peptide and the cAMP. The observed backshift of the activation curve suggested that the peptide was able to counteract the effect of cAMP. Interestingly, the fact that the measured $V_{1/2}$ was not more negative than the controls implies that in an HEK293T cell endogenous cAMP is not so crucial in determining the activation voltage of the HCN4. So another possible explanation of the observed effect may consider the fact that the c-di-GMP has always been present during the formation of the channel. This may cause an alteration of the voltage dependence that is independent from the endogenous cAMP. This second hypothesis implies an effect of c-di-GMP and CLP that has not been observed so far. For this reason, before further speculating, it is more reasonable to test whether the direct effect of c-di-GMP on HNC4 gating is actually due to the relative dilution timing of the two messengers. This can be done in further experiments by performing measurements with perforated patches.

Dilution problems may be an explanation also for the fact that the ability to counteract cAMP effect seemed to be concentration dependent. In Lolicato et al. (2014), the c-di-GMP and the cAMP were delivered via the pipette into the cytoplasm together. In the present experiments, on the contrary, the whole-cell configuration causes a decrease in the concentration of the cytoplasmatic c-di-GMP, while the concentration of cAMP is increasing. In the present study it was possible to measure a backshift of the activation curve by a few mV only with non-saturating concentrations of cAMP in the recording pipette. The results of these experiments suggest that the recordings conditions and the perfusion of the cells with second messengers can be crucial for the response of the cells.

More conclusions from this study can be drawn about the synthetic phytochrome BphS and its antagonist YhjH. The data show that the combined BphS-YhjH system is not properly light-regulated. Both the ELISA assays and immune fluorescence measurements reveal a high dark activity of the system. Both assays were unable to detect any difference in the c-di-GMP concentration between cells kept in the dark or exposed to stimulating red light. Moreover both assays indicate that the c-di-GMP concentration in cells expressing BphS-YhjH was about the same as in cells expressing the constitutively active enzyme Slr1143. It is well known that the light regulated BphS enzyme is leaky meaning that it also synthesizes c-di-GMP in the dark. For this reason it is generally co-expressed with the phosphodiesterase YhjH, which should balance the c-di-GMP production in the dark. This means that the actual c-di-GMP concentration in a cell is a delicate equilibrium between c-di-GMP synthesis and destruction. In this scenario an elevated c-di-GMP concentration in the dark could result from an insufficient activity of the phosphodiesterase. This interpretation is indirectly supported by the present data. In experiments in which BphS was expressed without the YHjH phosphodiesterase, the resulting c-di-GMP concentration was not much different compared to cells in which both enzymes were co-expressed. The results of these experiments imply that the YHjH phosphodiesterase is not sufficiently active for balancing the dark activity of the BphS cyclase. In the case of a large dark background in c-di-GMP synthesis it is not surprising that red light is not able to

stimulate an elevated level of the second messenger. The data strongly suggest that the expression and/or function of the YHjH phosphodiesterase needs to be improved in order to make this system suitable as an optogenetic tool.

The prominent dark activity of the BphS cyclase and the concomitant elevated c-di-GMP concentration in these cells predict that also the activation curve of HCN4 should be shifted in these cells with respect to non-transfected controls. This predicted shift however is not detected in the present experiments. The voltage dependence of the HCN4 channel in HEK293 cells was not different between cells co-transfected with Bphs-YhjH and control cells. The result of these data cannot be finally explained here. However, a comparison between the different panels in Fig. 4.20 may suggest a possible explanation of the conundrum. The fluorescent values on the x-axis of graphs A, B and E, which are an indirect measure of the expression levels for the cyclases, show that the Slr1143-IRES-TdTomato reaches higher maximal expression levels than the BphS-2A-YhjH-2A-TdTomato construct. For patch clamp experiments with HEK293 cells expressing Slr1143 always the brightest cells were chosen for measurements. Based on the data of Fig. 4.20 it is reasonable to assume that these cells were also those with the highest concentration of c-di-GMP. Hence the shift of the activation curve from Slr1143 expressing cells may be generated by high concentrations of c-di-GMP. The electrical experiments with BphS-2A-YhjH expressing cells were done in a different manner. In this case the cyclase/phosphdiestearse were co-transfected with a plasmid containing GFP. In this case the fluorescence intensity is not a measure for the expression of the cyclase. In this scenario it is reasonable to speculate that cells were choses for the electrical recordings in which the BphS/YhjH expression was not optimal and hence the c-di-GMP concentration below a functional concentration threshold. In further experiments it will be necessary to measure HCN4 channel gating in Slr1143 and BphS-2A-YhjH expressing cells with the same protocol. Based on the data from Fig. 4.20, which suggest a large range of expression between individual cells and a linear correlation between cyclase expression and c-di-GMP concentration, the fluorescent tagged cyclase would be the method of choice. The large cell to cell variability (Fig. 4.20) also implies that a much larger of cells has to be measured in patch clamp experiments for a robust insight into the effect of the cyclase activity on HCN4 activity.

The main goal of the present study was the development of an optogentic tool, which is able to modulate HCN4 activity by penetrating red light. The present work does not provide such a tool but presents some major advances. The data strongly support that a precise regulation of c-di-GMP concentration by red light requires a better compensation of the dark activity of the BphS enzyme. It has been shown in previous studies that a tuning of the expression of YhjH is crucial for obtaining this desired effect (Ryu et al., 2014). In the present study, YhjH is not contributing to the final concentration of c-di-GMP neither in cells kept in the dark nor in those exposed to red light. It is therefore reasonable to think that the expression of the phosphodiesterase must be increased.

One approach to achieve this goal could be obtained by transfecting a different amount of DNA for the two proteins. For this purpose YhjH could be moved to a different plasmid, under the same promoter. In this way one plasmid will contain only BphS and the other only YhjH. The two plasmids could be transfected together into HEK293T by using different concentrations for each plasmid. For example the DNA for BphS and YhjH could used in a 1:2 or 1:3 ratio in co-transfections. By optimizing this ratio it might be possible to find a good balance between the two antagonistic enzymes and to achieve a robust increase in c-di-GMP concentration in response to light.

An alternative approach could involve the tuning of protein synthesis, taking advantage of the work by Ferreira and colleagues (Ferreira et al., 2013). These authors show different ways by which it is possible to decrease the translation of a gene of interest. In one strategy the translation initiation site (TIS) could be modified. This is a short sequence, which is recognized by the ribosome and is composed of three bases upstream the methionine, the start codon and the first base after it. Many human genes present the conserved motif (G/C)CCAUGGG as a TIS. The insertion of an UUU triplet right before the start codon causes a decrease in the expression of the protein up to -50%. In this way it might be possible to favour the expression of the phosphodiesterase over the cyclase. For a more fine regulation of the translation levels, a small ORF, coding for only two amino acids, can be inserted 5 bases upstream the gene of interest (uORF). By using different combinations of triplets before the start codon of the target gene and of the uORF, it is possible to decrease the synthesis of a protein from-50% to -99%.

In addition to the previous method, which increase the activity the phosphodiesterase over the cyclase, also improvement in the light sensitivity of the cyclase could help in the construction of the desired optogenetic tool. Such a cyclase with an higher light-dependent activity, was recently developed by the group of Prof. Gomelsky at the Wyoming University (unpublished data). In further work this protein might be expressed at a very low concentration in cells. The dark activity of this protein might then be better compensated by YhjH. Because of the increased light sensitivity the improved cyclase might then produce a sufficient rise in c-di-GMP concentration for modulation of HCN4 gating.

6

MATERIALS AND METHODS

6.1 Molecular Biology

PCRs

PCRs were performed for different purposes: insertion of mutations, preparation of inserts for cloning, screening of colonies by colony-PCR. Two thermal cyclers have been used in this work: BioRad Tm100 and Biolab Cycler48 (Bio-Rad, Hercules, CA, USA; Biolab, Bebensee, Germany). The polymerases for the reactions were Phusion and Taq from ThermoFisher (Waltham, MA, USA) and NEB (Ipswich, MA, USA). All the reactions were prepared according to the manufacturer's instructions. For GC-rich sequences, the appropriate buffer was used. When DMSO was needed, its final concentration never exceeded 3%. The oligonucleotides (Sigma-Aldrich, St. Louis, MO, USA) were diluted in sterile ddH_2O to a final concentration of 100 uM and kept at -20 °C.

Phusion polymerase was used to amplify a gene of interest, to add flanking sequences or for overlapping PCRs. The thermal cycler protocols were designed according to the instructions provided with the enzyme. The 3-steps protocol, with annealing temperature at Tm - 4°C, worked well in most of the cases. All the PCR products were separated by gel electrophoreses on 0.8-1% agarose gels with 0.6 µg/mL MidoriGreen in 1x TAE (Tris-Acetate-EDTA) buffer. The DNA was then gel-purified and quantified as described below.

Taq polymerase was chosen for colony-PCRs. Colonies were picked with a pipette tip and re-suspended in 10 µL of sterile ddH_2O. 1 µL of each cell suspensions was then added to the reaction mixtures, while the rest was left at 4°C. Thermal cycler 3-steps protocols were designed according to the manufacturer's instructions. Once the positive colonies were determined by gel electrophoreses, the respective cell suspensions were re-inoculated in 8 to 130 mL of LB (Luria-Bertani) medium with appropriate antibiotic selection and grown for 16 hours (250 r.p.m. at 37°C) for mini/midi preparations (see below).

GEL EXTRACTION

The bands of interest (PCR products or linearized plasmids) were cut out from agarose gels using an ethanol-sterilized scalpel and transferred into 2 mL reaction tubes. Two different kits have been used in this work: Zymoclean Gel DNA Recovery from ZymoResearch (Freiburg, Germany) and QIAquick PCR & Gel Purification Kit from Quiagen (Hilden, Germany). The protocols of the two kits are the same:

1) Three volumes of the appropriate buffer (e.g. for 100 mg of gel slice 300 µl of buffer) were added to the gel slices and the latter were melted at 50-55°C for 10 minutes. 2) The gel slices melted in the buffer were loaded onto purification columns provided with the kit. 3) The columns were centrifuged for 1-2 minutes at $\geq$ 13000 x g (Sigma centrifuges, model 1-14) and the flow-through was discarded. 4) Columns were then

washed with the indicated buffer and centrifuged at 13000 x g. 5) The DNA was eluted with the recommended volume of water. DNA concentration of the samples was determined as described below.

DNA CONCENTRATION QUANTIFICATION

DNA sample concentration was determined with a UV-Vis spectrophotometer (*NANODROP ONE*^{C} from ThermoFisher, Waltham, MA, USA). Water was used for the blank measurement; the same volume of DNA samples was next loaded on the spectrophotometer. The drops of blank and DNA samples form a liquid column of known height between two pedestals. Light from a xenon flashlamp passes through this column and is detected by the internal spectrometer. A graph with the absorbance of the sample as a function of the wavelengths appears on the screen within few seconds, together with a table containing the concentrations of the samples in ng/µL, the 260/280 ratio and the 260/230 ratio.

TRANSFORMATION OF COMPETENT BACTERIAL CELLS

DNA was transformed in competent *E. coli* cells (Dh5α strain) via heat shock. 10 ng DNA was added to 50 µL of competent cells and the mixture was incubated on ice for 30 minutes. Afterwards, the cells were left at 42°C for 1 minute (dry bath) and then brought back onto ice for 5 minutes. 200 µL LB medium without antibiotics was added to the cells and the incubated on a shaker at 250 rpm for 30 minutes at 37°. Cell suspensions were centrifuged at 4000 rpm (Sigma centrifuges, model 1-14) for 4 minutes and almost all the medium was discarded. Cells were resuspended in the small volume of medium, which remained in the tube (~50 µL) by gently tapping the pellet. The re-suspended cells were then spread on a petri dish containing solid LB-Agar (15 g Agar/1L LB) and the appropriate antibiotic. Cells were grown overnight (16 hours) on the LB-Agar layer.

DNA EXTRACTION FROM BACTERIAL CELLS

Plasmid DNA purification from *E.coli* cultures was done with miniprep or midiprep kits. For minipreps were used two kits: GenElute Plasmid miniprep kit from Sigma-Aldrich (St. Louis, Missouri, USA) and ZR plasmid miniprep kit from Zymo (Freiburg, Germany). For midipreps, NucleoBond Xtra Midi kit from Macherey-Nagel (Duren, Germany) was employed. Cells taken from a colony or a glycerol stock were grown for 16 hours in 8 mL (miniprep) or 130 mL (midiprep) of LB medium (37°C, 250 rpm). The first passages of the two protocols are basically the same and they include: centrifugation of the cells, resuspension of the cell pellet, alkaline lysis at room temperature (RT) for 2-5 min and termination of the alkaline lysis with a neutralization buffer. After this procedure a precipitate of cell debris is visible. The following steps are different between miniprep and midiprep protocols. For a midiprep, the lysate is first passed through a filter (provided with the kit) in order to eliminate cell debris, before going on a purification column (also provided with the kit). The filter and the column were both washed with the proper buffers and then the

DNA was eluted. The DNA is mixed with 0.7 volumes of 2-propanol for precipitation. After a centrifugation (15000 x g for 30 minutes at 4 °C, BIOFUGE primoR), the DNA pellet was dried at room temperature and resuspended in ddH_2O. For minipreps, the cell debris were eliminated by centrifugation and only the supernatant was loaded on a purification column. The columns were then washed with the indicated buffer and the DNA was finally eluted with the recommended volume of water. DNA concentration was determined as previously described.

PLASMIDS DIGESTION WITH RESTRICTION ENZYMES

DNA digestions have been performed by using FastDigest restriction enzymes (FD) from ThermoFischer (Waltham, MA, USA). These products have two important advantages: 1) different enzymes can work in the same buffer, 2) the reaction time is very short (1 µg of plasmid DNA can be digested in 5-10 minutes). A reaction mix of 20 µL included: 2 µL of 10x FDGreen buffer + 1 µg DNA + 1 µL enzyme + ddH_2O up to 20 µL. The reaction mixtures were incubated at 37°C for 5-10 minutes in a dry bath. FD Green Buffer includes a density reagent and two tracking dyes; the reactions were therefore directly loaded on an 1% agarose gel with 0.6 µg/mL Midori Green in 1x TAE buffer for electrophoreses. After checking the digestion result, a gel extraction was performed as previously described.

ENZYME-FREE CLONING

For this project I decided to use an enzyme-free cloning approach called AQUA cloning (Beyer et al., 2015). This DNA assembly method relies on *in vivo* processing by *E. coli*: homologous recombination allows the generation of circular plasmids from DNA fragments sharing overlapping homologous regions (a cut plasmid and inserts). The gene of interest was amplified by PCR and regions of homology to a linearized expression vector were introduced. Primers were designed to add flanking regions of 32 bp upstream and downstream. The PCR products were separated by gel electrophoreses on 0.8-1% agarose gel with 0.6 µg/mL MidoriGreen in 1x TAE buffer and gel extraction was performed as described before. Plasmids were linearized using FD restriction enzymes from Thermo Fisher (Waltham, MA, USA) and gel-purified. The DNA fragments (expression vector and insert) were then mixed in a 1.5 mL tube as follows:

Linearized plasmid	12 ng / Kb plasmid
Insert	molar ratios of 3:1 (insert:vector)
H_2O	up to 10 µL
Final Volume	10 µL

The DNA mixture was incubated for 30 minutes at RT and 30 minutes at 50°C. The DNA was then added to a 50 µL aliquot of competent DH5α cells. The tubes containing the DNA-cell mixture were kept on ice for 30 minutes, after which a heat shock was performed. The reaction tubes were therefore transferred for 45 seconds to a dry bath at 42°C before transferring them back on ice for 10 more minutes. At this point 500 µL of LB medium was added to the cells, which were incubated on a shaker (250 r.p.m.) for 1 hour at 37°C. After a quick centrifugation (4000 x g for 4 minutes Sigma centrifuges, model 1-14), most of the medium was discarded and the cells were resuspended in ~50 µL of LB. The small volume of medium with re-suspended cells was then spread on LB-agar plates containing appropriate antibiotics. The next day the colonies were screened via colony-PCR. Positive colonies were re-inoculated in LB medium with appropriate antibiotic selection and grown for mini/midiprep. The DNA was then sequenced by EurofinsGenomics (Luxembourg).

6.2 HEK293T cells culture and transfection

HEK293T CELL LINE MAINTENANCE

HEK293T cells were cultured in DMEM (Dulbecco's Modified Eagle Medium, Euroclone, Pero, Italy) and DMEM/F-12 (1:1 mixture of Dulbecco's Modified Eagle Medium and Nutrient Mixture F-12, Millipore, Burlington, MA, USA) supplemented with 10% fetal bovine serum and 1% Pen Strep (100 U/mL of penicillin and 100 µg/ml of streptomycin), both from Sigma-Aldrich. Cells were grown in 25 mm^2 flasks (Sartstedt, Numbrecht, Germany), stored in a 37 °C humidified incubator with 5% CO_2. DMEM/F-12 without phenol-red was used for experiments with red light. Cells were split every 3-4 days. After the medium was removed, 1 mL of trypsin or accutase (both from Sigma-Aldrich, St. Louis, MO, USA) was added. Cells were then incubated for 2 minutes at RT with trypsin or 4 minutes at 37 °C with accutase. The enzymatic reaction was stopped by adding 5 mL of fresh and pre-heated medium. The desired amount of cell suspension was added to a new flask pre-filled with 5 mL medium. The same cell suspension was also used to seed the cells in 35 mm petri dishes (Sartstedt, Numbrech, Germany) pre-filled with 2 mL of fresh medium. The latter cells were used for transfections. After 25 to 30 passages, the transfection efficiency started to get worse. At this point new cells were thawed from a stock to start a new line. HEK293T cell stocks were stored as aliquots in liquid nitrogen with medium and DMSO. When an aliquot was thawed, the cells were immediately centrifuged to separate them from DMSO. The pellet was re-suspended in 1mL of fresh medium and transferred to a new flask containing 5 mL of fresh medium.

TRANSFECTION OF HEK293T CELLS

Two transfection protocols have been used in this work for HEK293T cells.

1. *Turbofect transfection protocol*. The following transfection mix was prepared in a 1.5 mL reaction tube: 100 µL of serum-free medium, up to 1µg of each plasmid, 2µL of turbofect/µg DNA (turbofect transfection reagent from ThermoFisher, Waltham, MA, USA). The transfection mix was vortexed and incubated at RT for 20 minutes. After these 20 minutes the transfection mix was added drop-wise to petri dishes with a cell confluence between 60% and 80%. The dishes were gently shaken to achieve even distribution of the transfection mix. This transfection method does not require changing of the medium.
2. *Calcium phosphate transfection method*. Two 1.5 mL tubes were prepared. The first one was filled with 500 µL of 2x Hepes Buffer Solution (280 mM NaCl, 50 mM HEPES, 1.5 mM Na_2HPO_4, pH 7.09 with 5M NaOH). The second tube was filled in the following order: up to 6 µg of each plasmid, 62 µL $CaCl_2$ 2M, H_2O up to 500 µL. The content of this tube was added drop-wise to the first one, while gently tapping the latter to ensure good mixing. After incubation at RT for 10 minutes, 500 µL of the transfection mix was added in a 35 mm petri dish with a cell confluence between 60% and 80%. Cells were transferred back into the incubator and the medium was changed after 4 hours.

6.3 Jurkat cells culture and transfection

JURKAT CELL LINE MAINTENANCE

Jurkat cells were cultured in RPMI (Roswell Park Memorial Institute 1640 medium, Millipore, Burlington, MA, USA) supplemented with 10% fetal bovine serum and 1% Pen Strep (100 U/mL of penicillin and 100 µg/ml of streptomycin), both from Sigma-Aldrich. Cells were grown in 75 mm^2 flasks (Sartstedt, Numbrech, Germany), stored in a 37 °C humidified incubator with 5% CO_2. RPMI without phenol-red was used for experiments with NIR.

The cells were split every four days. Jurkat are not adherent cells so they don't need to be detached from the flask with enzymes. A new flask was prepared with 15 mL of fresh pre-heated medium, then 15 mL of the cell culture was transferred to this new flask. The cells were visually checked with a microscope periodically. Healthy Jurkat cells appear round, with small wing-shaped extensions. When the cells started to look unhealthy (not round and without extensions) a new line was started as described for HEK293T.

TRANSFECTION OF JURKAT CELLS

Jurkat cells are more difficult to transfect than HEK293T cells. For the present work I used a protocol, which had been established in previous work (Voos et al. 2018). The transfection reagent used in this protocol is lipofectamine 2000 (Invitrogen, Carlsband, CA, USA).

The cell concentration in the culture flask was determined with a cell-counter (NanoEnTek, Seoul, Korea). An aliquot of 50 µL of cell culture was mixed with 50 µL of Tryphan Blue, which stains dead cells. 10 µL of this blue sample was loaded on a counting slide for inspection in the cell counter. The counter provides information about cell concentration and viability. For transfections, 1.4 – 1.7 x 10^6 cells were pelleted and re-suspended in 100 µL of fresh pre-heated medium. In another 1.5 mL tube, 1µg of DNA (for double transfections 0.5 µg of each DNA) was mixed with 6 µL lipofectamine 2000. After 5 minutes of incubation at RT, 250 µL of serum-free medium was added. After one more minute of incubation at RT, the transfection mix was transferred in the first tube to be mixed with the cells. This tube was then incubated at 37°C for 5 hours, after which the cells were seeded in 35 mm petri dishes together with 2 mL of fresh medium.

6.4 Electrophysiology

24 hours after transfection, HEK293T cells were split in 35mm petri dishes to obtain dispersed single cells. After 3-4 hours cells were ready for patch-clamp experiments, which were performed at RT.

EXPERIMENTAL SETUP AND ANALYSIS

For experiments at TU Darmstadt the glass pipettes were prepared with a vertical puller (model P-P 830 from Narishige, Suginami, Japan). Borosilicate capillaries (1.5-1.8 x 1000 mm, Kimble, Vineland, NJ, USA) were pulled and then coated with Sigmacote (Sigma-Aldrich, St. Louis, MO, USA). The capillaries were then dried for 5 to 6 days. For recordings at the University of Milan, a horizontal puller (P-97 Flaming/Brown from Sutter, Novato, CA, USA) was used to pull borosilicate capillaries (1.5mm O.D., 0.86 I.D. capillaries from Sutter, Novato, CA, USA). Both pullers were set to obtain pipettes with a resistances of 3–5 MΩ. Pipettes were filled with the intracellular solution, which contained: 10 mM NaCl, 130 mM KCl, 1 mM egtazic acid (EGTA), 0.5 mM $MgCl_2$, 2 mM ATP (Mg salt) and 5 mM HEPES–KOH buffer (pH 7.4). Where indicated, Adenosine 3',5'-cyclic monophosphate (cAMP, Sigma-Aldrich) was added to the intracellular solution. The medium was removed from the 35 mm petri dish before recordings and substituted with the extracellular solution, which contained: 110 mM NaCl, 30 mM KCl, 1.8 mM $CaCl_2$, 0.5 mM $MgCl_2$ and 5 mM HEPES–KOH buffer (pH 7.4).

Fluorescent cells were approached with the glass pipette and sealed against the pipette tip by gentle suction. After obtaining a good seal (seal resistance > 1GΩ), HCN4 currents were measured in the whole-cell configuration. In Milan a Dagan 3900A amplifier (Degan, Minneapolis, MN, USA) and an Axon Digidata 1322 A/D converter (Axon Instruments, San Jose, CA, USA) were used for the recordings. The recorded current traces were analyzed with Axon pClamp9. In TU Darmstadt the same measurements were performed with a HEKA EPC9 (HEKA, Lambrecht/Pfalz, Germany), which includes in a single instrument the amplifier and the A/D converter. Currents were in this case analyzed with PatchMaster v2x90.2 a software from HEKA. To elicit and record HCN4 currents voltage step protocols were applied to the cells. Each protocol was composed by many cycles, each of them divided in 3 segments. In the first and the last segment the voltage was clamped at -30 mV (1 second) and -40 mV (7 seconds), respectively. Test voltages were applied in the second segment (4.5 seconds), starting from -30 mV, in -15 mV increments. Usually, protocols were composed of 10 cycles to cover a range of voltages from -30 to -165 mV.

The current traces were analyzed to investigate the voltage dependence of the channel. In the Results and Discussion chapters, I explain the types of analysis that I performed and the rationale behind them. The analysis and the preparation of the figure were done with the Originpro (OriginLab, Northampton, MA, USA) or Igorpro (WaveMetrics, Lake Oswego, OR, USA).

6.5 ELISA assays for quantification of intracellular c-di-GMP

PREPARATION OF CELL EXTRACT SAMPLES

ELISA assays were performed in order to quantify the intracellular c-di-GMP concentration. For this purpose cell extracts had to be prepared. Cells were transfected with the constructs of interest and after 24 hours the transfection efficiency was checked under a microscope (usually 30-40 % of transfected cells). Cells were detached from the dishes with accutase and the reaction was stopped with 2mL medium. Cells were transferred into a 2 mL tube and centrifuged (800 x g, 3 min, BIOFUGE, primoR); the supernatant was discarded. For the lysis of the collected cells three methods for different assays were used during the course of this work. The reasons for using three different approaches are explained in Results and Discussion. The three different methods are as follows:

1. Cells were resuspended in PBS to a final concentration of 1 x 10^6 cells/mL. The cell membranes were then broken by 3 freeze/thaw cycles.
2. Cells were resuspended in an 1% Triton buffer (150 mM NaCl, 2 mM EDTA, 1% Triton, 10 mM Tris-HCl pH 7.4) to a final concentration of 1 x 10^6 cells/mL. The lysis buffer was added cold to the cell pellets. Cells were resuspended by pipetting and vortexing. After that, cells were incubated on ice for 30 minutes.
3. Cell pellets were resuspended in a buffer containing acetonitrile, methanol and H_2O (2:2:1) to a final concentration of 1 x 10^6 cells/mL. Cells were incubated on ice for 15 minutes and at 95°C for 5 minutes.

The lysates obtained with these methods were cleared of cell debris by centrifugation (5 min, 14000 x g, 4°C, BIOFUGE primoR). The supernatants were collected and stored at -20°C.

ELISA ASSAY

For this work the General Cyclic Diguanylate ELISA Kit (EIAab, Wuhan, China) was used. This assay is based on the competitive immunoassay technique. General information about competitive ELISA can be found in Results and Discussion, where I introduce this technique. The assay was performed according to the manufacturer's instructions. Before the assay all the reagents were brought to room temperature. Samples, standards and reagents were loaded in two replicates in 96-well plate with a multi-channel pipette. The incubation steps were performed at 37°C in a sterile incubator. During these incubation steps, the plate was carefully sealed to avoid contamination. After each incubation step, the reagents were removed from the wells by pipetting plus gently tapping the plate on a paper towel. After the last step of the assay procedure, the absorbance values of the wells were measured with a special spectrophotometer designed to read multi-well plates (Epoch2 from BioTek, Winooski, VT, USA). Absorbance values of the standards were used to obtain a calibration curve, from which concentration values of the samples could be extrapolated. For this analysis an online software called MyAssay was used (www.myassays.com).

6.6 Immuno-fluorescence of Jurkat Cells

PREPARATION OF THE CELLS

As explained in the Results and Discussion, I quantified the production of interferon β (IFN-β) in Jurkat cells in response to the presence of c-di-GMP with immunofluorescence. Cells were transfected with the constructs of interest as described in chapter 6.2. 24 hours after transfection, the following treatments were applied:

1. Cells were transferred into 2 mL reaction tubes and centrifuged (1800 rpm, RT, 5 minutes, Sigma centrifuges, model 1-14). The medium was discarded and the pellet resuspended in 1 mL PBS. After centrifugation, the PBS supernatant was removed from the tube. All following centrifugation steps were performed as the aforementioned one.

2. The pellet was resuspended in 1 mL of 4% Paraformaldehyde (in PBS). Cells were incubated at RT for 30 minutes on a shaker at 400 rpm.

3. Cells were isolated by centrifugation from the Paraformaldehyde supernatant and resuspended in 1 mL of 0.2% Triton X-100 (in PBS). Cells were then incubated on a shaker with Triton X-100 at RT for 10 minutes (400 rpm). After this incubation the cells were pelleted and the Triton X-100 was discarded. This step was repeated twice.

4. The cells were washed with 1 mL PBS.

5. After PBS was removed, the cells were resuspended in 0.5 mL of primary antibody (20 µg/mL, anti-IFN-β rabbit polyclonal antibody, ThermoFisher), to which they were exposed overnight (16 hours, 4°C, 300 rpm).

6. The next day the samples were centrifuged to eliminate the antibody. The cell pellet was resuspended in 1 mL of Tween20 (Polyethylene glycol sorbitan monolaurate) 0.05% (in PBS) and centrifuged again.

7. The Tween20 was discarded and substituted with 500 µL secondary antibody (1 µg/mL, AlexaFluo goat anti-rabbit, Invitrogen, Carlsbad, CA, USA). Cells were incubated with the antibody for 1 hour, at RT on a shaker at 400 rpm. After this incubation the cells were pelleted.

8. The pellet was washed with 1 mL of Tween20 0.05% (in PBS) and centrifuged.

9. The cells were resuspended in 500 µL PBS.

IMAGING AT THE CONFOCAL MICROSCOPE

Jurkat cells were imaged on a confocal laser scanning microscope (CLSM) (LeicaTCS SP5; Leica mycrosystem CMS GmbH, Wetzlar, Germany). The cell samples were examined using an immersion objective (HCX PL APO 100x). Two laser lights were used for exciting the fluorescent tags. The first was an 488 nm Argon laser with an intensity of 20%. The second was a green 561 nm laser at intensity of 40%. The filter used for this type of analysis was a dual band pass filter (458-514 nm). For the green GFP-like emission signal the detector HyD1 was used, while for the red signal was collected by HyD2 detector. Each detector covered a range of wavelengths ±20 nm around the absorption peak. The cells were measured in PBS. Each cell sample was loaded on a 25 mm coverslip fixed between two aluminum rings. The coverslip was then fixed to the microscope plate.

Images of the cells were taken using the software LAS AF Version 2.60 (Leica Leica mycrosystem CMS GmbH). The images were acquired with a scanning frequency of 200 Hz and the pixel size was set to 1024x1024. Pictures were then analyzed with the software Fiji (Bethesda, MD, USA) to quantify the fluorescence intensities. The analysis that was done on the images acquired at the microscope is presented in the Results and Discussion part.

7

BIBLIOGRAPHY

Aldridge M.e., Forest K.T. (2011) Bacterial phytochromes: More than meets the light. *Critical Reviews in Biochemistry and Molecular Biology, 46, 1: 67-88.*

Arrigoni C., Schroeder I., Romani G., Van Etten J.L., Thiel G., Moroni A. (2013) The voltage-sensing domain of a phosphatase gates the pore of a potassium channel. *Journal of General Physiology 141 (3): 389-95*

Bamberg E., Tittor J., Oesterhelt D. (1993) Light-driven proton or chloride pumping by halorhodopsin. *Proceedings of the National Academy of Sciences of the United States 90 (2): 639-643.*

Banghart M., Borges K., Isacoff E., Trauner D., Kramer R.H. (2004) Light-activated ion channels for remote control of neuronal firing. *Nat Neurosci., 7(12):1381-6.*

Barbuti A., DiFrancesco D. (2008) Control of cardiac rate by "funny" channels in health and disease. *Ann. N.Y. Acad. Sci., 1123: 213–223*.

Baruscotti M., Barbuti A., Bucchi A. (2010) The cardiac pacemaker current. J Mol Cell Cardiol., 48(1): 55-64.

Bell D.C., Yao H., Saenger R.C., Riley J.H., Siegelbaum S.A. (2004) Changes in local S4 environment provide a voltage-sensing mechanism for mammalian hyperpolarization-activated HCN channels. *J Gen Physiol., 123(1): 5-19*

Beyer H.M., Gonschorek P., Samodelov S.L., Meier M., Weber W., Zurbriggen M.D. (2015) AQUA cloning: c versatile and simple enzyme-free cloning approach. PLoS One 11; 10(9): e0137652.

Bezanilla F. (2008) How membrane proteins sense voltage. *Nature Reviews Molecular Cell Biology 9: 323-332.*

Biel M., Wahl-Schott C., Michalakis S., Zong x. (2009) Hyperpolarization-activated cation channels: from genes to function. *Physiol Rev* 89: 847–885.

Biel S., Aquila M., Hertel B., Berthold A., Neumann T., DiFrancesco D., Moroni A., Thiel G., Kauferstein S.(2016) Mutation In S6 domain of HCN4 channel in patient with suspected Brugada syndrome modifies channel function. *Pflugers Arch.,468(10):1663-71.*

Blunck R., Batulan Z. (2012) Mechanism of electromechanical coupling in voltage-gated potassium channels. *Frontiers in Pharmacology, 3: 1-16.*

Börjesson S. I. and Elinder F. (2008) Structure, function, and modification of the voltage sensor in voltage-gated ion channels. *Cell Biochem Biophys 52: 149–174.*

Boyden E.S., Zhang F., Bamberg E., Nagel G., Deisseroth K. (2005) Millisecond-timescale, genetically targeted optical control of neural activity. *Nature Neuroscience 8 (9): 1263-1268.*

Boyden E.S. (2011) A history of optogenetics: the development of tools for controlling brain circuits with light. *F1000 Biology Reports 2011, 3:11.*

Boyle P.M., Karathanos T.V., Trayanova N.A. (2018) Cardiac Optogenetics: 2018. *JACC Clin Electrophysiol., 4(2):155-167.*

Brown H.F., DiFrancesco D., S.J. Noble (1979) How does adrenaline accelerate the heart? *Nature vol. 280: 235-236.*

Burdette D.L., Monroe K.M., Sotelo-Troha K., Iwig J.S., Eckert B., Hyodo M., Hayakawa Y., Vance R.E. (2011) STING is a direct innate immune sensor of cyclic di-GMP. *Nature 478 (7370): 515-8.*

Burdette, D. L., Vance, R. E. (2013) STING and the innate immune response to nucleic acids in the cytosol. *Nature Immunology, 14(1): 19–26.*

Burgie E.S., Vierstra R.D. (2014) Phytochromes: an atomic perspective on photoactivation and signaling. *The Plant Cell, Vol. 26: 4568–4583.*

Christen M., Christen B., Folcher M., Schauerte A., Jenal U. (2005) Identification and Characterization of a Cyclic di-GMP-specific Phosphodiesterase and Its Allosteric Control by GTP. *THE JOURNAL OF BIOLOGICAL CHEMISTRY Vol. 280, No. 35: 30829 –30837.*

Christie (2007) Phototropin Blue-Light Receptors. *Annual Review of Plant Biology 58: 21–45.*

Cosentino C., Alberio L., Gazzarrini S., Aquila M., Romano E., Cermenati S., Zuccolini P., Petersen J., Beltrame M., Van Etten J.L., Christie J.M., Thiel G., Moroni A. (2015) Engineering of a light-gated potassium channel. *Science 348:707-710.*

Crick F.H. (1979) Thinking about the brain. *Scientific American 241 (3): 219-32.*

D'Argenio D.A., Miller S.I. (2004) Cyclic di-GMP as a bacterial second messenger. *Microbiology, 150: 2497–2502.*

Deisseroth K. (2011) Optogenetics. *Nature Methods* 8: 26–29.

Deisseroth K. (2015) Optogenetics: 10 years of microbial opsins in neuroscience. *Nature Neuroscience, volume 18, Number 9.*

DiFrancesco D., Ferroni A., Mazzanti M., Tromba C. (1986) Properties of the hyperpolarizing-activated current (if) in cells isolated from the rabbit sino-atrial node. *J. Physiol., 377, pp. 61-88*.

DiFrancesco D., Tortora, P. (1991). Direct activation of cardiac pacemaker channels by intracellular cyclic AMP. Nature, 351(6322): 145–147.

DiFrancesco D. (1993) Pacemaker Mechanisms in Cardiac Tissue. *Annual Review of Physiology, 55(1), 455–472*.

DiFrancesco D. (2010) The role of the funny current in pacemaker activity. *Circ Res., 106(3):434-46.*

DiFrancesco M.L., Gazzarrini S., Arrigoni C., Romani G., Thiel G., Moroni A. (2015) Engineering a Ca2+ sensitive (bio) sensor from the pore-moduke of a potassium channel. *Sensors 15:4913-4924.*

DiVentura B., Kuhlman B (2016) Go in! Go out! Inducible control of nuclear localization. *Curr Opin Chem Biol. 34: 62-71*

Fenno L.E., Yizhar O., Deisseroth K. (2011) The Development and Application of Optogenetics *Annual. Review of. Neuroscience 34: 389-412.*

Folcher M., Oesterle S., Zwicky K., Thekkottil T., Heymoz J., Hohmann M., Christen M., Daoud El-Baba M., Buchmann P., Fussenegger M. (2014) Mind-controlled transgene expression by a wireless-powered optogenetic designer cell implant. *Nature Communications, 5(1).*

Gross C., Saponaro A., Santoro B., Moroni A., Thiel G., Hamacher K. (2018) Mechanical transduction of cytoplasmic-to-transmembrane-domain movements in a hyperpolarization-activated cyclic nucleotide-gated cation channel. *J Biol Chem., 293(33): 12908-12918*

Hayoz S., Tiwari P.B., Piszczek G., Üren A., Brelidze T.I. (2017) Investigating cyclic nucleotide and cyclic dinucleotide binding to HCN channels by surface plasmon resonance. *PLoS One12(9): e0185359.*

Hille, B. (2001) Ionic channels of excitable membranes. *Sinauer Sunderland MA.*

Kalia D., Merey G., Nakayama S., Zheng Y., Zhou J., Luo Y., Guo M., Roembke B.T., Sintim H.O. (2013) Nucleotide, c-di-GMP, c-di-AMP, cGMP, cAMP, (p)ppGpp signaling in bacteria and implications in pathogenesis. *Chem. Soc. Rev.* 42: *305-341.*

Larsson H. P., Baker O. S., Dhillon D. S., Isacoff E. Y. (1996) Transmembrane movement of the shaker K^+ channel S4. *Neuron Vol. 16, 387–397.*

Lee C.H., MacKinnon R. (2017) Structures of the human HCN1 hyperpolarization-activated channel. *Cell 168: 111–120.*

Lolicato M., Nardini M., Gazzarrini S., Möller S., Bertinetti D., Herber F.W., Bolognesi M., Martin H., Fasolini M., Bertrand J.A., Arrigoni C., Thiel G., Moroni A. (2011) Tetramerization dynamics of C-terminal domain underlies isoform-specific cAMP gating in Hyperpolarization-activated Cyclic Nucleotide-gated channels. *The journal of biological chemistry Vol. 286, No. 52: 44811–44820*

Long S. B., Campbell E. B., MacKinnon R. (2005) Voltage Sensor of Kv 1.2: structural basis of the electromechanical coupling. *Science Vol. 309: 903-908.*

Ludwig A., Zong X., Jeglitsch M., Hofmann F., Biel M. (1998) A family of hyperpolarization-activated mammalian cation channels. *Nature, 393: 587–591.*

Ludwig A., Zong X., Stieber J., Hullin R., Hofmann F., Biel M. (1999) Two pacemaker channels from human heart with profoundly different activation kinetics. *The EMBO Journal, 18(9): 2323–2329.*

Männikko R., Elinder F., Larsson H. P. (2002) Voltage-sensing mechanism is conserved among ion channels gated by opposite voltages. *Nature Vol. 419, 837-841.*

McWhirter S.M., Barbalat R., Monroe K.M., Fontana M.F., Hyodo M., Joncker N.T., Ishii K.J., Akira S., Colonna M., Chen Z.J., Fitzgerald K.A., Hayakawa Y., Vance R.E. (2009) A host type I interferon response is induced by cytosolic sensing of the bacterial second messenger cyclic-di-GMP. *J Exp Med. 206(9):1899-911.*

Mei Y., Zhang F. (2012) Molecular Tools and Approaches for Optogenetics. *Biological psychiatry 71:1033–1038.*

Nagel G., Szellas T., Huhn W., Kateriya S., Adeishvili N., Berthold P., Ollig D., Hegemann P., and Bamberg E. (2003) Channelrhodopsin-2, a directly light-gated cation-selective membrane channel. *Proceedings of the National Academy of Sciences of the United States Vol. 100, No. 24: 13940–13945.*

Niopek D., Benzinger D., Roensch J., Draebing T., Wehler P., Eils R., Di Ventura B. (2014) Engineering light-inducible nuclear localization signals for precise spatiotemporal control of protein dynamics in living cells. *Nat Commun. 2014 5:4404.*

Niopek D., Wehler P., Roensch j. Eils R., Di Ventura B. (2016) Optogenetic control of nuclear protein export. *Nat Commun. 7:10624.*

Pape H.C. (1996) Queer current and pacemaker: the hyperpolarization- activated cation current in neurons. *Annu Rev. Phyiol. 1996 58:299-327*

Pham E., Mills E., Truong K. (2011) A Synthetic Photoactivated Protein to Generate Local or Global Ca2+ Signals. *Chemistry & Biology 18: 880–890.*

Piatkevich K.D., Subach F.D., Verkhusha V.V. (2013) Engineering of bacterial phytochromes for near-infrared imaging, sensing, and light-control in mammals. *Chem. Soc. Rev.*42, 3441

Plugge B., Gazzarrini S., Nelson M., Cerana R., Van Etten J.L., Derst C. DiFrancesco D., Moroni A. Thiel G. (2000) A Potassium Channel Protein Encoded by Chlorella Virus PBCV-1. *Science 287: 1641-44*

Pusch M., Neher E. (1988) Rates of diffusional exchange between small cells and a measuring patch pipette. Pflugers Arch. 411(2): 204-11.

Rockwell N.C. and Lagarias J.C. (2010) A Brief History of Phytochromes. *ChemPhysChem, 11: 1172 – 1180.*

Römling U., Galperin M.Y., Gomelsky M. (2013) Cyclic di-GMP: the First 25 Years of a Universal Bacterial Second Messenger. *Microbiol Mol Biol Rev. 77(1): 1–52.*

Römling U., Galperin M.Y. (2017) Discovery of the second messenger cyclic di-GMP. *Methods Mol Biol. 1657: 1-8.*

Ross P., Weinhouse H., Aloni Y., Michaeli D., Weinberger-Ohana P., Mayer R., Braun S., de Vroom E., van der Marel G.A., van Boom J.H., Benziman M. (1987) Regulation of cellulose synthesis in Acetobacter xylinum by cyclic diguanylic acid. *Nature 325(6101): 279-81.*

Rost B.R., Schneider-Warme F., Schmitz D., Hegemann P. (2017) Optogenetic Tools for Subcellular Applications in Neuroscience. *Neuron, 96(3): 572-603.*

Ryu M.H. and Gomelsky M. (2014) Near-infrared Light Responsive Synthetic c-di-GMP Module for Optogenetic Applications. *ACS Synth. Biol., 3: 802−810*.

Ryu M.H., Fomicheva A., Moskvin O.V., Gomelsky, M. (2017) Optogenetic Module for Dichromatic Control of c-di-GMP Signaling. *Journal of Bacteriology, 199 (18).*

Santoro B., Grant S.G.N., Bartsch D., Kandel E.R. (1997) Interactive cloning with the SH3 domain of N-src identifies a new brain specific ion channel protein, with homology to Eag and cyclic nucleotide-gated channels. *PNAS, 94 (26): 14815-14820.*

Santoro B., Liu D.T., Yao H., Bartsch D., Kandel E.R., Siegelbaum S.A., Tibbs G.R. (1998) Identification of a gene encoding a hyperpolarization-activated pacemaker channel of brain. *Cell, 93(5): 717-29.*

Santoro B. and Tibbs G. (1999) The HCN Gene Family: molecular basis of the hyperpolarization-activated pacemaker channels. *Ann N Y Acad Sci., 868:741-64.*

Saponaro A., Pauleta S.R., Cantini F., Matzapetakis M., Hammann C., Donadoni D., Hu L., Thiel G., Banci L., Santoro B., Moroni A. (2014) Structural basis for the mutual antagonism of cAMP and TRIP8b in regulating HCN channel function. Proc *Natl Acad Sci U S A, 111(40):14577-82.*

Saponaro A., Cantini F., Porro A., Bucchi A., DiFrancesco D., Maione V., Donadoni C., Introini B., Mesirca P., Mangoni M.E., Thiel G., Banci L., Santoro B., Moroni A. (2018) A synthetic peptide that prevents cAMP regulation in mammalian hyperpolarization-activated cyclic nucleotide-gated (HCN) channels. *eLife 2018;7:e35753*

Scicchitano P., Carbonara S., Ricci G., Mandurino C., Locorotondo M., Bulzis G., Gesualdo M., Zito A., Carbonara R., Dentamaro I., Riccioni G., Ciccone M.M. (2012) HCN Channels and Heart Rate. *Molecules, 17(4): 4225-35.*

Shao J., Xue S., Yu G., Yu Y., Yang X., Bai Y., Zhu S., Yang L., Yin J., Wang Y., Liao S., Guo S., Xie M., Fussenegger M., Ye H. (2017). Smartphone-controlled optogenetically engineered cells enable semiautomatic glucose homeostasis in diabetic mice. *Science Translational Medicine, 9 (387), eaal2298.*

Shi W., Wymore R.,Yu H., Wu J., Wymore R.T., Pan Z., Robinson R.B., Dixon J.E., McKinnon D., Cohen I.S. (1999). Distribution and prevalence of hyperpolarization-activated cation channel (HCN) mRNA expression in cardiac tissues. *Circ Res., 85(1): 1-6.*

Sineshchekov O.A., Jung K.H., Spudich J.L. (2002) Two rhodopsins mediate phototaxis to low- and high-intensity light in Chlamydomonas reinhardtii. *Proc Natl Acad Sci U S A., 99(13): 8689-94.*

Strickland D., Moffat K., Sosnick T.R. (2008) Light-activated DNA binding in a designed allosteric protein. PNAS, vol. 105, n 31: 10709–10714.

Takala H., Björling A., Berntsson O., Lehtivuori H., Niebling S.,Hoernke M., Kosheleva I., Henning R., Menzel A., Ihalainen J.A., Westenhoff S. (2014) Signal amplification and transduction in phytochrome photosensors. *Nature, 509(7499): 245-248.*

Vaccari T., Moroni A., Rocchi M., Gorza L., Bianchi M.E., Beltrame M., DiFrancesco D. (1999) The human gene coding for HCN2, a pacemaker channel of the heart. *Biochim Biophys Acta 1446: 419–425.*

Vemana S., Pandey S., Larsson H.P. (2004) S4 movement in a mammalian HCN channel. *J Gen Physiol., 123(1): 21-32.*

Voos P., Fuck S., Weipert F., Babel L., Tandl D., Meckel T., Hehlgans S., Fournier C., Moroni A., Rödel F., Thiel G. (2018) Ionizing Radiation Induces Morphological Changes and Immunological Modulation of Jurkat Cells. *Front Immunol.,9: 922.*

Wang Y., Wang F., Wang R., Zhao P., Xia Q. (2015). 2A self-cleaving peptide-based multi-gene expression system in the silkworm Bombyx mori. *Scientific Reports, 5 (1): 16273*

Wagner J.R., Brunzelle J.S., Forest K.T., Vierstra R.D. (2005) A light-sensing knot revealed by the structure of the chromophore-binding domain of phytochrome. *Nature, 438(7066): 325-31.*

Zagotta W.N., Olivier N.B., Black K.D., Young E.C., Olson R., Gouaux e. (2003) Structural basis for modulation and agonist specificity of HCN pacemaker channels. *Nature, vol 425: 200-205*

Zemelman B.V., Lee G. A. and Miesenbock G. (2002) Selective Photostimulation of Genetically ChARGed Neurons. *Neuron, Vol. 33: 15–22.*

Zhang F., Wang L.P., Brauner M., Liewald J.F., Kay K., Watzke N., Wood P.G., Bamberg E., Nagel G., Gottschalk A., Deisseroth K. (2007) Multimodal fast optical interrogation of neural circuitry. *Nature 5 ;446 (7136): 633-639.*

Zhou Y., Morais-Cabral J.H., Kaufman A., MacKinnon R. (2001). Chemistry of ion coordination and hydration revealed by a K+ channel–Fab complex at 2.0 Å resolution. *Nature, 414: 43–48.*